NASA CR-72558

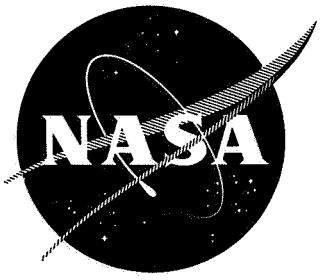

CONTRACTOR REPORT

THEORY OF DROPLET VAPORIZATION IN THE REGION OF THE THERMODYNAMIC CRITICAL POINT

by

Jose A. Manrique

prepared for

NATIONAL AERONAUTICS AND SPACE ADMINISTRATION

June 2, 1969

NASA Grant NGR 50-002-017

Technical Management
NASA Lewis Research Center
Cleveland, Ohio
Chemistry and Energy Conversion Division
Paul R. Wieber

THE UNIVERSITY OF WISCONSIN
DEPARTMENT OF MECHANICAL ENGINEERING
Madison, Wisconsin

NASA CR-72558

CONTRACTOR REPORT

THEORY OF DROPLET VAPORIZATION IN THE REGION OF THE THERMODYNAMIC CRITICAL POINT

by

Jose A. Manrique

prepared for

NATIONAL AERONAUTICS AND SPACE ADMINISTRATION

June 2, 1969

NASA Grant NGR 50-002-017

Technical Management
NASA Lewis Research Center
Cleveland, Ohio
Chemistry and Energy Conversion Division
Paul R. Wieber

THE UNIVERSITY OF WISCONSIN
Department of Mechanical Engineering
Madison, Wisconsin

THEORY OF DROPLET VAPORIZATION IN THE REGION OF THE THERMODYNAMIC CRITICAL POINT

JOSE A. MANRIQUE

Under the Supervision of
Associate Professor Gary L. Borman

ABSTRACT

Analysis of the vaporization of a spherical droplet in a stagnant inert atmosphere including property variations with temperature and pressure and surface regression is applied by numerical computation to the case of liquid carbon dioxide vaporizing in gaseous nitrogen. Ambient temperatures of 375-1600°K and pressures of 70-120 atmospheres were used in the calculations. Non-ideal effects are shown to be important. It is shown that for sufficiently high pressures no steady-state exists and that a droplet can reach and exceed its critical temperature by an intrinsically unsteady process. Comparisons are made with low density film theories and film theory with properties corrected for non-ideal effects. Some calculations of the effects of sinusoidal pressure oscillations on vaporization are also included.

SUMMARY

A mathematical model of a spherical liquid droplet vaporizing in an inert gas with ambient temperatures and pressures such that the droplet may approach or exceed its thermodynamic critical temperature was investigated by numerically integrating the equations of change. Hydrodynamic and gravitational effects are not included in the analysis, and the liquid phase is assumed to have a uniform but time dependent temperature. The boundary layer is thus spherical and the independent variables are radial distance and time. Non-ideal effects associated with high pressure mixtures, solubility of the gas into the liquid droplet, variation of the thermophysical properties through the boundary layer, and the effects of total pressure on vapor pressure and enthalpy of vaporization are included in the analysis.

Calculated vaporization histories of a carbon dioxide droplet vaporizing in a nitrogen atmosphere are reported for ambient temperatures of 375-1600°K and ambient pressures of 70-120 atmospheres.

The theory indicates that at sufficiently high pressures a droplet cannot attain steady state conditions. By steady state it is implied that all the energy transferred to the droplet surface is carried away entirely by the mass transfer while the liquid remains at a constant temperature.

The results indicate that all of the non-ideal effects, hitherto neglected in vaporization analyses, are important in the critical region. Furthermore, the unsteady heating up of the droplet is most important under high pressure conditions. Under supercritical pressure and high ambient temperature conditions a droplet can reach and exceed its thermodynamic critical temperature, thus becoming a dense mass of vapor, by an intrinsically unsteady process.

Comparisons with a low pressure unsteady film theory model are reported. The comparisons indicate that vaporization times can be estimated with reasonable accuracy by this low pressure model over a wide range of temperatures and pressures, provided the effects of total pressure on vapor pressure and enthalpy of vaporization are properly taken into account under high density conditions.

The effects of superimposed gas phase sinusoidal pressure oscillations of relatively small amplitude upon the droplet vaporization process were calculated. The computations indicate that the relaxation times in the gas phase are very short and the overall effect of the pressure oscillations is negligibly small.

ACKNOWLEDGMENTS

The author wishes to express his deepest gratitude and appreciation to Professors Gary L. Borman, Phillip S. Myers, and Otto A. Uyehara for the inspiration, invaluable counsel and assistance he received from them. He is especially grateful and it is impossible for him to say enough in thanks for the wise advice and limitless help he received from Professor Gary L. Borman.

The author wishes to express his thanks to the National Aeronautics and Space Administration for its financial support, and to Mr. Paul R. Wieber of the Lewis Research Center who acted as contract monitor. He is also grateful to the Wisconsin Alumni Research Foundation and to the Instituto Tecnologico y de Estudios Superiores de Monterrey for their partial financial support, and to the University of Wisconsin Computing Center for the use of its facilities.

The author wishes to acknowledge with thanks the invaluable assistance received from Dean William R. Marshall of the University of Wisconsin Engineering Experiment Station, and to Dean Jose Emilio Amores and Dr. Carlos Trevino of the Instituto Tecnologico y de Estudios Superiores de Monterrey. He is indebted to the faculty members of the University of Wisconsin Mechanical Engineering Department,

and wishes to express special appreciation to Professors Richard A. Gaggioli and John W. Mitchell.

TABLE OF CONTENTS

NOMENCLATURE

A, A, B, b = parameters in Redlich-Kwong equation of state

$\underline{A}$, $\underline{B}$, ... = variables defined by Equations [3.31] to [3.37]

b_1, b_2 = constants in Equation [3.66]

$\underline{A}'$, $\underline{B}'$, ... = variables defined by Equations [4.9] to [4.16]

C_1, C_2 = constants defined by Equations [1.16]and [1.17]

C_3 = constant defined by Equation [1.18]

C' = parameter in Equation [A.9]

c = molar density, g-mole/cm^3

c_i = molar concentration of component i, g-mole/cm^3

c_p = molar specific heat, cal/g-mole°K

c_{pi} = molar specific heat of component i, cal/g-mole°K

$\bar{c}_{pi}$ = partial molal specific heat of i, cal/g-mole°K

$\bar{c}_r$ = pseudo-reduced density defined by Equation [A.22]

D_{AB} = binary diffusivity defined by Equation [1.9], cm^2/sec

F = function in Equation [2.17]

f_i = fugacity of component i, atm.

f' = frequency, Hz.

$\bar{g}$ = parameter defined by Equation [A.21]

H_i = molar enthalpy of component i, cal/g-mole

$\bar{H}_i$ = partial molal enthalpy of component i, cal/g-mole

h = parameter in Redlich-Kwong equation of state

J = conversion factor, cal/atm cm^3

K_v = vaporization rate constant, cm^2/sec

k = thermal conductivity, cal/cm sec °K

k_L, k_R = thermal conductivities in Brokaw's method and defined by Equations [A.29] and [A.30], cal/cm sec °K

$\bar{M}$ = mean molecular weight defined by Equation [A.27], gm/g-mole

M_i = molecular weight of component i, gm/gm-mole

m_d = droplet mass in molar units, g-mole

N = parameter defined by Equation [4.24]

N_i = molar flux of component i with respect to stationary coordinates, g-mole/cm^2 sec

P = total pressure, atm

$\bar{P}$ = average pressure, atm

P' = amplitude of sinusoidal pressure oscillation, atm

$\bar{P}_c$ = pseudocritical pressure defined by Equation [A.26], atm

P_{ci} = critical pressure of component i, atm

p_i = partial pressure of component i, atm

p_v = vapor pressure, atm

Q = heat flux, cal/cm^2 sec

Q' = amplitude of sinusoidal heat flux oscillation, cal/cm^2 sec

q = function defined by Equation [A.31]

R = gas constant, atm cm^3/g-mole °K, or cal/g-mole °K

r = radial distance in spherical coordinates, cm

r_o = droplet radius, cm

r^* = radial distance near edge of boundary layer, cm

s = space increment in Equation [2.21]

T = temperature, °K

$\tilde{T}$ = asymptotic temperature, °K

$\bar{T}_c$ = pseudocritical temperature defined by Equation [A.25], °K

T_{ci} = critical temperature of component i, °K

T_{cij} = critical temperature characteristic of the i-j interaction, °K

T_{qs} = function defined by Equation [3.39], °K

T_{ss} = steady state droplet temperature, °K

t = time, sec

t_v = vaporization time, sec

V_{i0} = velocity of component i with respect to stationary coordinates, cm/sec

V_{iy} = velocity of component i relative to the droplet surface, cm/sec

v = molar volume, cm^3/g-mole

$\bar{v}_c$ = pseudocritical volume defined by Equation [A.23], cm^3/g-mole

v_{ci} = critical volume of component i, cm^3/g-mole

v_{cij} = critical volume characteristic of the i-j interaction, cm^3/g-mole

w = molar vaporization rate, g-mole/sec

x_i = mole fraction of component i

$\tilde{x}_i$ = asymptotic mole fraction of component i

x_{qs} = function defined by Equation [3.40]

Y = dependent variable in Equation [2.17]

y = radial distance from droplet surface, cm

y^* = radial distance near edge of boundary layer, cm

Z = independent variable in Equation [4.23], cm

z = compressibility factor, Pv/RT

$\bar{z}_c$ = pseudocritical compressibility factor defined by Equation [A.24]

$(\dot{})$ = indicates differentiation with respect to time

Greek Letter

α = thermal diffusivity

γ = ratio of ideal gas specific heats

λ = latent heat of vaporization, cal/g-mole

Ω_a, Ω_b = constants in Redlich-Kwong equation of state

ω_i = acentric factor of component i

Superscripts

ℓ = liquid phase

v = vapor phase

o = low pressure value

Subscripts

A = species A

B = species B

i = component i

j = component j

(i, j) = coordinate point in finite-difference grid

∞ = ambient conditions

LIST OF FIGURES

INTRODUCTION

In high pressure combustion chambers, such as those encountered in Diesel engines and liquid propellant rocket motors, the influence of the droplet vaporization process on engine performance is of primary importance.

While many investigations on single droplet vaporization have been carried out in the past, relatively few have dealt with high pressure conditions where the droplets may approach or exceed their thermodynamic critical temperature. Among these investigations dealing with high pressure environmental conditions, Wieber[32*] applied a low pressure semi-empirical vaporization model[10] to investigate the vaporization process in the region of the critical point. He concluded that a fuel droplet vaporizing under high pressure conditions can reach its critical temperature before the vaporization process is completed, and that small pressure disturbances may lead to combustion instability in this region. Spalding[27] analyzed the unsteady combustion of single droplets under high pressure conditions by using a point source model and the theory of unsteady heat conduction. Rosner[24] has modified Spalding's point source model by taking into account the

---

*Superscript numbers designate references which are listed alphabetically by first author at the end.

finite dimensions of the droplet. The underlying assumption in References 24 and 27 is that the droplet rapidly becomes a dense vapor and subsequently burns like an initially well defined "puff of gas". Although a number of the assumptions involved in Spalding's point source theory and Rosner's distributed source theory depart from reality, a more recent experimental investigation by Faeth[11] on the burning of fuel droplets, indicates that these models give reasonably accurate predictions except in the early part of the process. Recent liquid temperature measurements by Dominicis[9] indicate that, under high enough pressure conditions, there is a regime where a liquid droplet heats up continuously from its injection conditions approaching or exceeding its critical temperature. Therefore, it is now clear that at high pressures a liquid droplet may reach its critical temperature becoming a dense vapor before the vaporization process is completed.

However, previous analytical investigations have not taken into account the non-ideal effects associated with the high pressure conditions prevailing in a combustion chamber, nor the effects of pressure upon the thermophysical mixture properties. Thus, many of the assumptions ordinarily made in vaporization studies have become questionable, giving rise to a need for a more fundamental understanding of the vaporization process in the region where a droplet may reach its critical temperature.

The present investigation attempts to illuminate the understanding of the vaporization phenomenon under high pressure conditions by means of a theoretical approach which makes use of the equations of change, including the effects of high pressure mixtures as well as the effects of temperature and pressure upon the physical properties. Such a treatment although complicated by uncertainties in the determination of the thermodynamic and transport properties of binary mixtures at high pressures (whose components may exhibit anomalous behavior in the vicinity of their critical points or the entire mixture may behave abnormally elsewhere) nevertheless should provide a means for understanding the experimental data. Applications are made to a carbon dioxide droplet vaporizing in nitrogen under high pressure conditions. This selection of components was made because both are nonpolar and of relatively simple molecular structure.

The text which follows is divided into four sections. The first section presents a rather simple mathematical formulation for steady state droplet vaporization under low pressure ambient conditions. Although a similar treatment may be found elsewhere in the literature[21], the low pressure analysis is repeated here in order to establish the specific areas which require revision in the analytical formulation of the vaporization process in the critical region. Steady state droplet vaporization under high pressure conditions

is considered in the second section, including the non-idealities present in the system as well as the variation of the physical properties in the gaseous film surrounding the droplet. The unsteady vaporization process is considered in section three by means of an entirely unsteady one-dimensional analysis. Finally, the effects of relatively small amplitude sinusoidal pressure oscillations on the unsteady vaporization process at high pressures are briefly discussed in section four. Such perturbations are important in the analysis of rocket combustion instability models[32].

I. STEADY STATE VAPORIZATION AT LOW AMBIENT PRESSURES

This study is begun by considering a very simplified one-dimensional model of a droplet undergoing quasi-steady vaporization in an inert low pressure environment. Such a model is not realistic at the high levels of total pressure encountered in the thermodynamic critical region, for it ignores all the effects associated with high pressure mixtures.

Although numerous investigations on droplet vaporization at low pressure environmental conditions have been carried out in the past and a similar treatment may be found elsewhere[3,10,21], the purpose of the low pressure analysis which follows is to establish the specific areas which require revision in the analytical formulation of the vaporization process in the critical region, as well as to indicate the salient assumptions and thus the inherent limitations of the model.

Only steady state conditions are considered and therefore the heating-up period, which plays an important role in the vaporization process, will be ignored. Moreover, hydrodynamic and gravitational effects are not included in the analysis. By steady state, it is implied that all the energy

arriving at the droplet surface is carried away entirely by the mass transfer, while the liquid temperature remains at a constant value determined by the ambient conditions until the vaporization process is completed.

The model is first developed in general form for a binary system and then application is made to the vaporization of heptane and dodecadene droplets in air.

In the analysis that follows subscripts A and B refer respectively to the chemical species of the liquid droplet and inert gaseous environment.

Theoretical Model

A mass balance taken on a differential shell about a spherically symmetrical model of a quiescent droplet undergoing quasi-steady vaporization leads to the following differential equation

$$\frac{d}{dr}\left(r^2 N_A\right) = 0 \quad , \quad r > r_o \qquad [1.1]$$

where N_A is the molar flux of component A with respect to stationary coordinates, r is the radial distance measured from the droplet center, and r_o is the droplet radius. Equation [1.1] indicates that for the case of unidirectional diffusion, i.e., stagnant environment, the molar flow rate of species A, $w = 4\pi r^2 N_A$, is constant with respect to the

radial distance.

Similarly, an energy balance on a spherical shell surrounding a droplet leads to the differential equation

$$\frac{d}{dr}(r^2 N_A H_A) = \frac{d}{dr}\left(r^2 k \frac{dT}{dr}\right) \quad , \quad r > r_o \qquad [1.2]$$

where H_A is the molar enthalpy of component A in the vapor film and k is the thermal conductivity of the gaseous mixture. This relation equates the energy transferred by the mass motion of component A to that transferred by heat conduction. Viscous dissipation, emission and absorption of radiant energy, and the Dufour energy flux, i.e., energy flux due to concentration gradients, are assumed to be physically negligible. Furthermore, it is assumed that the total pressure of the system is constant.

Ideal gas behavior has been assumed in the formulation of the energy equation, for in ideal gas mixtures there is a complete indifference of each component to the presence of others, and thus the molar enthalpy of component A depends only upon temperature. Therefore, by the chain rule

$$\frac{dH_A}{dr} = \frac{dH_A}{dT}\frac{dT}{dr} = c_{pA}\frac{dT}{dr} \qquad [1.3]$$

where $c_{pA} = c_{pA}(T)$ is the molar specific heat at constant pressure of component A in the ideal gas state.

Using the above expressions and assuming constant thermal conductivity the equation of energy becomes

$$\frac{d^2T}{dr^2} + \left(\frac{2}{r} - \frac{w\, c_{pA}}{4\pi r^2 k}\right)\frac{dT}{dr} = 0 \qquad [1.4]$$

Under steady state conditions, all the energy transferred to the droplet surface by heat conduction is carried away entirely by the mass transfer. Hence it follows that

$$4\pi r^2 k \frac{dT}{dr} = \lambda w \qquad \text{at} \quad r = r_o \qquad [1.5]$$

where $\lambda = \lambda(T)$ is the latent heat of vaporization of pure liquid A. Equation [1.5] establishes that the energy required to evaporate the liquid is not affected by the presence of component B.

Since the ambient temperature is specified

$$T = T_\infty \qquad \text{at} \quad r = \infty \qquad [1.6]$$

The equation of energy, [1.4], and its boundary conditions, [1.5] and [1.6], can be readily integrated for the case of constant properties in terms of the still undetermined rate of vaporization. After carrying out the required integration, the following expression for the temperature profile in the gaseous mixture surrounding the droplet is obtained

$$T = T_\infty - \frac{\lambda}{c_{pA}} \exp\left(\frac{w\, c_{pA}}{4\pi k r_o}\right)\left[1 - \exp\left(-\frac{w\, c_{pA}}{4\pi k r}\right)\right] \qquad [1.7]$$

The steady state liquid temperature is now obtained from the above expression replacing the radial distance, r, by the droplet radius, r_o. Thus, the steady state droplet temperature is:

$$T_{ss} = T_\infty - \frac{\lambda}{c_{pA}} \left[\exp\left(\frac{w\, c_{pA}}{4\pi k r_o} \right) - 1 \right] \qquad [1.8]$$

Since the temperature profile as well as the steady state temperature expressions are given in terms of the molar flow rate, it is necessary to determine it from the equation of continuity in terms of thermophysical properties.

The molar flux of species A with respect to stationary coordinates is given by Fick's first law for ordinary diffusion in the form[2]

$$N_A = x_A(N_A + N_B) \quad -cD_{AB} \frac{dx_A}{dr} \qquad [1.9]$$

where x_A is the mole fraction of component A, c is the molar density of the mixture, and D_{AB} is the binary diffusivity. The above relationship is the defining equation for D_{AB}. The transport of mass due to temperature gradients (the Soret effect) is assumed to be physically negligible in Equation [1.9], which states that the molar flux of A results from the bulk motion of the mixture and the diffusion superimposed to the bulk flow.

Under the assumption of unidirectional diffusion, i.e.,

$N_B = 0$, Equation [1.9] simplifies to

$$N_A = - \frac{c\, D_{AB}}{1 - x_A} \frac{dx_A}{dr} \qquad [1.10]$$

For ideal gases the molar density of the mixture is determined by the equation of state $c = P/RT$. Furthermore, by Dalton's law, the mole fraction of component A in the mixture is equal to its partial pressure divided by the total pressure of the system, $x_A = p_A/P$. Therefore, introducing these simplifications the equation of continuity, [1.1], becomes

$$\frac{d}{dr}\left(- \frac{r^2 P D_{AB}}{RT(P - p_A)}\right)\frac{dp_A}{dr} = 0 \qquad [1.11]$$

with the boundary conditions of

$$p_A = p_v \quad \text{at} \quad r = r_o \qquad [1.12]$$

and

$$p_A = 0 \quad \text{at} \quad r = \infty \qquad [1.13]$$

where $p_v = p_v(T)$ is the vapor pressure of pure liquid A in thermodynamic equilibrium with its vapor at a given temperature. Equation [1.12] assumes that the vapor pressure of the pure liquid is not affected by the presence of component B in the gaseous mixture surrounding the droplet.

Assuming that the binary diffusivity is also constant, the above equation of continuity and its boundary conditions can be readily integrated to determine the rate of vaporization

as well as the partial pressure profile of component A in the film. Carrying out the necessary integration, the following expressions for the steady state molar flow rate and partial pressure profile, respectively, are obtained:

$$w = \frac{4\pi r_o}{T_{ss} c_{pA} - \lambda} \left[\frac{P D_{AB} c_{pA}}{R} \ln \frac{P}{P - p_v} - k(T_\infty - T_{ss}) \right] \quad [1.14]$$

and

$$\frac{p_A}{P} = 1 - \exp\left[C_1 \left(\exp \frac{-w c_{pA}}{4\pi k r} - 1 \right) - \frac{C_2}{r} \right] \quad [1.15]$$

where

$$C_1 = \frac{kR\,\lambda}{P D_{AB} c_{pA}^2} \exp \frac{w c_{pA}}{4\pi k r_o} \quad [1.16]$$

$$C_2 = \frac{wR}{4\pi P D_{AB}} \left(T_{ss} - \frac{\lambda}{c_{pA}} \right) \quad [1.17]$$

Hence, for some given ambient conditions and droplet size, Equations [1.8] and [1.14] simultaneously determine the steady state droplet temperature and its corresponding rate of vaporization. Under steady state conditions the molar flow rate is directly proportional to the droplet radius, whereas the liquid temperature depends only upon the properties and ambient conditions.

It is of interest to estimate the vaporization time spent by a droplet under steady state conditions after the governing equations have been solved. Since the liquid temperature is

constant, from Equation [1.8]

$$\frac{w\, c_{pA}}{4\pi k r_o} = \text{constant} = C_3 \qquad [1.18]$$

This may be verified since the properties are assumed to be constant and the vaporization rate is proportional to the droplet radius. Using a mass balance

$$w = -4\pi r_o^2 c_A^{\ell} \frac{dr_o}{dt} \qquad [1.19]$$

where c_A^{ℓ} is the molar density of the liquid. Thus, combining the above two relations and integrating the resulting differential equation, the vaporization time spent under steady state conditions is

$$t_v = \frac{1}{K_v} (2r_o)^2 \qquad [1.20]$$

where the vaporization rate constant, K_v, is defined by

$$K_v = \frac{2w}{\pi r_o c_A^{\ell}} = \frac{8C_3\, k}{c_{pA} c_A^{\ell}} \qquad [1.21]$$

Equation [1.20] indicates that the vaporization time, t_v, is directly proportional to the square of the droplet diameter.

Applications

Some steady state calculations were performed using

heptane and dodecadene droplets vaporizing in air under atmospheric pressure conditions for various values of air temperature in the range 440-830°K. Property correlations were obtained from References 3 and 21. The specific heat at constant pressure of the fuel vapor, and the binary diffusivity were evaluated at the arithmetic average temperature in the mixture. The thermal conductivity of the air-vapor film was evaluated at the arithmetic average temperature in the mixture and for an air-vapor mixture equal to one-half the concentration at the droplet surface.

Figures 1.1 and 1.2 show typical temperature and partial pressure profiles in the film surrounding an arbitrary 813-micron-radius heptane droplet vaporizing in air at 444 and 555°K.

The steady state results were found to agree with the calculated and/or experimental results of Reference 21 which uses a low pressure semi-empirical vaporization model[10].

In order to determine the effect of property variations in the air-vapor film, variable properties were introduced in the equations of change. The numerical solution of the governing equations indicated that the effect is negligibly small at atmospheric pressure for the temperature range investigated.

Summary of Results and Assumptions

Summarizing the above analysis, the following conclusions are drawn:

i. The rate of vaporization is directly proportional to the droplet radius.

ii. The steady state liquid temperature does not depend upon the droplet size.

iii. The vaporization time spent under steady state conditions is proportional to the square of the droplet diameter.

iv. For the ambient temperature range investigated, the constant mean properties assumption is a valid one under atmospheric pressure conditions.

A list of the assumptions that were introduced in the analysis is given below:

i. Spherical symmetry. This means that gravitational and hydrodynamic effects are not considered.

ii. Steady state. The heat transfer to the droplet is carried away by the mass transfer. Under these conditions the droplet remains at constant temperature until complete vaporization takes place.

iii. The inert gas surrounding the droplet is stationary, i.e., unidirectional diffusion, with the liquid surface movement effect on diffusion neglected.

iv. Low pressure environmental conditions. Therefore, the vapor film surrounding the droplet obeys the equation of state of ideal gases.

v. The total pressure in the system is constant.

vi. There exists thermodynamic equilibrium at the droplet interface, and the pure liquid vapor pressure as well as the energy required to evaporate it are not affected by the presence of the inert environment.

vii. Viscous dissipation, radiant energy exchange, and coupled effects associated with transport processes, such as the Dufour and Soret effects, are assumed to be physically negligible.

viii. The specific heat of the diffusing vapor, c_{pA}, the binary diffusivity, D_{AB}, and the thermal conductivity, k, are constant.

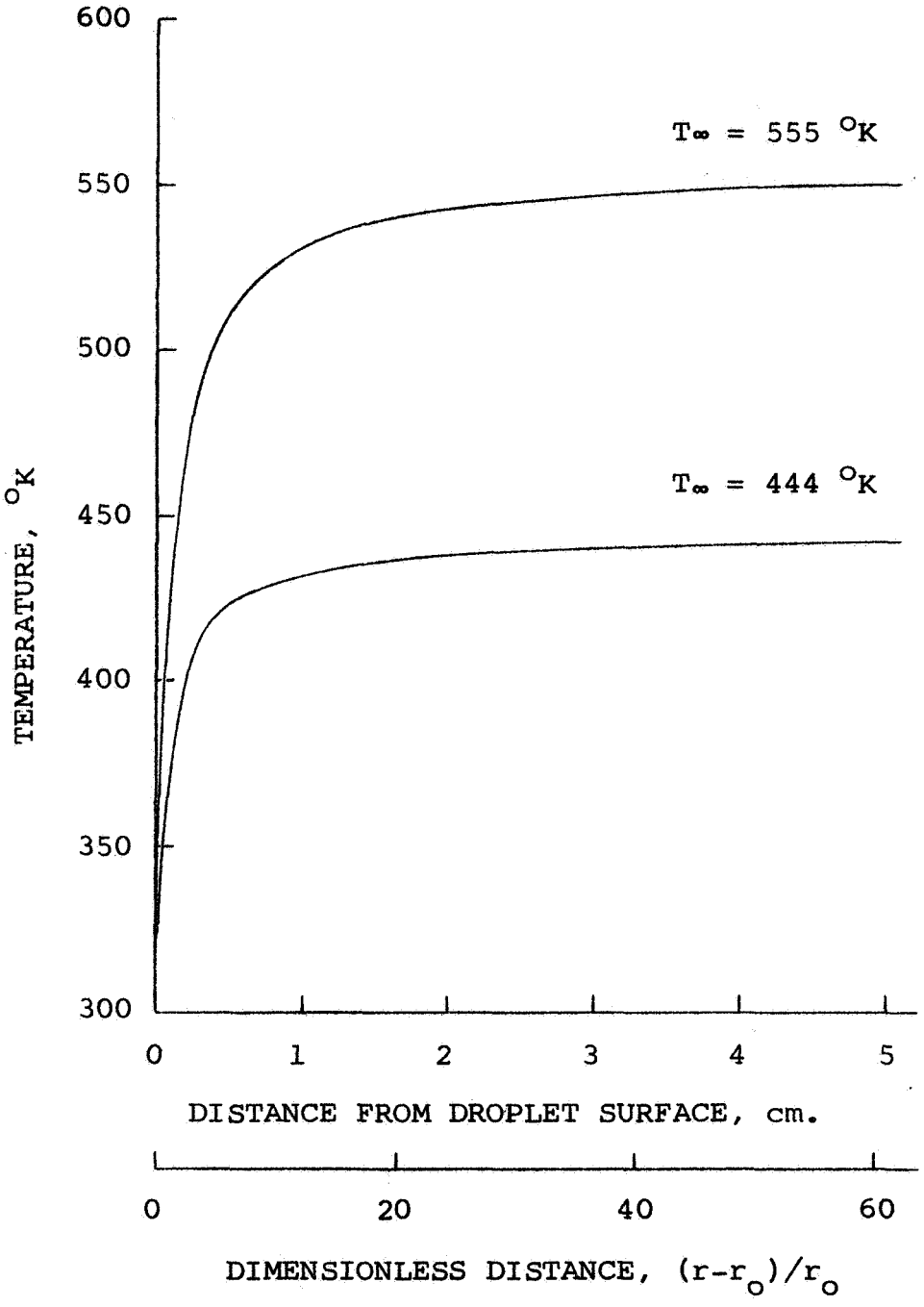

Figure 1.1. Temperature profiles in the film surrounding a n-heptane droplet vaporizing in air. Total pressure = 1 atm.

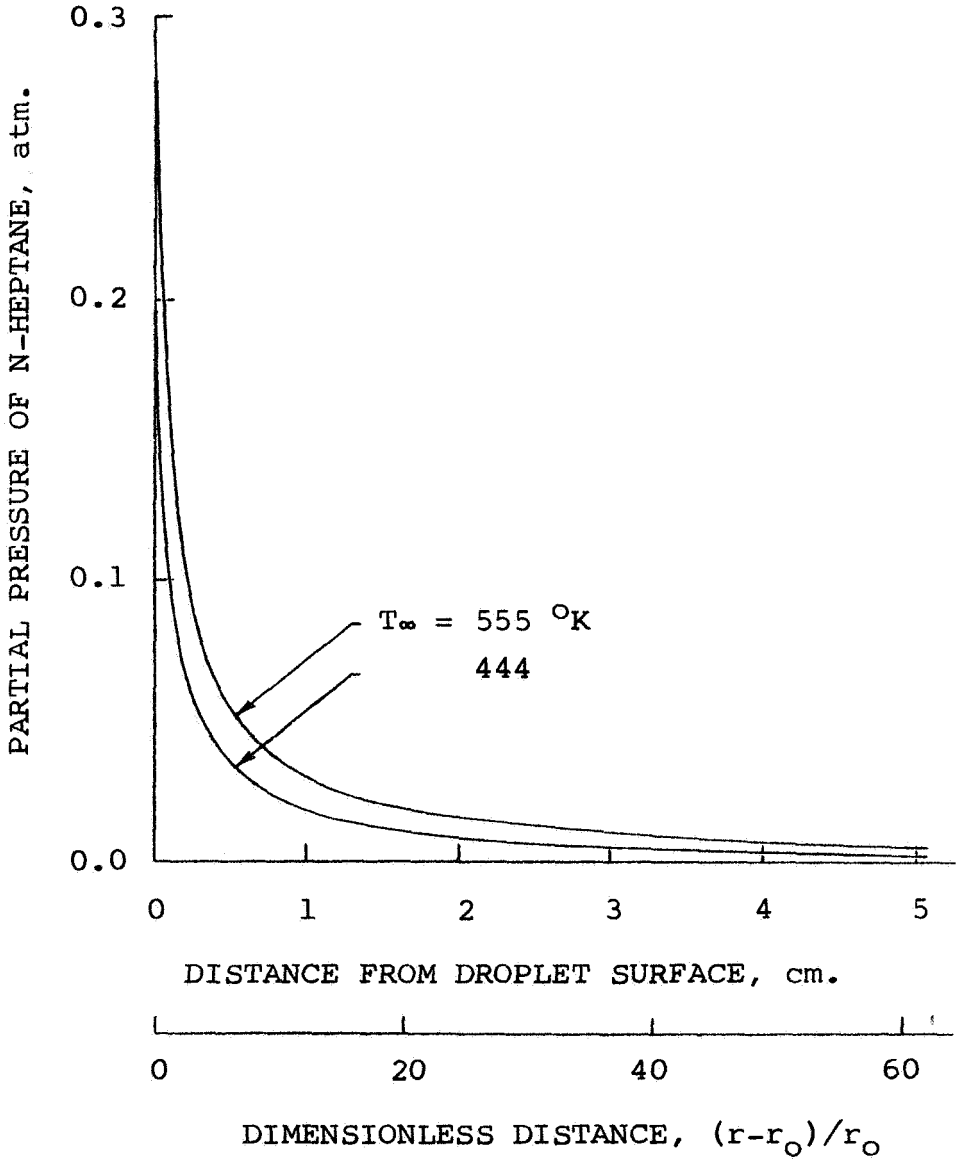

Figure 1.2. Partial pressure profiles in the film surrounding a n-heptane droplet vaporizing in air. Total pressure = 1 atm.

II. STEADY STATE VAPORIZATION AT HIGH AMBIENT PRESSURES

The underlying assumptions in the previous vaporization analysis are that ideal gas behavior is obeyed in the gaseous mixture surrounding a vaporizing droplet, constant thermophysical properties, and the indifference of the liquid phase to the presence of the inert environment. Certainly none of these assumptions are valid under high levels of total pressure as those encountered in the critical region.

Therefore, the purpose of this section is to include in a quasi-steady analysis the effects of non-ideal mixtures, variation of the physical properties through the boundary layer, the effect of total pressure on the vapor pressure and the enthalpy of vaporization.

This analysis is further complicated by uncertainties in the determination of thermodynamic and transport properties of binary mixtures under high pressure.

As in the previous study, only steady state conditions are considered to simplify the analysis and concentrate on the non-ideal effects. The basic relationships are first derived for a binary system. These relationships are then applied to a liquid carbon dioxide droplet undergoing steady state vaporization in a nitrogen atmosphere. This selection of components was made because both are non-polar and of

relatively simple molecular structure.

Thermodynamic equilibrium is assumed at the liquid-vapor interface when calculating the thermophysical properties there. The entire liquid droplet is assumed to be at a uniform temperature and absorption of nitrogen into the liquid phase is assumed to be confined to a very thin layer at the droplet surface. Since vaporization rates may be large enough that thermodynamic equilibrium at the droplet interface may not be attained, this topic is briefly discussed as well as the difficulties encountered.

Only unidirectional ordinary diffusion is taken into account and thus the regression of the droplet surface is neglected. Viscous dissipation, radiant energy exchange, and the transport of energy due to concentration gradients (the Dufour effect) are assumed to be physically negligible.

In the analysis that follows, subscripts A and B refer respectively to the chemical species of the diffusing vapor and inert environment.

Theoretical Model

Governing Equations

A mass balance on a spherically symmetrical shell surrounding a droplet undergoing quasi-steady vaporization leads to the differential equation

$$\frac{d}{dr}(r^2 N_A) = 0 \quad , \quad r>r_o \qquad [2.1]$$

where N_A is the molar flux of component A with respect to stationary coordinates. Equation [2.1] assumes unidirectional diffusion. As it will become apparent, this assumption is most valid for low density systems. The error introduced under high pressure conditions may be estimated by calculating the ratio of molar fluxes N_B/N_A at the droplet surface. The actual molar flux of component B may be approximated by $N_B = cx_B(dr_o/dt)$. Furthermore, by continuity, the molar flux of the diffusing vapor is $N_A = -c_A^{\ell}(dr_o/dt)$. Hence, it follows that

$$\left|\frac{N_B}{N_A}\right| = (1 - x_A)\,\frac{c}{c_A^{\ell}} \quad , \quad r = r_o \qquad [2.2]$$

For a given value of total pressure in the system, as the droplet temperature increases the density ratio, c/c_A^{ℓ}, increases but the concentration of component B, $(1-x_A)$, decreases. In the range of environmental conditions studied here, the flux ratio varies from 5 to 17 percent.

It should be noted that an accurate description of the absorption of component B into liquid A requires a knowledge of diffusion in the liquid phase. In the absence of such data only limiting cases are considered.

An energy balance on a spherically symmetric shell surrounding a droplet leads to

$$\frac{d}{dr}(r^2 N_A \bar{H}_A) = \frac{d}{dr}\left(r^2 k \frac{dT}{dr}\right) \quad , \quad r>r_o \qquad [2.3]$$

where $\overline{H}_A$, the partial molal enthalpy of component A in the vapor film, and k, the thermal conductivity of the mixture, are in general functions of temperature, pressure, and composition. Of course for low values of total pressure in the system the above equation of energy reduces to[1.2].

Since the total pressure is essentially constant, by the chain rule

$$\frac{d\overline{H}_A}{dr} = \frac{\partial \overline{H}_A}{\partial x_A} \frac{dx_A}{dr} + \overline{c}_{pA} \frac{dT}{dr} \qquad [2.4]$$

and

$$\frac{dk}{dr} = \frac{\partial k}{\partial x_A} \frac{dx_A}{dr} + \frac{\partial k}{\partial T} \frac{dT}{dr} \qquad [2.5]$$

where the stoichiometric relation $x_A + x_B = 1$ must be satisfied.

The molar flux of component A in the gas phase is determined by Fick's first law for ordinary diffusion. Although there are many equivalent forms of Fick's first law for binary systems, the form used in this work,[1.9],does not have limitations[16]. Therefore, assuming that the molar flux of component B is relatively small compared to the one of A,

$$N_A = - \frac{cD_{AB}}{1 - x_A} \frac{dx_A}{dr} \qquad [2.6]$$

Introducing the above expressions the governing equations

of change become

$$\frac{d^2T}{dr^2} + \left(\frac{2}{r} + \frac{1}{k}\frac{\partial k}{\partial T}\frac{dT}{dr} + \frac{1}{k}\frac{\partial k}{\partial x_A}\frac{dx_A}{dr} - \frac{w}{4\pi r^2 k}\bar{c}_{pA}\right)\frac{dT}{dr}$$

$$- \frac{w}{4\pi r^2 k}\frac{\partial \bar{H}_A}{\partial x_A}\frac{dx_A}{dr} = 0 \qquad [2.7]$$

and

$$\frac{d}{dr}\left(-\frac{r^2 c D_{AB}}{1 - x_A}\frac{dx_A}{dr}\right) = 0 \qquad [2.8]$$

or integrating Equation [2.8]

$$w = 4\pi r^2 N_A = -\frac{4\pi r^2 c D_{AB}}{1 - x_A}\frac{dx_A}{dr} \qquad [2.9]$$

Boundary Conditions

To determine the boundary conditions, it is required that

$$x_A = 0 \quad \text{at} \quad r = \infty \qquad [2.10]$$

Furthermore, the temperature of the environment is specified as

$$T = T_\infty \quad \text{at} \quad r = \infty \qquad [2.11]$$

The boundary conditions at the droplet surface require special consideration. Assuming small departures from equilibrium at the interface, the concentration of species A in the gas phase, expressed as mole fraction, may be represented by the vapor-liquid equilibrium relationship:

$$x_A = x_A\,(T,P) \quad \text{at} \quad r = r_o \qquad [2.12]$$

Under steady state conditions, all the energy transferred to the droplet surface by heat conduction is carried away entirely by the mass transfer. Hence, it follows that:

$$4\pi r^2 k \frac{dT}{dr} = w(\overline{H}_A^v - \overline{H}_A^\ell) \quad \text{at} \quad r = r_o \qquad [2.13]$$

Before proceeding to the evaluation of both boundary conditions [2.12] and [2.13], let us analyze some simplifying assumptions. One commonly used approximation for Equation [2.12] is to express the mole fraction of component A in the gas phase, at the interface, as the vapor pressure of pure liquid A at the equilibrium temperature divided by the total pressure, i.e.,

$$x_A = p_v(T)/P \quad \text{at} \quad r = r_o \qquad [2.14]$$

This relationship, analogous to Equation [1.12], assumes that B is insoluble in A, that the equilibrium vapor pressure of pure liquid A is not affected by the presence of component B, and that the gaseous mixture obeys the equation of state for ideal gases. It will be shown that this approximation is far from being correct at the pressure levels encountered in the critical region. Another approximation commonly used, and made in Equation [1.5], is to replace the term $(\overline{H}_A^v - \overline{H}_A^\ell)$ in Equation [2.13] by the latent heat of vaporization of pure component A, evaluated at the equilibrium temperature. This is an over-simplification at high total pressures. The term $(\overline{H}_A^v - \overline{H}_A^\ell)$ is the amount of heat absorbed per mole when component

A evaporates from the liquid solution into the gaseous mixture, at T and P, whereas λ is the heat required to evaporate a pure substance from liquid into its vapor, at T and $p_v(T)$.

The trends predicted by the use of these simplified boundary conditions, although perfectly valid at low pressures, fail to be correct at high pressures.

Now, in order to determine the thermodynamic equilibrium conditions at the droplet interface, besides the temperature and pressure being equal in both phases, the fugacity (or chemical potential) of every component must be the same in both phases, i.e.,

$$\left.\begin{aligned} T &= \text{constant} \\ P &= \text{constant} \\ f_A^v &= f_A^\ell \\ f_B^v &= f_B^\ell \end{aligned}\right\} \quad [2.15]$$

Equation of State

To solve the governing equations of change and their boundary conditions a suitable equation of state has to be used. Choosing among available equations, the simple Redlich-Kwong equation of state was selected, for it has proved to be reliable[33] and is regarded as the best two-parameter equation now available[5]. It is of the form[22]

$$P = \frac{RT}{v-b} - \frac{a}{T^{0.5}v(v+b)} \quad [2.16]$$

where a and b may be taken as functions of composition and depend upon the particular components involved.

Boundary conditions [2.12] and [2.13] are computed basically from Equations [2.15] and [2.16]. The detailed working forms of the equations are presented in Appendix A.

Thermophysical Properties

The numerical integration of the equations of change requires knowledge of the partial molal enthalpy of component A, $\overline{H}_A$, the thermal conductivity of the mixture, k, as well as the coefficient of binary diffusion, D_{AB}, or the product cD_{AB}. Very few experimental data to be correlated are available on these properties for high pressure gaseous mixtures. The correlations used in this work are presented in Appendix A with some of their limitations.

Numerical Method of Solution

The numerical integration of the equations of change throughout the vapor film was carried out by using a recursive formula of the third category due to Heun[8]. It is of the form:

$$\frac{dY}{dr} = F(Y,r) \quad ; \quad Y(r_0) = Y_0 \qquad [2.17]$$

$$Y_{n+1} = Y_n + s\left[\frac{1}{4}F(Y_n,r_n) + \frac{3}{4}F\left(Y_{n+2/3},r_{n+2/3}\right)\right] \qquad [2.18]$$

$$Y_{n+2/3} = Y_n + \frac{2}{3}sF(Y_{n+1/3},r_{n+1/3}) \qquad [2.19]$$

$$Y_{n+1/3} = Y_n + \frac{1}{3}sF(Y_n, r_n) \qquad [2.20]$$

$$s = r_{n+1} - r_n \quad ; \; n = 0,1,2,\ldots \qquad [2.21]$$

The method is self-starting and there is no difficulty in altering the increment size, s, during the integration. The partial derivatives which appear in Equation [2.7] were determined by a centered difference technique.

Setting the total pressure, the integration process was initiated at the droplet surface by fixing its temperature. The vaporization rate, w, was iterated until the mole fraction of component A vanished at a large distance from the droplet. The proper ambient temperature results. Since the environmental conditions are approached asymptotically, the numerical integration in the vapor film was carried out to a certain radial distance, r^*, where the temperature profile did not change appreciably. At this point the equations of change were modified by assuming constant k, $\bar{c}_{pA}$, and cD_{AB}, and neglecting the last term in Equation [2.7] which is very small for $r \geq r^*$. These simplifications lead to the following asymptotic solutions where $\tilde{x}_A$ and $\tilde{T}$ are used to indicate that they hold only for $r \geq r^*$,

$$\tilde{x}_A(r) = 1 - \exp\left(\frac{-w}{4\pi cD_{AB}r}\right) \qquad [2.22]$$

and

$$T_\infty = \tilde{T}(r) - \frac{4\pi r^2 k}{w\bar{c}_{pA}} \frac{d\tilde{T}}{dr}\left[\exp\frac{w\bar{c}_{pA}}{4\pi rk} - 1\right]\Bigg|_{r = r^*} \qquad [2.23]$$

When the numerical and asymptotic solutions are matched at $r = r^*$, the iterated rate of vaporization, w_i, is equal to the steady state vaporization rate, w, and the temperature of the ambient gas results from Equation [2.23], satisfying all boundary conditions.

In order to obtain the solution of the equations of change and their boundary conditions, the rate of vaporization was iterated three or four times. When the mismatch index, $(x_A - \tilde{x}_A)\ (r^*)$, was a positive number, the rate of vaporization was increased. The iterative process was facilitated since, for values of w_i close to the steady state vaporization rate, w, the mismatch index mentioned above varies linearly with w_i.

Since temperature and composition gradients are very large near the droplet surface, the radial increment size in the numerical technique was varied from $0.025r_o$ near the surface to $0.1r_o$ near the edge of the boundary layer. The entire steady state solution takes approximately 15 seconds using a UNIVAC 1108 digital computer.

Applications to a CO_2-N_2 System

The components studied in the critical region were carbon dioxide (component A) vaporizing in a nitrogen (component B) atmosphere. The critical temperature of pure CO_2 is 304.2 ^oK and its critical pressure 72.9 atm.[23] This

selection of components was made because both are nonpolar and of relatively simple molecular structure.

First let us consider the boundary conditions. Figure 2.1 is a calculated fugacity-composition diagram for the CO_2-N_2 system under reduced conditions of $T/T_{cA} = 0.9$ and $P/P_{cA} = 1.3$. The upper portion of the figure depicts the variation of nitrogen fugacity with composition whereas the lower portion represents the variation of carbon dioxide fugacity. The broken lines determine the CO_2 composition in both liquid and gas phases for these isothermal and isobaric conditions as specified by the set of equations[2.15]. Repetitive application of the above technique yields Figure 2.2 which shows a composition-pressure diagram for reduced equilibrium isotherms of 0.90 and 0.95. Reduced conditions are based on the critical pressure and temperature of pure CO_2. For a given isotherm, the lower side of the solid curve shows the composition of carbon dioxide in the gas phase which is in equilibrium with a corresponding liquid phase composition represented by the upper side of the curve for different values of total pressure. On the lower pressure side the mole fraction of carbon dioxide in both phases is equal to unity when the total pressure of the system is equal to the vapor pressure corresponding to that isotherm. Above a certain pressure the mole fraction of carbon dioxide in the gas phase increases rather than decreases, with the result that at still higher pressures liquid and gas compositions become

equal at the critical mixing point. Accordingly, for a given isotherm, there exists a definite upper limit on the total pressure of the system above which steady state conditions cannot be attained. Therefore, states outside the envelope enclosed by points C, D, E, ... are intrinsically unsteady. Point C corresponds to the critical point of pure carbon dioxide. It is observed that the range of total pressures in order to achieve steady state temperatures becomes wider as the droplet temperature (which depends also on the ambient temperature) decreases in the region of the thermodynamic critical point of carbon dioxide.

The broken lines represent the ideal vapor phase compositions predicted by Equation [2.14]. It is apparent that this relationship does not hold at high levels of total pressure.

The behavior illustrated in Figure 2.2, which applies only at the droplet interface, may be understood qualitatively for the partial molal volume of carbon dioxide reverses its sign at high pressures. Unlike the molar volume of a pure substance, the partial molal volume of a component may be either postive or negative. Since the partial molal volume of a component represents the volume change which is experienced by the entire mixture when a very small amount of that component is added at constant temperature and pressure, the gaseous mixture tends to shift its properties from a gaseous to a liquid state.

Considering the approximations involved and that only very few pure component data are required, the agreement with experimental data of Reference 34 is found satisfactory. Near the critical mixing point the equilibrium results are extremely sensitive to small errors in the quantities involved and as a consequence, it was found that the critical points C, D, E, ..., are somewhat scattered. Observing Figure 2.1, it is noted that, as a critical mixing point is approached, the fugacity curves form an inflection point, and hence small errors in the fugacity calculations cause relatively larger errors in the composition results. In retrospect, it may have been preferable to determine, simultaneously with the equilibrium calculations, the critical points envelope by some other technique, such as the one outlined in Reference 6, in order to smooth the computed data.

Figure 2.3 shows the isothermal difference in the partial molal enthalpies of carbon dioxide across the droplet interface, $(\overline{H}_A^V - \overline{H}_A^\ell)$, as compared to its latent heat of vaporization, λ, for the same equilibrium isotherms.

At points C, D, and E of Figure 2.3, the difference in the partial molal enthalpy of carbon dioxide across the interface becomes equal to zero since the temperature, pressure, and composition are identical in both phases. The broken lines represent the latent heat of vaporization of carbon dioxide evaluated at $T/T_{cA} = 0.90, 0.95$ by means of the generalized enthalpy deviation charts of Lydersen, Greenkorn,

and Hougen[14]. Thus, even at a subcritical temperature of carbon dioxide, the difference in enthalpy across the interface may vanish.

Figure 2.4 shows a typical pressure-volume diagram for the carbon dioxide-nitrogen system under thermodynamic equilibrium conditions. This diagram compares favorably well with the experimental results of Reference 18.

Figure 2.5 illustrates graphically the departures from the equation of state of ideal gases in the gas phase at the droplet interface as a function of pressure for the isotherm $T/T_{cA} = 0.90$.

Thus far complete thermodynamic equilibrium at the interface has been assumed. Considering that the rates of vaporization may be large enough that thermodynamic equilibrium at the interface may not be attained, let us analyze the boundary conditions and their results by assuming that nitrogen is insoluble in liquid carbon dioxide. In other words, let us postulate that very few of the nitrogen molecules in the gas phase that strike the interface have sufficient time to penetrate and become dissolved in the liquid phase.

For this situation, the computed values of carbon dioxide mole fraction in the gas mixture are generally higher than those obtained under thermodynamic equilibrium conditions. Furthermore, for a given isotherm, the mole fraction of CO_2 in the gas phase starts increasing at a certain value of total

pressure lower than in the corresponding equilibrium case (approximately 80 atmospheres for the 0.90 reduced isotherm). One difficulty is encountered with this hypothesis: since the critical points, where the temperature, pressure, and composition are the same in both phases, cannot exist as a consequence of the postulate, there is no clear transition from two to one phase states. Although the difference in enthalpies, $\overline{H}_A^v - H_A^\ell$, across the interface does not vanish at any isotherm different from the critical of carbon dioxide due to the above difficulty, it does follow the same trends as those predicted under thermodynamic equilibrium conditions.

Approximate calculations show that the partial molal enthalpy of CO_2 in the liquid solution is nearly the same as the one for pure liquid CO_2, at the same temperature and pressure. Thus, there is a negligibly small temperature difference between the core of the droplet and its interface.

Figures 2.6 and 2.7 show typical temperature and composition profiles in the mixture surrounding an arbitrary 1000-μ-radius droplet. Both temperature and composition variations in the mixture are confined to a region of the order of several droplet diameters. At a given value of total pressure, the boundary layer increases with increasing ambient temperature and, at a fixed droplet temperature decreases with increasing total pressure.

Property variations in the film surrounding a droplet are shown in Figure 2.8. For the conditions illustrated in

this figure, the mixture compressibility factor changes from a value of about 0.68 to unity in a small radial distance of the order of one droplet radius from the surface.

Figures 2.9 and 2.10 show that the higher the ambient temperature, the higher the rate of vaporization and the higher the steady state temperature, under fixed pressure conditions. As carbon dioxide approaches its critical point, essentially no nitrogen surrounds the droplet and hence a large temperature difference between the ambient and droplet must exist so that heat may be conducted to the droplet surface. These figures also show that, for the same ambient conditions, there is a small difference between the computed steady state temperatures and mass vaporization rates by using in the model either one of the two assumptions at the interface previously discussed, i.e., thermodynamic equilibrium and no nitrogen solubility in liquid carbon dioxide. However, it should be pointed out that for values of total pressure higher than the critical pressure of CO_2, the difference between the computed steady state results is greater; e.g., at ambient conditions of approximately 84 atm. and 1290^{o}K the rates of vaporization differ by about 24 percent and the steady state temperatures by seven percent. Since the equilibrium postulate is thermodynamically consistent, the results reported hereafter use this assumption.

Cross plots of steady state temperatures and vaporization rates are shown in Figures 2.11 and 2.12. These curves are

terminated on the right at the critical mixing line since points at higher pressures do not correspond to steady state solutions and can only be reached by an unsteady process. For a given liquid temperature the vaporization rate and nitrogen temperature decrease rapidly with increased pressure. The vaporization rate tends to level off and increases slightly as the critical mixing line is approached. For a given nitrogen temperature the steady state temperature and vaporization rate increase as the pressure of the system is increased. The higher the pressure, the higher the rate of increase of the steady state temperature with ambient temperature. Schematically, Figure 2.13 indicates that for all those environmental conditions to the left of the line defined by points C, D, E, ..., whose absissae are determined by the critical mixing pressures (point C is fixed by the critical pressure of CO_2), the liquid droplet heats up from its injection temperature to its steady state temperature remaining at this condition until the vaporization process is completed. Of course the droplet may not attain its steady state temperature if the injection conditions are such that the vaporization process is terminated before steady state conditions are reached. On the other hand, for all the ambient conditions to the right of the mentioned line, the droplet continuously heats up from its injection conditions until the vaporization process is completed.

Near the critical mixing line, where the change of enthalpy at the droplet interface is small, slight inaccuracies in the determination of the critical mixing pressure cause larger inaccuracies in the enthalpy of vaporization and consequently, the steady state results may be affected. To analyze the overall sensitivity of the model to this type of inaccuracy, a change of approximately five percent was made in the critical mixing pressure of the 0.96 carbon dioxide critical isotherm. This caused a difference in the enthalpy of vaporization of the order of 30 percent at 102 atmospheres. However, under nitrogen conditions of 850°K and 102 atmospheres the calculated steady state results are virtually the same.

Vaporization times may be readily estimated from the foregoing results. Using the equation of continuity for the diffusing vapor leaving the droplet, $w = - 4\pi r_o^2 c_A^{\ell} (dr_o/dt)$, and noting that the rate of vaporization is proportional to the droplet radius, from the numerical results, the following expression for the vaporization time spent under steady state conditions is obtained:

$$t_v = \frac{1}{K_v} (2r_o)^2 \qquad [2.24]$$

where the vaporization rate constant, K_v, is given by

$$K_v = \frac{2w}{\pi r_o c_A^{\ell}} \qquad [2.25]$$

The above two expressions are completely analogous to Equations [1.20]and [1.21]. For some given environmental

conditions, the vaporization rate constant K_v may be obtained from Figure 2.12 and the pure CO_2 molar density from Reference 14.

Comparisons with a Low Pressure Model

It is of interest to compare the foregoing computed CO_2-N_2 results with those predicted by Equations [1.8] and [1.14] under the same ambient conditions. For convenience, the presented above steady state formulation under high pressure conditions is referred here as the high pressure QS model, whereas the simplified formulation which yielded Equations [1.8] and [1.14] is referred as the low pressure model. In the comparisons which follow, average low pressure values for the physical properties in the vapor film were used in Equations [1.8] and [1.14].

Figure 2.14 shows the steady state conditions predicted by both models as a function of total pressure and a nitrogen temperature of 600°K. Other steady state results under a system pressure of 72.9 atmospheres (critical pressure of carbon dioxide) are presented in Figure 2.15.

The following conclusions may be drawn from the calculations:

1. The low pressure model may predict more than one or no analytical solution at high pressure levels as is illustrated in Figure 2.14. Although the broken line solutions may

arbitrarily be considered unrealistic, the results are beclouded by the fact that the solution is not unique.

ii. At low ambient temperatures and high system pressures, the rates of vaporization predicted by the low pressure model are lower than those given by the high pressure QS model, e.g., at 475°K and 115 atmospheres the low pressure model vaporization rate is about 35 percent lower than the high pressure QS model vaporization rate.

iii. At high ambient temperatures and a system pressure equal to the critical pressure of CO_2, the rates of vaporization given by the low pressure model are higher than those predicted by the high pressure QS model, e.g., at 1600°K and 72.9 atmospheres the low pressure model rate of vaporization is about 22 percent higher than the high pressure QS model mass vaporization rate.

The steady state temperatures predicted by the low pressure model are in general higher than those obtained with the high pressure QS model, under the same environmental conditions. As a consequence, the low pressure model adjusts itself to the increase in the total pressure of the

system by decreasing the latent heat of vaporization and increasing the vapor pressure at the interface, along the pure CO_2 saturation curve, thus reducing in part the large property discrepancies between these models; e.g., at 600°K and 72.9 atmospheres, the increase in the steady state temperature reduces the difference in the heats of vaporization of these models from about 56 percent to 50 percent and the CO_2 mole fractions at the interface from approximately 32 percent to 23 percent.

Although the results given by the models are not completely different under the same ambient conditions, it nevertheless may be considered fortuitous that the low pressure model estimates the steady state conditions without larger discrepancies, for the low pressure model is unrealistic in itself at high levels of total pressure.

Concluding Remarks

Summarizing the present analysis, the following remarks are made:

i. It is evident from the foregoing study that for a given value of ambient temperature there is an upper limit in the total pressure of the system above which steady state conditions cannot be obtained in the vaporization process. This implies that for pressures above this limit the droplet

continuously heats up from its injection conditions until complete disappearance. This remark seems to be supported by liquid temperature measurements[9] which indicate that at high pressures the temperature rises continuously throughout the droplet lifetime. Therefore, supercritical temperatures may only be reached at supercritical pressures by an unsteady process.

ii. Non-ideal effects cannot be ignored. The effect of the inert gas pressure on the vapor pressure is appreciable at high levels of total pressure and the heat of vaporization is drastically modified.

iii. By assuming constant mean physical properties in the equations of change, [2.7] and[2.9], the steady state temperature is predicted without significant difference but the vaporization rate is approximately 35 percent higher than the corresponding variable properties case, under ambient conditions of 72.9 atmospheres and 1600°K.

iv. The assumption of unidirectional diffusion in the steady state regime becomes gradually less valid as the ambient temperature is decreased and the pressure in the system is increased.

v. In agreement with previous studies the time of vaporization spent under steady state conditions is proportional to the square of the droplet diameter.

vi. Because experimental data are not available for comparison purposes, the accuracy of the model is difficult

to assess. The uncertainties in the properties of high pressure mixtures certainly may affect the absolute values reported.

vii. Comparing the results obtained with those given by a simplified low pressure model, Equations [1.8] and [1.14], it is observed that the simplified model does have more than one or no analytical solutions at high pressure levels. Furthermore, under some given ambient conditions of temperature and pressure, the simplified model predicts steady state conditions which physically cannot be obtained as may be understood from Figure 2.2. This clearly indicates that the low pressure model is not properly posed for high pressure environmental conditions.

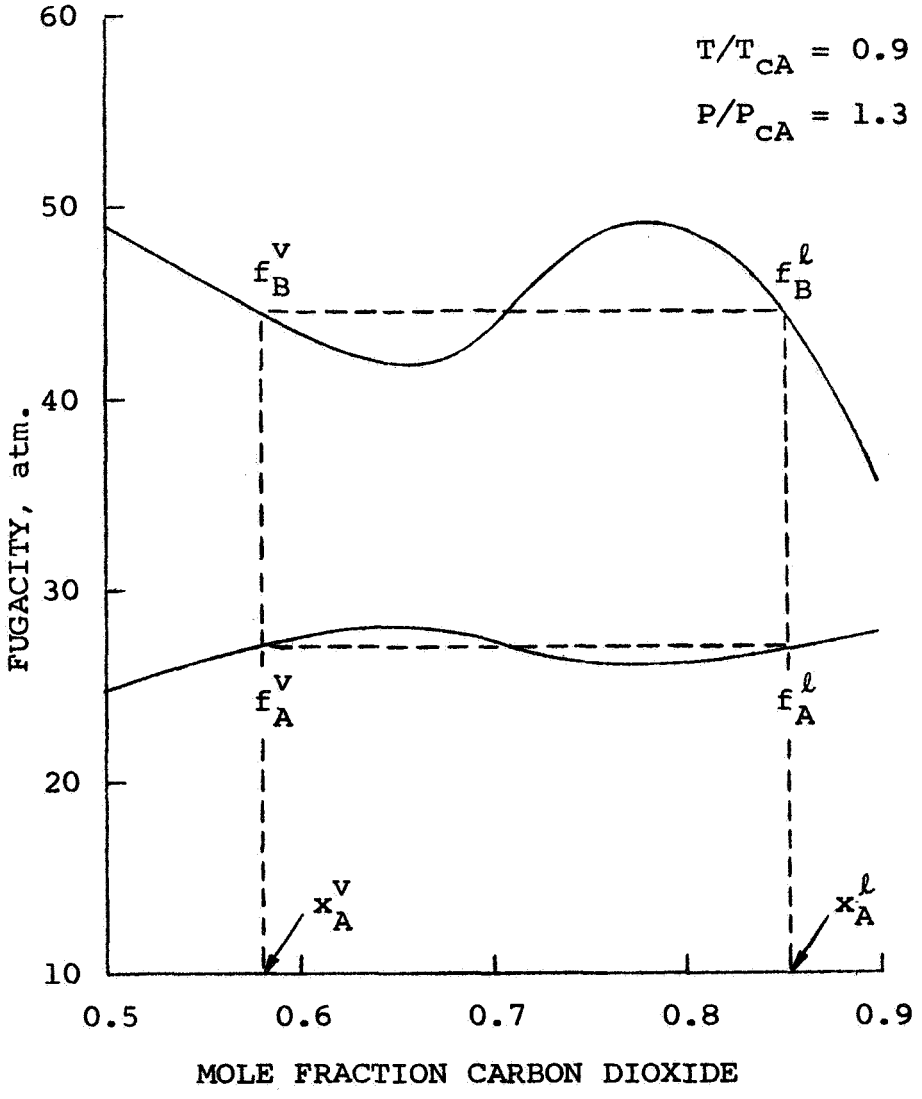

Figure 2.1. Fugacity-composition diagram for the carbon dioxide-nitrogen system under isothermal and isobaric conditions.

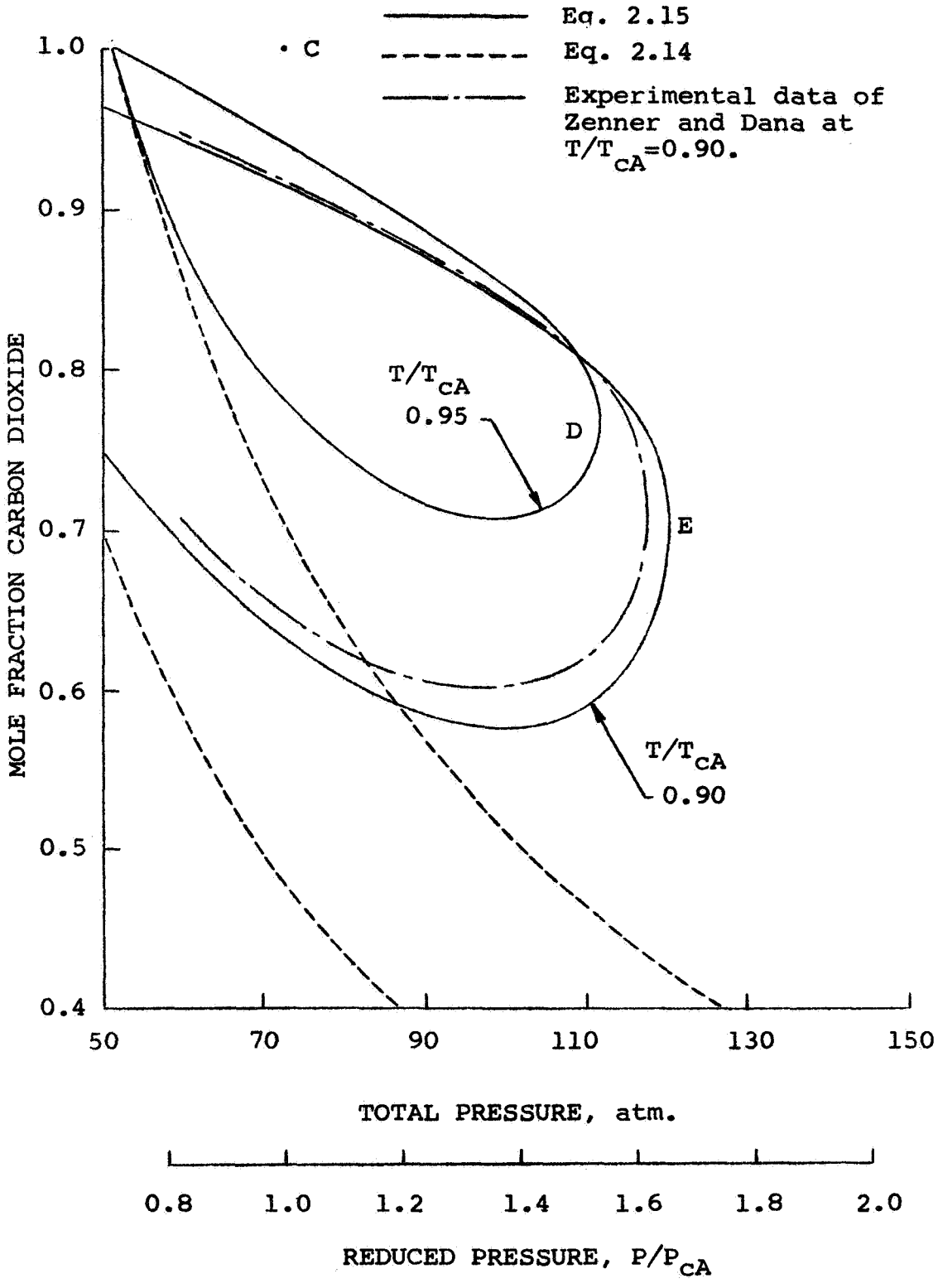

Figure 2.2. Calculated vapor-liquid equilibrium isotherms for the carbon dioxide-nitrogen system. (C = critical point of CO_2)

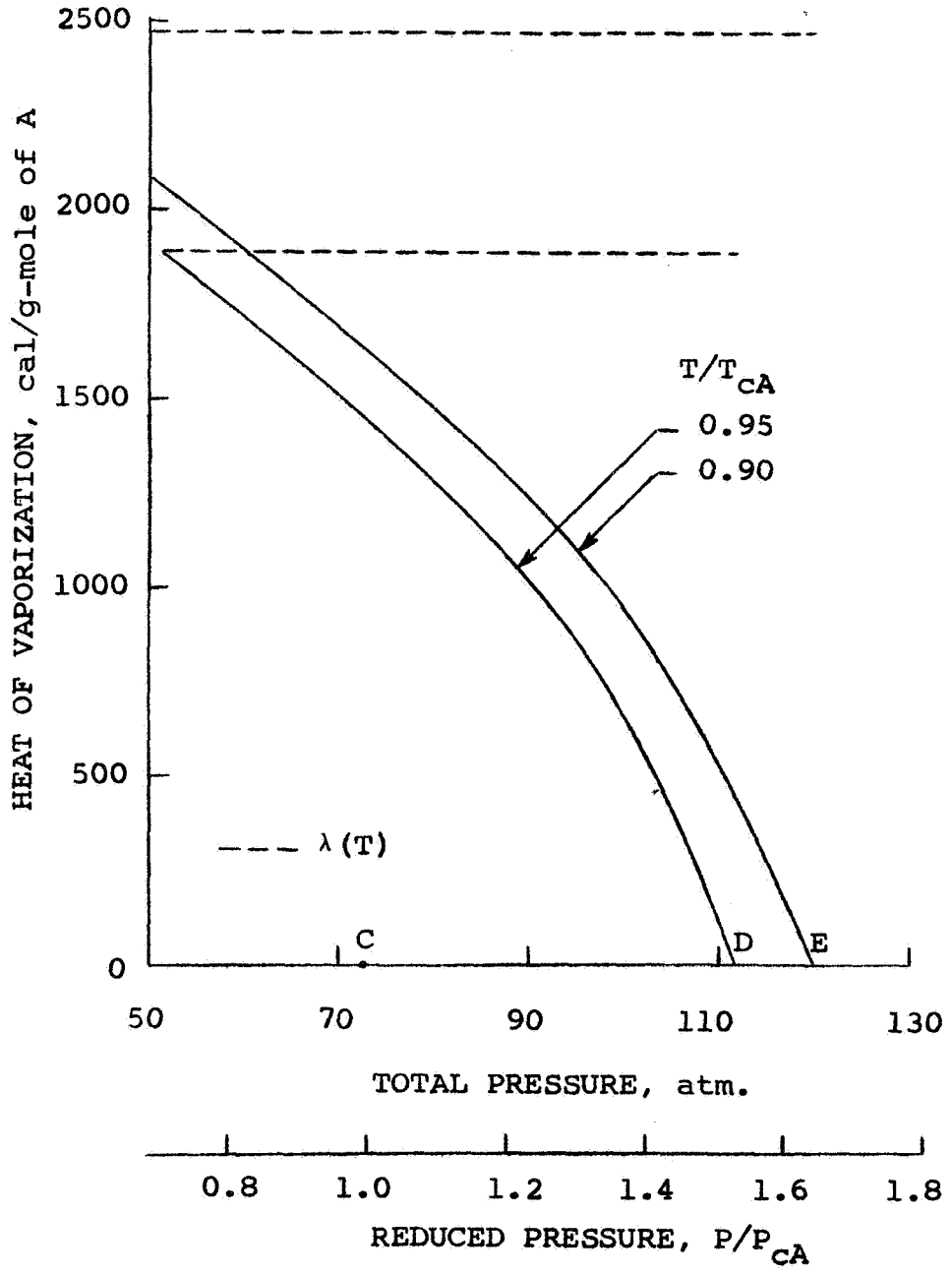

Figure 2.3. Isothermal difference in the partial molal enthalpies of carbon dioxide as a function of total pressure.

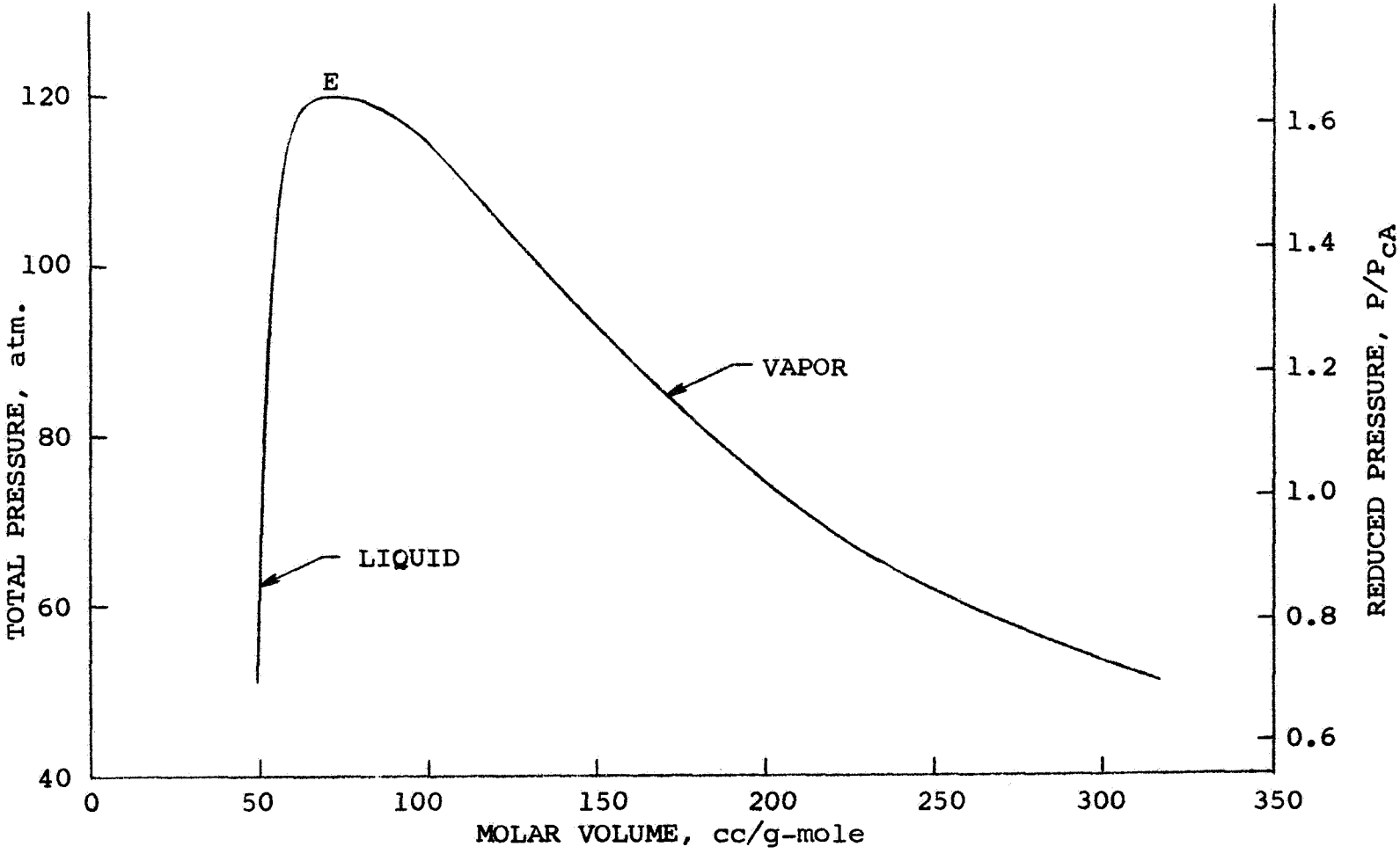

Figure 2.4. Pressure-molar volume diagram for the carbon dioxide-nitrogen system at $T/T_{cA} = 0.90$.

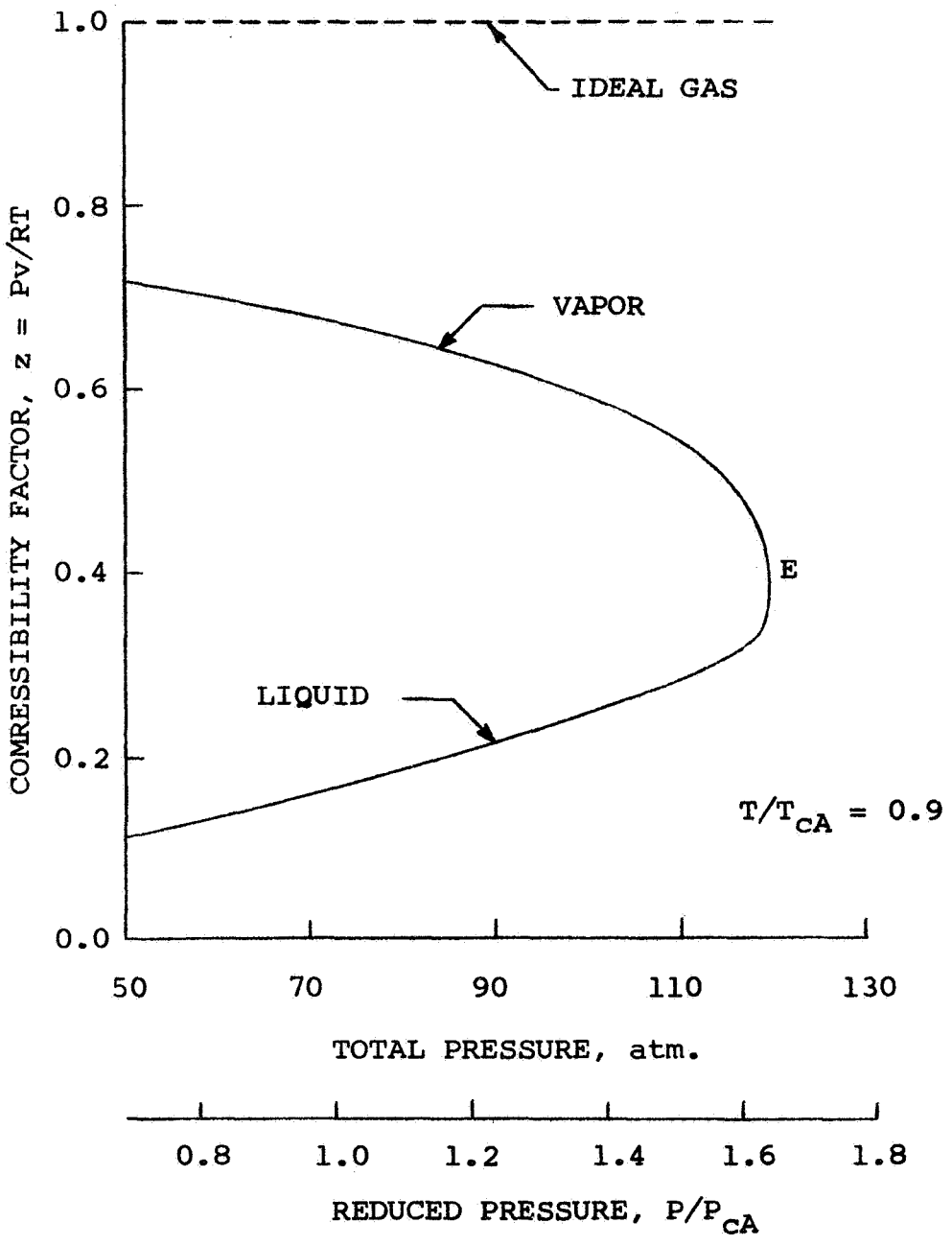

Figure 2.5. Compressibility factor-pressure diagram for the carbon dioxide-nitrogen system.

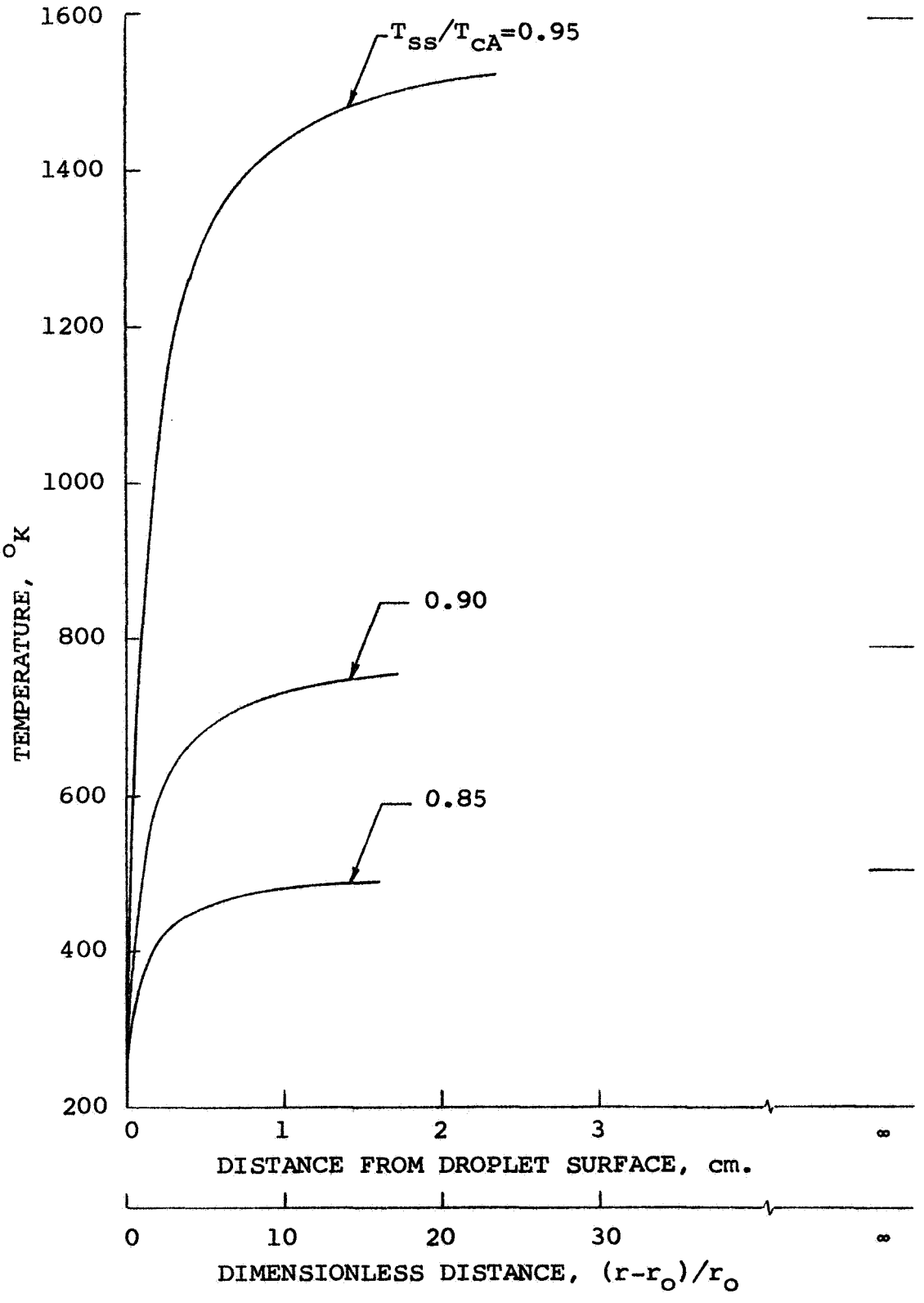

Figure 2.6. Temperature profiles in the film surrounding a 1000-micron carbon dioxide droplet vaporizing in nitrogen. $P = P_{cA}$.

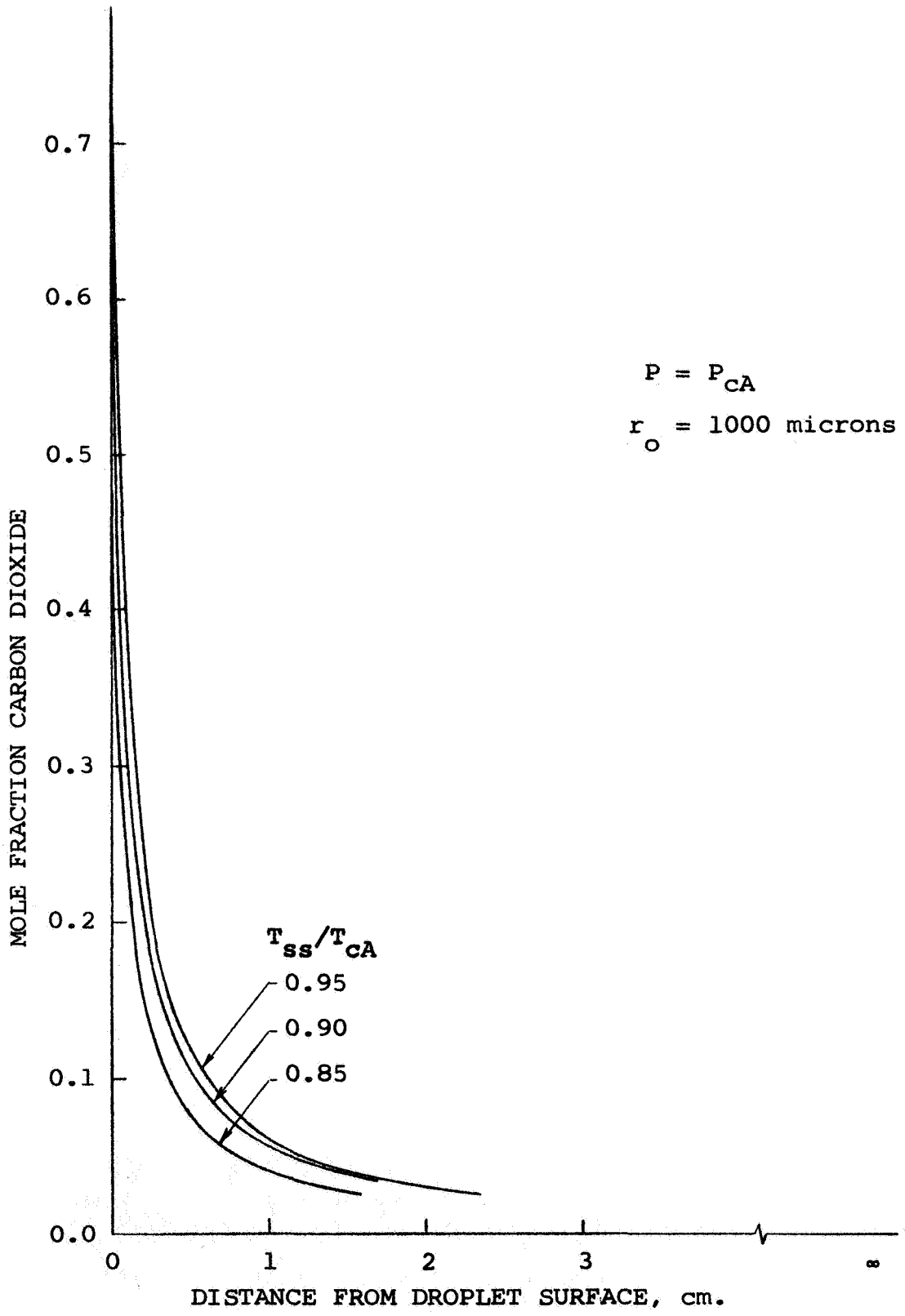

Figure 2.7. Composition profiles in the film surrounding a carbon dioxide droplet.

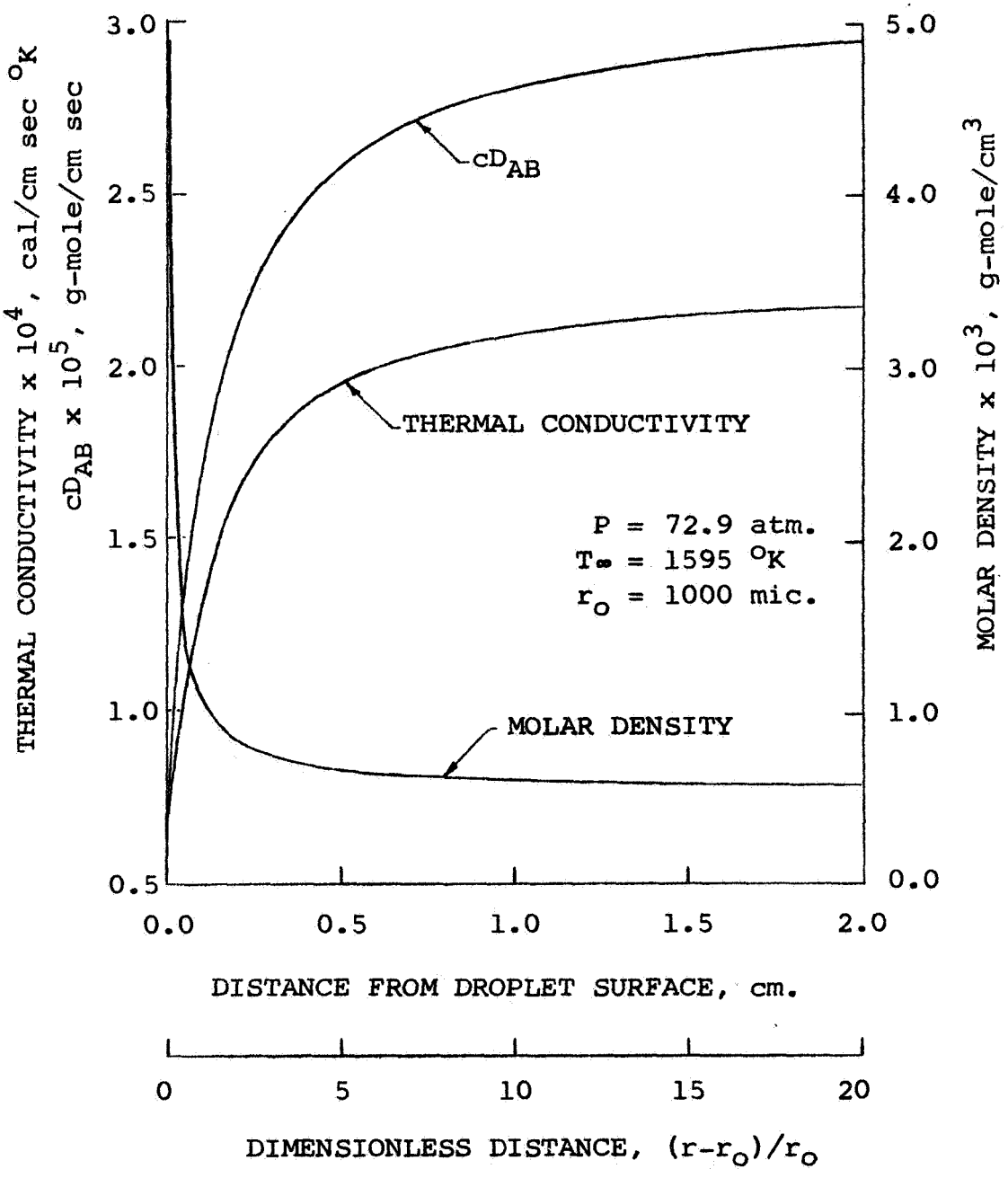

Figure 2.8. Property variations in the film surrounding a carbon dioxide droplet vaporizing in nitrogen.

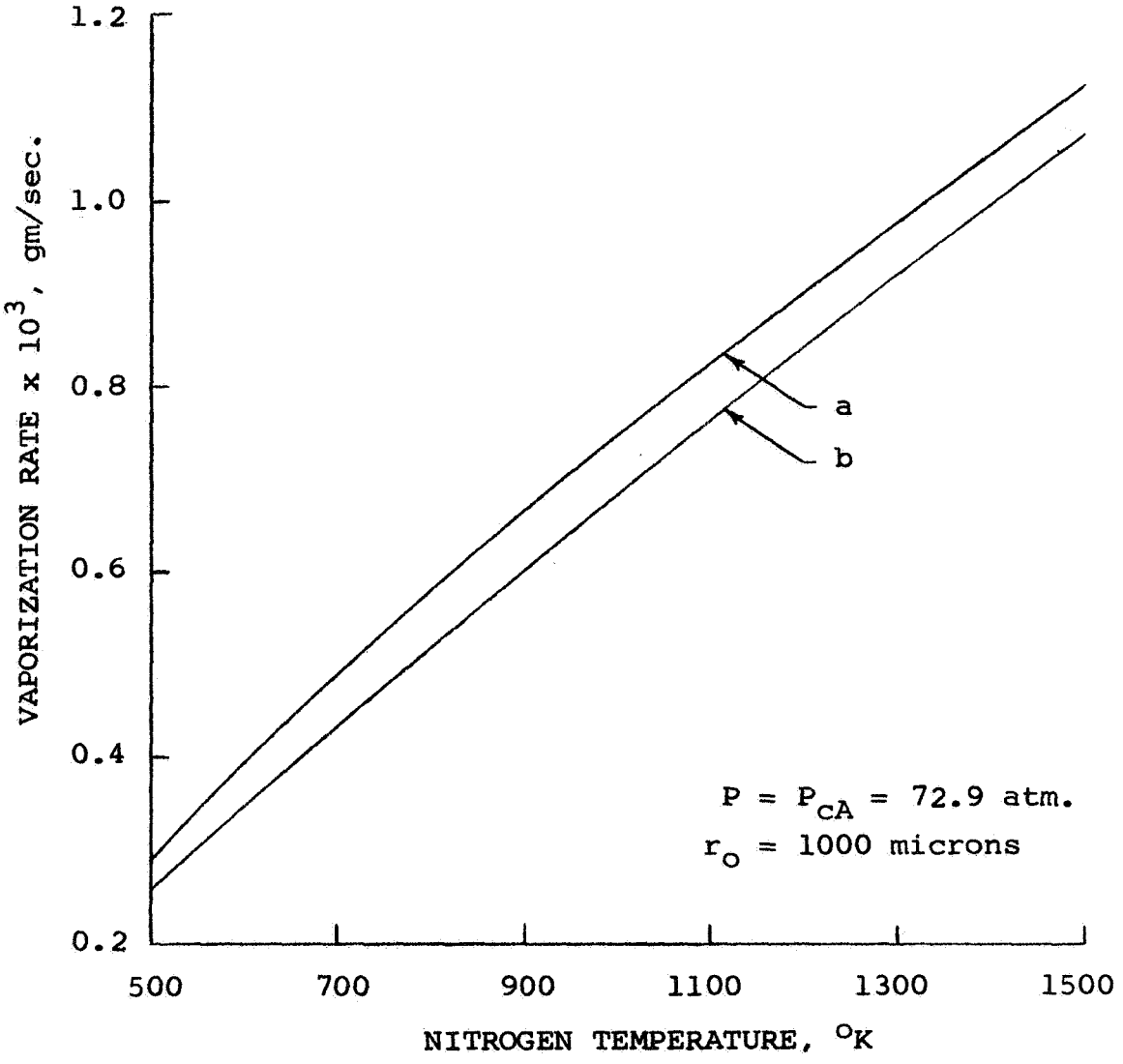

Figure 2.9. Variation of mass vaporization rate with nitrogen temperature; a) assuming thermodynamic equilibrium at the interface and b) assuming that N_2 is insoluble in CO_2 liquid.

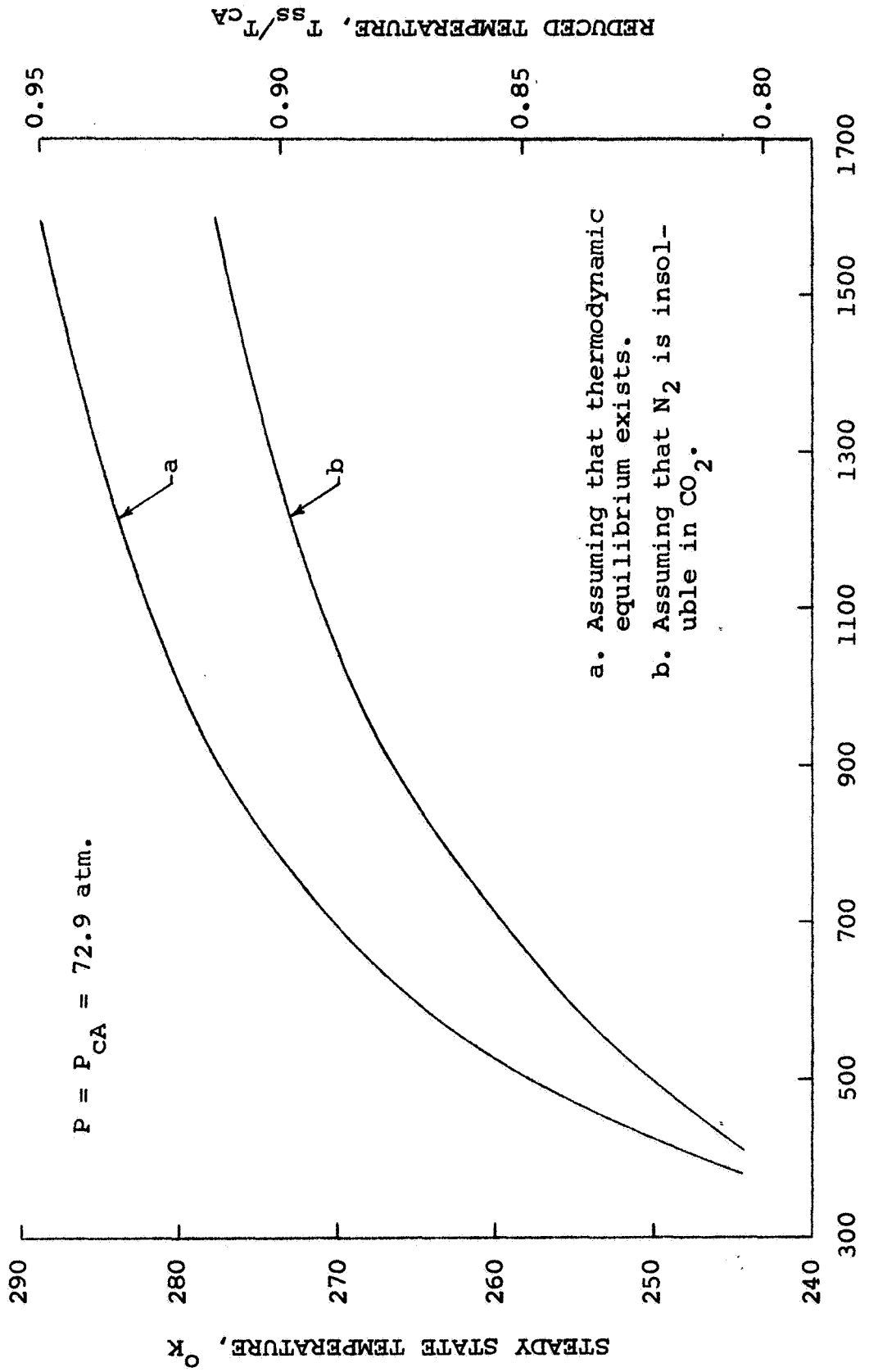

Figure 2.10. Steady state temperature as a function of nitrogen temperature.

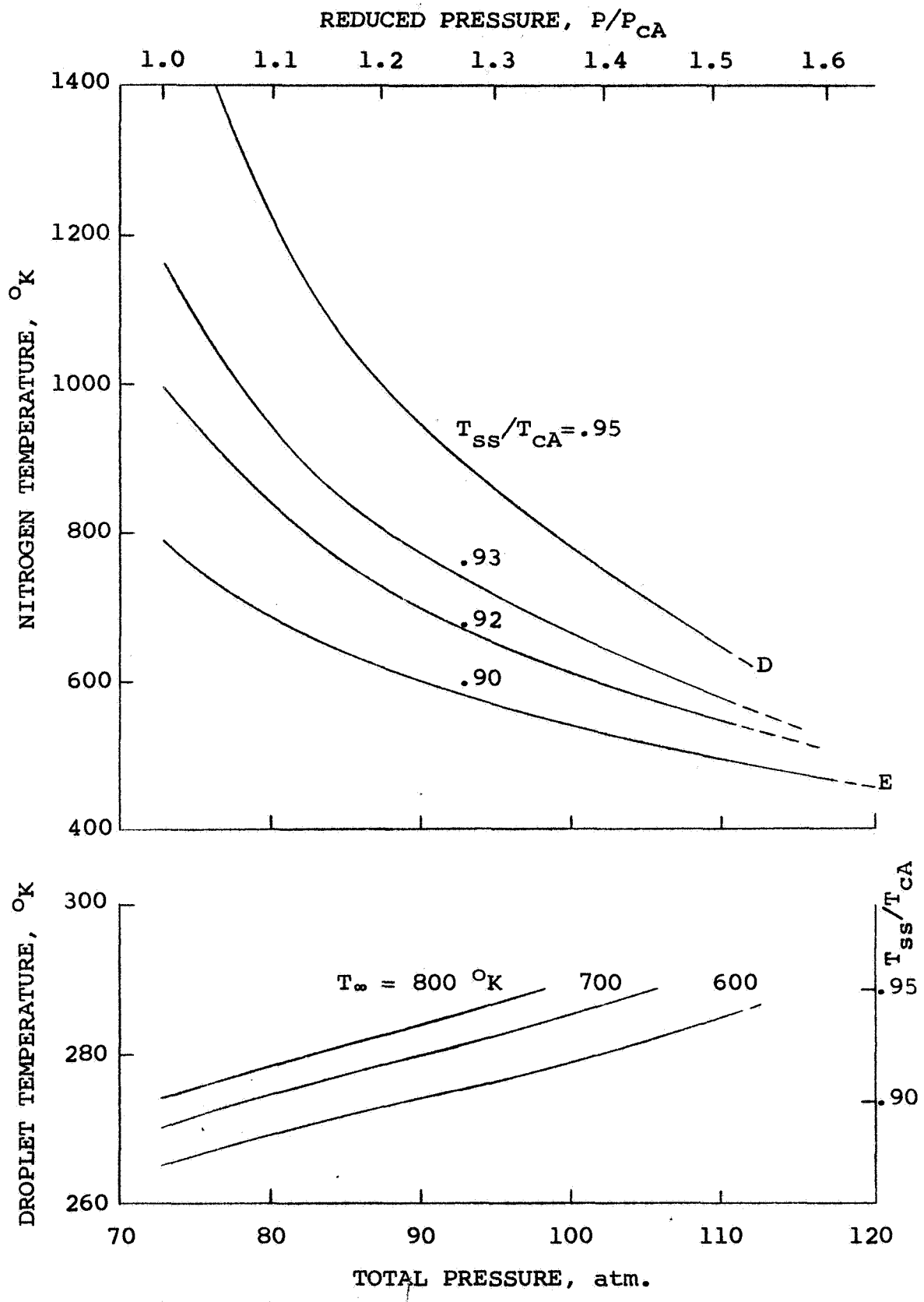

Figure 2.11. Steady state temperatures.

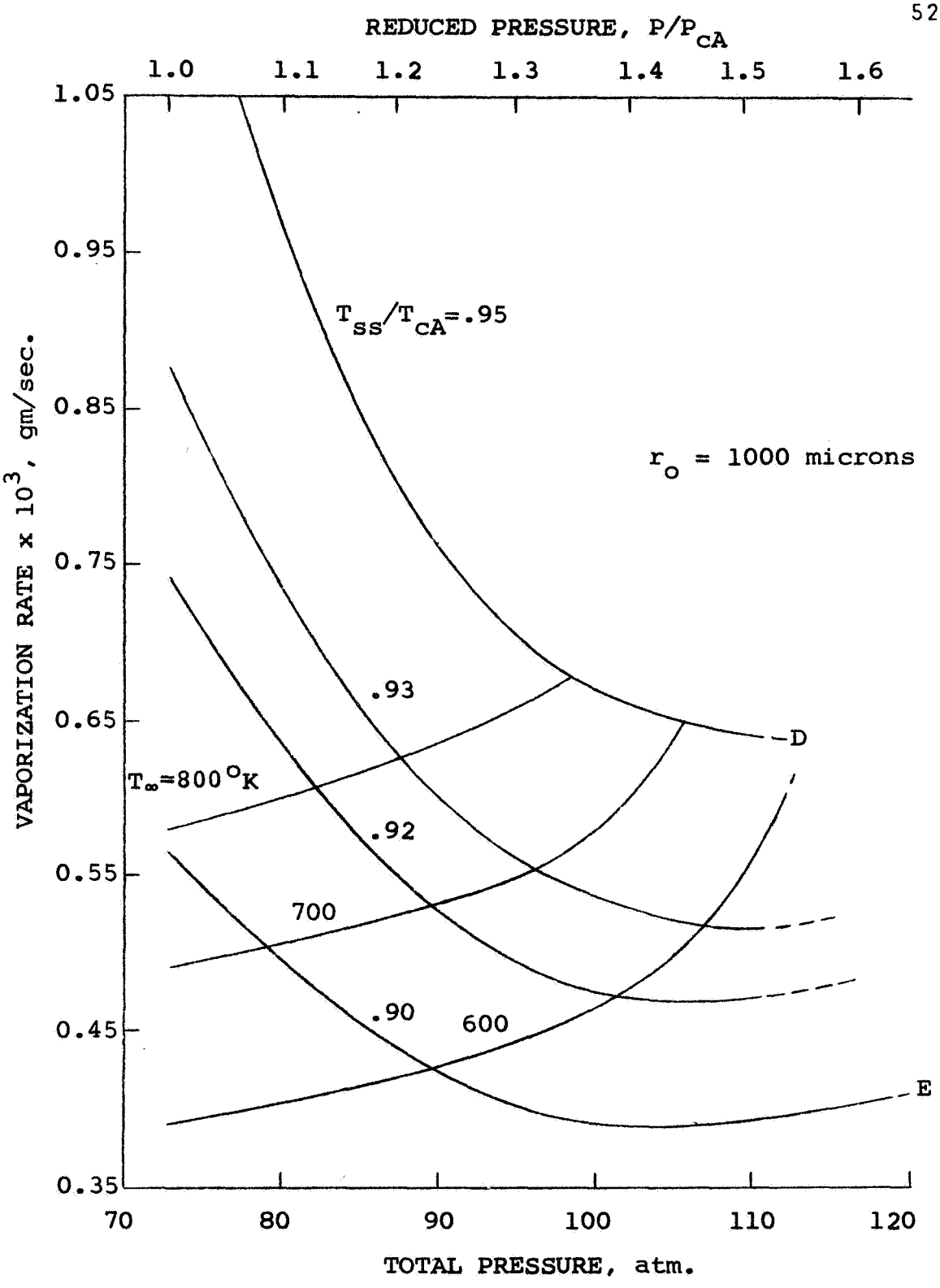

Figure 2.12. Effect of pressure and temperature on mass vaporization rate.

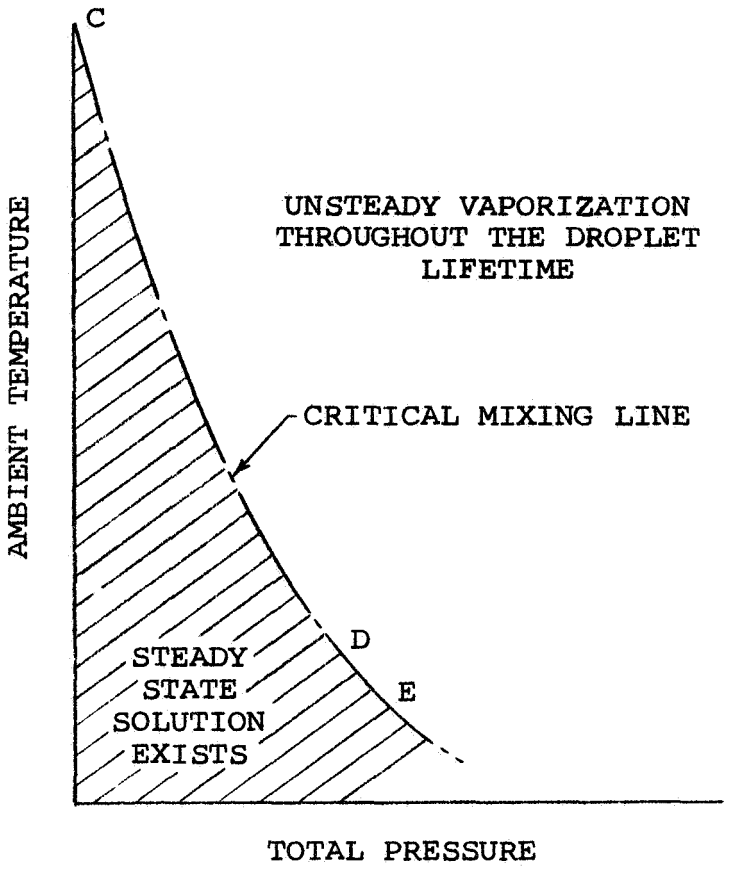

Figure 2.13. Schematic diagram illustrating ambient conditions where steady state solutions exist.

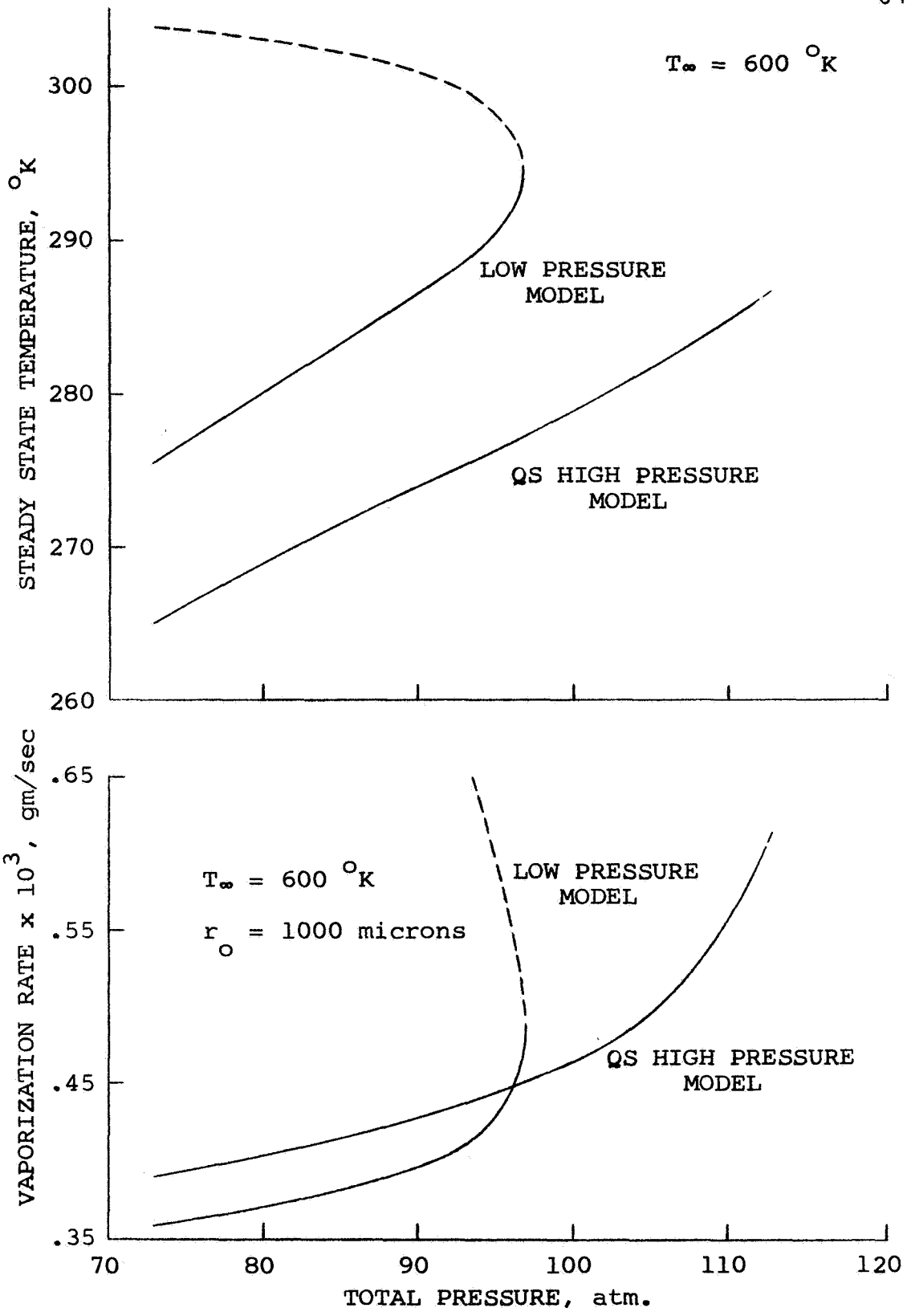

Figure 2.14. Comparison of calculated steady state results.

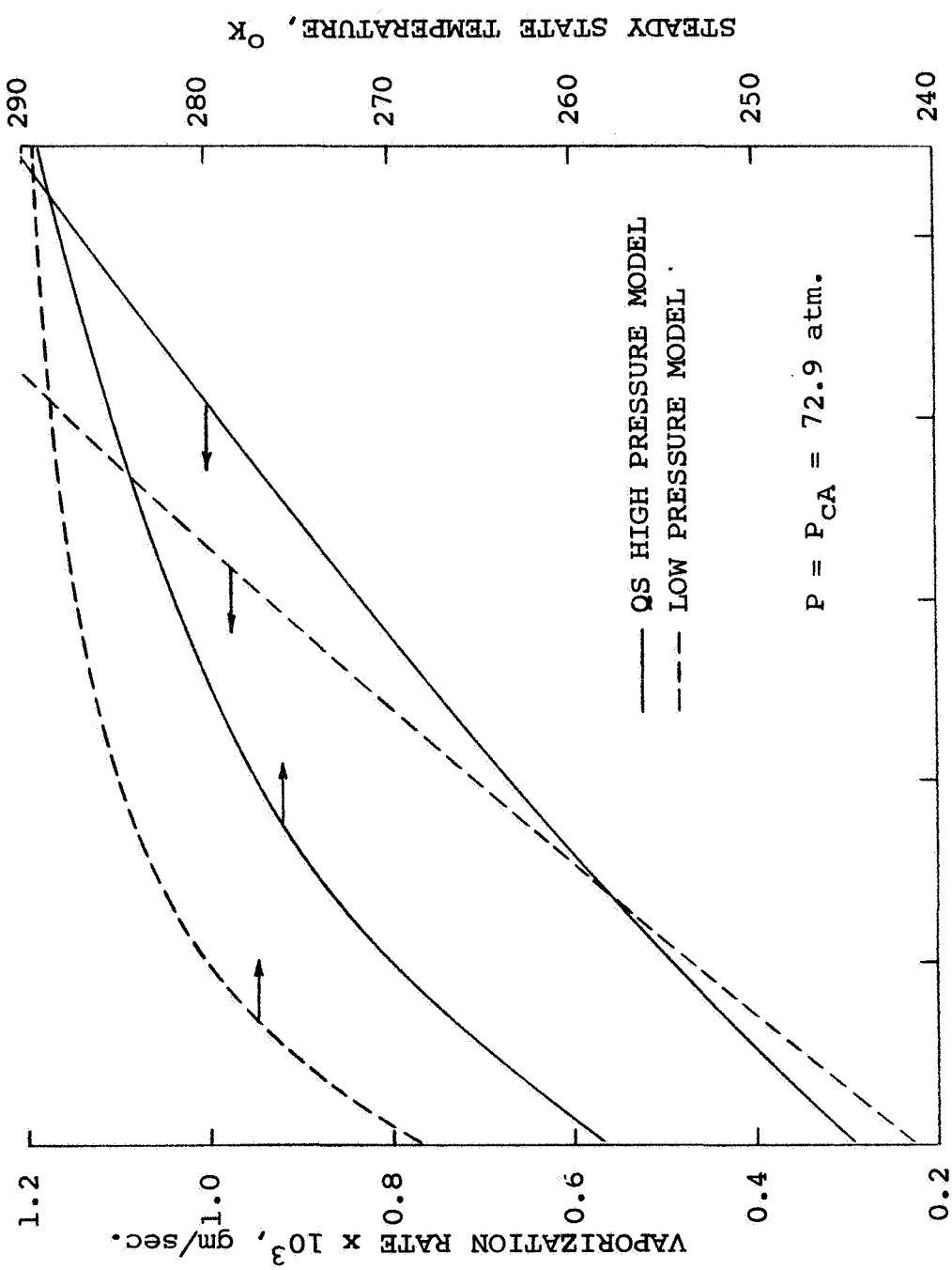

Figure 2.15. Comparison of calculated steady state results.

III. UNSTEADY DROPLET VAPORIZATION AT HIGH AMBIENT PRESSURES

Thus far, only steady state conditions have been considered, ignoring the unsteady heating-up period of the droplet. It is the purpose of this section to analyze the entire vaporization process including the heating-up of the droplet from its initial conditions, the regression of the droplet surface caused by evaporation, and the inherent transient effects in the gaseous phase.

The basic relationships are first derived in general form for a spherically symmetric model of a droplet undergoing vaporization in an inert atmosphere. These relationships are then applied to a carbon dioxide droplet vaporizing in nitrogen. Thermodynamic equilibrium at the droplet interface (when it exists) will be assumed. The entire liquid droplet is assumed to have a uniform temperature and the amount of nitrogen dissolved into liquid carbon dioxide is confined to a very thin layer at the droplet surface. Viscous dissipation, radiant energy exchange, and coupling effects between transport processes, such as the transport of energy due to concentration gradients and the transport of mass due to temperature gradients, are assumed to be physically negligible. All the non-ideal effects associated with dense

mixtures, as well as the variation of the thermophysical properties through the boundary layer are taken into account.

In the analysis that follows subscript A refers to the chemical species of the droplet, and B to the inert environment.

Theoretical Model

Governing Equations

The fully unsteady one-dimensional treatment of the vaporization process in the gaseous phase can be described by the equation of continuity of species A, the equation of energy, and an appropriate equation of state.

A mass balance of species A in a spherically symmetric shell surrounding a droplet leads to the differential equation

$$\frac{\partial c_A}{\partial t} + \frac{1}{r^2}\frac{\partial}{\partial r}(r^2 c_A V_{AO}) = 0 \quad , \quad r>r_o(t) \qquad [3.1]$$

where c_A is the molar concentration of component A in the gaseous mixture, V_{AO} is the velocity of A relative to stationary coordinates, and $r_o = r_o(t)$ is the droplet radius.

Similarly, a mass balance for the entire mixture leads to the differential equation

$$\frac{\partial c}{\partial t} + \frac{1}{r^2}\frac{\partial}{\partial r}(r^2 c V_{MO}) = 0 \quad , \quad r>r_o(t) \qquad [3.2]$$

where c is the molar density of the mixture, and V_{MO} is the molar average velocity of the mixture defined by

$$V_{M0} = x_A V_{A0} + x_B V_{B0} \qquad [3.3]$$

Neglecting viscous dissipation, radiant energy exchange, the Dufour energy flux, and assuming constant pressure in the system, an energy balance leads to the differential equation

$$\frac{\partial}{\partial t}(c_A \bar{H}_A + c_B \bar{H}_B) + \frac{1}{r^2}\frac{\partial}{\partial r}(r^2 c_A V_{A0} \bar{H}_A + r^2 c_B V_{B0} \bar{H}_B) = \frac{1}{r^2}\frac{\partial}{\partial r}\left(r^2 k \frac{\partial T}{\partial r}\right) \quad , \quad r>r_o(t) \qquad [3.4]$$

where c_i is the molar concentration of component i, $\bar{H}_i$ is the partial molal enthalpy of component i, V_{i0} is the velocity of i with respect to stationary coordinates, k is the thermal conductivity of the mixture, and $T = T(r,t)$ is the temperature distribution in the gas phase.

The molar density c is determined by an equation of state, namely

$$c = c(T,P,x_A) \qquad [3.5]$$

The above equations of change can be written more conveniently in terms of molar fluxes and composition gradients by introducing Fick's first law for ordinary diffusion, as Fourier's law for heat conduction was introduced in Equation [3.4]. Thus, the molar fluxes of species A and B may be expressed in the form

$$N_A = c_A V_{A0} = c x_A V_{M0} - c D_{AB} \frac{\partial x_A}{\partial r} \qquad [3.6]$$

and

$$N_B = c_B V_{BO} = cx_B V_{MO} + cD_{AB} \frac{\partial x_A}{\partial r} \qquad [3.7]$$

The above two expressions are entirely analogous to Equation [1.9] since $cV_{MO} = N_A + N_B$.

Therefore, substituting [3.6] and [3.7] into the equations of change, they may be arranged in the following form:

$$c \frac{\partial x_A}{\partial t} + cV_{MO} \frac{\partial x_A}{\partial r} = \frac{1}{r^2} \frac{\partial}{\partial r} \left(r^2 cD_{AB} \frac{\partial x_A}{\partial r}\right) \qquad [3.8]$$

$$\frac{\partial c}{\partial t} + \frac{1}{r^2} \frac{\partial}{\partial r} (r^2 cV_{MO}) = 0 \qquad [3.9]$$

$$cx_A \frac{\partial \bar{H}_A}{\partial t} + cx_B \frac{\partial \bar{H}_B}{\partial t} + N_A \frac{\partial \bar{H}_A}{\partial r} + N_B \frac{\partial \bar{H}_B}{\partial r}$$

$$= \frac{1}{r^2} \frac{\partial}{\partial r} \left(r^2 k \frac{\partial T}{\partial r}\right) \qquad [3.10]$$

and

$$c = c(T, P, x_A) \qquad [3.11]$$

The partial molal enthalpy of each component, $\bar{H}_A$ and $\bar{H}_B$, the thermal conductivity of the mixture, k, and the binary diffusivity, D_{AB}, are in general functions of temperature, pressure, and composition. For convenience, the product cD_{AB} will be considered as a single variable, for it may be regarded as a function of temperature and a weak function of pressure. The correlations to determine these thermodynamic and transport properties are presented in Appendix A. The

molar density of the mixture, c, will be determined by the Redlich-Kwong equation of state, Equation [2.16].

Since the total pressure of the system is essentially constant, by the chain rule

$$\frac{\partial \overline{H}_A}{\partial t} = \frac{\partial \overline{H}_A}{\partial T}\frac{\partial T}{\partial t} + \frac{\partial \overline{H}_A}{\partial x_A}\frac{\partial x_A}{\partial t} \qquad [3.12]$$

$$\frac{\partial \overline{H}_A}{\partial r} = \frac{\partial \overline{H}_A}{\partial T}\frac{\partial T}{\partial r} + \frac{\partial \overline{H}_A}{\partial x_A}\frac{\partial x_A}{\partial r} \qquad [3.13]$$

$$\frac{\partial \overline{H}_B}{\partial t} = \frac{\partial \overline{H}_B}{\partial T}\frac{\partial T}{\partial t} + \frac{\partial \overline{H}_B}{\partial x_A}\frac{\partial x_A}{\partial t} \qquad [3.14]$$

$$\frac{\partial \overline{H}_B}{\partial r} = \frac{\partial \overline{H}_B}{\partial T}\frac{\partial T}{\partial r} + \frac{\partial \overline{H}_B}{\partial x_A}\frac{\partial x_A}{\partial r} \qquad [3.15]$$

$$\frac{\partial k}{\partial r} = \frac{\partial k}{\partial T}\frac{\partial T}{\partial r} + \frac{\partial k}{\partial x_A}\frac{\partial x_A}{\partial r} \qquad [3.16]$$

$$\frac{\partial (cD_{AB})}{\partial r} = \frac{\partial (cD_{AB})}{\partial T}\frac{\partial T}{\partial r} \qquad [3.17]$$

$$\frac{\partial c}{\partial t} = \frac{\partial c}{\partial T}\frac{\partial T}{\partial t} + \frac{\partial c}{\partial x_A}\frac{\partial x_A}{\partial t} \qquad [3.18]$$

and

$$\frac{\partial c}{\partial r} = \frac{\partial c}{\partial T}\frac{\partial T}{\partial r} + \frac{\partial c}{\partial x_A}\frac{\partial x_A}{\partial r} \qquad [3.19]$$

where the stoichiometric relation $x_A + x_B = 1$ must be satisfied.

Equations [3.6] to [3.19] determine the evolution with time of the one-dimensional profiles $x_A = x_A(r,t)$, $T = T(r,t)$, and $V_{MO} = V_{MO}(r,t)$ in the gas phase.

In order to integrate numerically the governing equations, a finite differences grid will be imposed on the gaseous mixture. Since the droplet radius is time dependent, the following transformation is introduced here for later convenience:

$$y = r - r_o(t) \qquad [3.20]$$

Thus, by the chain rule

$$\frac{\partial x_A}{\partial t}(r,t) = \frac{\partial x_A}{\partial t}(y,t) - \dot{r}_o(t)\,\frac{\partial x_A}{\partial y}(y,t) \qquad [3.21]$$

$$\frac{\partial x_A}{\partial r}(r,t) = \frac{\partial x_A}{\partial y}(y,t) \qquad [3.22]$$

$$\frac{\partial^2 x_A}{\partial r^2}(r,t) = \frac{\partial^2 x_A}{\partial y^2}(y,t) \qquad [3.23]$$

$$\frac{\partial T}{\partial t}(r,t) = \frac{\partial T}{\partial t}(y,t) - \dot{r}_o(t)\,\frac{\partial T}{\partial y}(y,t) \qquad [3.24]$$

$$\frac{\partial T}{\partial r}(r,t) = \frac{\partial T}{\partial y}(y,t) \qquad [3.25]$$

$$\frac{\partial^2 T}{\partial r^2}(r,t) = \frac{\partial^2 T}{\partial y^2}(y,t) \qquad [3.26]$$

and

$$V_{MO}(r,t) = V_{My}(y,t) + \dot{r}_o(t) \qquad [3.27]$$

where V_{My} is the velocity of the mixture relative to the droplet surface.

The equation of continuity for the mixture may be integrated to obtain the velocity distribution. Thus, in the independent variables y and t,

$$V_{My}(y,t) = \frac{r_o^2}{(y+r_o)^2}\left[V_{My}(0,t) + \dot{r}_o\right]\frac{(c)_{y=0}}{c} - \dot{r}_o\left[1 - \frac{1}{(y+r_o)^2 c}\int_0^y (y+r_o)^2\left(\frac{\partial c}{\partial x_A}\frac{\partial x_A}{\partial y} + \frac{\partial c}{\partial T}\frac{\partial T}{\partial y}\right)dy\right] - \frac{1}{(y+r_o)^2 c}\int_0^y (y+r_o)^2\left(\frac{\partial c}{\partial x_A}\frac{\partial x_A}{\partial t} + \frac{\partial c}{\partial T}\frac{\partial T}{\partial t}\right)dy \qquad [3.28]$$

Under steady state conditions and unidirectional diffusion the above expression reiterates that the rate of vaporization is constant with the radial distance.

Similarly, the equations of continuity for species A and energy become, in the independent variables y and t,

$$\frac{\partial x_A}{\partial t} = \underline{A}\frac{\partial^2 x_A}{\partial y^2} + \left[\underline{B}\frac{\partial T}{\partial y} + \frac{2\underline{A}}{(y+r_o)} - V_{My}\right]\frac{\partial x_A}{\partial y} \qquad [3.29]$$

$$\frac{\partial T}{\partial t} = \underline{C}\frac{\partial^2 T}{\partial y^2} + \left[\underline{D}\frac{\partial x_A}{\partial y} + \underline{E}\frac{\partial T}{\partial y} + \frac{2\underline{C}}{(y+r_o)} - V_{My}\right]\frac{\partial T}{\partial y}$$

$$- \underline{AF} \frac{\partial^2 x_A}{\partial y^2} + \left[\underline{G} \frac{\partial x_A}{\partial y} - \underline{BF} \frac{\partial T}{\partial y} - \frac{2\underline{AF}}{(y+r_o)} \right] \frac{\partial x_A}{\partial y} \qquad [3.30]$$

where

$$\underline{A} = \frac{(cD_{AB})}{c} \qquad [3.31]$$

$$\underline{B} = \frac{1}{c} \frac{\partial (cD_{AB})}{\partial T} \qquad [3.32]$$

$$\underline{C} = \frac{k}{c\, c_p} = \alpha \qquad [3.33]$$

$$\underline{D} = \frac{1}{c\, c_p} \left[\frac{\partial k}{\partial x_A} + cD_{AB}(\bar{c}_{pA} - \bar{c}_{pB}) \right] \qquad [3.34]$$

$$\underline{E} = \frac{1}{c\, c_p} \frac{\partial k}{\partial T} \qquad [3.35]$$

$$\underline{F} = \frac{1}{c_p} \left[x_A \frac{\partial \bar{H}_A}{\partial x_A} - (1-x_A) \frac{\partial \bar{H}_B}{\partial x_A} \right] \qquad [3.36]$$

$$\underline{G} = \frac{(cD_{AB})}{c\, c_p} \left(\frac{\partial \bar{H}_A}{\partial x_A} - \frac{\partial \bar{H}_B}{\partial x_A} \right) \qquad [3.37]$$

and

$$c_p = x_A \bar{c}_{pA} + x_B \bar{c}_{pB} \qquad [3.38]$$

The governing equations of change must be supplied with an appropriate set of initial and boundary conditions.

Initial Conditions

Numerical difficulties are certainly encountered if one

attempts to consider the injection of a liquid droplet into pure component B, for no boundary layer exists at t = 0. A common approach to treat this singularity is to start the numerical solution with assumed profiles for small values of time. While this approach may be valid for certain problems, the assumed profiles may lead to unrealistic solutions due to the extremely nonlinear behavior of the differential equations. Therefore, the initial conditions to be considered here are those of a droplet of radius r_o (0) vaporizing under quasi-steady conditions and maintained at its initial temperature, $T^{\ell}(0)$, for $t \leq 0$. Although these conditions are difficult to be satisfied exactly in practice, it is considered that these initial conditions are better than the assumption of uncoupled profiles in the gas phase.

Thus,

$$T(y,0) = T_{qs}(y) \quad , \quad y \geq 0 \qquad [3.39]$$

and

$$x_A(y,0) = x_{qs}(y) \quad , \quad y \geq 0 \qquad [3.40]$$

where $T_{qs}(y)$ and $x_{qs}(y)$ are respectively the temperature and composition profiles in the vapor film surrounding a droplet of radius r_o (0) and temperature $T^{\ell}(0)$ undergoing quasi-steady vaporization. The governing equations which yield these initial conditions are the same as those presented in the previous steady state section, modifying boundary condition [2.13] in

order to take into account the excess energy arriving at the droplet surface which is not carried away by the mass transfer, since the droplet is not vaporizing under steady state conditions.

Boundary Conditions

The boundary conditions for Equations [3.28], [3.29], and [3.30] are now described.

Since the ambient conditions are specified,

$$T(\infty,t) = T_\infty \qquad , t \geq 0 \qquad [3.41]$$

and

$$x_A(\infty,t) = 0 \qquad , t \geq 0 \qquad [3.42]$$

At the droplet surface,

$$T(0,t) = T^{\ell}(t) \qquad , t \geq 0 \qquad [3.43]$$

and

$$x_A(0,t) = x_A(T,P) \qquad , t \geq 0 \qquad [3.44]$$

Assuming small departures from equilibrium, Equation [3.44] is determined by the vapor-liquid equilibrium relationship $x_A = x_A(T,P)$. However, as it was pointed out in the previous section, the critical mixing points envelope delineates the region where two phases in a binary system can coexist in thermodynamic equilibrium. Therefore, for those states outside the critical mixing line, where a gaseous phase surrounds the postulated core of the liquid droplet, boundary

condition [3.44] may be determined via an overall conservation equation, such as

$$m_d(0) - m_d(t) = \int_{r_o(t)}^{\infty} 4\pi r^2 c x_A dr - \int_{r_o(0)}^{\infty} 4\pi r^2 (c x_A)_{t=0} dr$$

$$= \int_0^t w dt \qquad [3.45]$$

where $m_d(t)$ is the mass of the droplet, and w is the rate of vaporization. The above relationship indicates that the total amount of component A in the system is constant. The practicality of Equation [3.45] will be discussed later.

The velocity $V_{My}(0,t)$, which appears in Equation [3.28], can be determined using the following relationship:

$$V_{My}(y,t) = x_A V_{Ay}(y,t) + x_B V_{By}(y,t) \qquad [3.46]$$

Since it is assumed that the velocity of component B relative to the droplet surface is nearly equal to zero at $y = 0$, it follows that

$$V_{My}(0,t) = -\frac{1}{c} \frac{(cD_{AB})}{1 - x_A} \frac{\partial x_A}{\partial y} \Bigg|_{y=0} \qquad [3.47]$$

In order to determine the liquid temperature, and the position of the droplet surface, additional equations are required. These are supplied by the following equations of

energy and continuity in the liquid phase:

$$4\pi r_o^2 k \left.\frac{\partial T}{\partial y}\right|_{y=0} = m_d c_{pA}^{\ell} \frac{dT^{\ell}}{dt} + w(\bar{H}_A^v - \bar{H}_A^{\ell}) \qquad [3.48]$$

$$w = 4\pi r_o^2 \left(-\frac{cD_{AB}}{1-x_A}\frac{\partial x_A}{\partial y} + cx_A \frac{dr_o}{dt}\right)_{y=0} \qquad [3.49]$$

$$= -4\pi r_o^2 c_A^{\ell} \frac{dr_o}{dt} - \frac{4}{3}\pi r_o^3 \frac{dc_A^{\ell}}{dt} \qquad [4.50]$$

Therefore, the set of equations [3.28], [3.29], [3.30], [3.39], [3.40], [3.41], [3.42], [3.43], [3.44], [3.47], [3.48], [3.49], and [3.50] describe the entire vaporization process.

Numerical Method of Solution

The numerical solution of the governing equations in the film clearly poses a problem. While an implicit technique may have numerical stability advantages, the nature of the equations seems to preclude any solution, for if it would be feasible, it would involve the simultaneous solution of an enormous amount of nonlinear algebraic equations. Therefore, an explicit scheme was contrived to solve the governing equations in the gaseous film. Since the technique itself may be of interest, it is described in detail below.

A grid was imposed on the gaseous mixture surrounding the droplet as shown in Figure 3.1. Forward differences were used to determine the time derivatives, and centered differences to determine the space derivatives. Thus, for

any variable u(y,t)

$$\frac{\partial u}{\partial t} \doteq \frac{u_{i,j+1} - u_{i,j}}{\Delta t} \qquad [3.51]$$

$$\frac{\partial u}{\partial y} \doteq \frac{u_{i+1,j} - u_{i-1,j}}{2\Delta y} \qquad [3.52]$$

$$\frac{\partial^2 u}{\partial y^2} \doteq \frac{u_{i+1,j} - 2u_{i,j} + u_{i-1,j}}{(\Delta y)^2} \qquad [3.53]$$

The integrals which appear in Equation [3.28] were determined by the trapezoidal rule as in

$$\int_0^y u \, d\bar{y} \doteq \frac{\Delta y}{2}\left[u_{0,j} + u_{i,j} + 2(u_{1,j} + u_{2,j} + \cdots + u_{i-1,j})\right] \qquad [3.54]$$

Therefore, substituting the above finite-difference relationships into Equations [3.28], [3.29], and [3.30]:

$$\underline{X}_{i,j} = \underline{A}_{i,j}\frac{x_{i+1,j} - 2x_{i,j} + x_{i-1,j}}{(\Delta y)^2} + \left[\underline{B}_{i,j}\frac{T_{i+1,j} - T_{i-1,j}}{2\Delta y} + \frac{2}{i\Delta y + r_{oj}}\underline{A}_{i,j} - \frac{r_{oj}^2 c_{0,j}}{(i\Delta y + r_{oj})^2 c_{i,j}}(V_{0,j} + \dot{r}_{oj}) + \dot{r}_{oj}(1 - \underline{H}_{i,j}) + \frac{r_{oj}^2}{(i\Delta y + r_{oj})^2 c_{i,j}}\frac{\Delta y}{2}\left(c_{x0,j}\frac{x_{0,j+1} - x_{0,j}}{\Delta t} + c_{T0,j}\frac{T_{0,j+1} - T_{0,j}}{\Delta t}\right)\right.$$

$$+ \frac{\Delta y}{(i\Delta y + r_{oj})^2 c_{i,j}} \sum_{n=1}^{i-1} (n\Delta y + r_{oj})^2 \left(c_{xn,j} \right.$$

$$\left. \frac{x_{n,j+1} - x_{n,j}}{\Delta t} + c_{Tn,j} \frac{T_{n,j+1} - T_{n,j}}{\Delta t} \right) \left(\frac{x_{i-1,j} - x_{i-1,j}}{2\Delta y} \right)$$

$$; \; i = 1, 2, \ldots \qquad [3.55]$$

$$\underline{T}_{i,j} = \underline{C}_{i,j} \frac{T_{i+1,j} - 2T_{i,j} + T_{i-1,j}}{(\Delta y)^2} + \left[\underline{D}_{i,j} \frac{x_{i+1,j} - x_{i-1,j}}{2\Delta y} \right.$$

$$+ \underline{E}_{i,j} \frac{T_{i+1,j} - T_{i-1,j}}{2\Delta y} + \frac{2}{i\Delta y + r_{oj}} \underline{C}_{i,j}$$

$$- \frac{r_{oj}^2 c_{O,j}}{(i\Delta y + r_{oj})^2 c_{i,j}} (V_{O,j} + \dot{r}_{oj}) + \dot{r}_{oj} (1 - \underline{H}_{i,j})$$

$$+ \frac{r_{oj}^2}{(i\Delta y + r_{oj})^2 c_{i,j}} \frac{\Delta y}{2} \left(c_{xO,j} \frac{x_{O,j+1} - x_{O,j}}{\Delta t} \right.$$

$$\left. + c_{TO,j} \frac{T_{O,j+1} - T_{O,j}}{\Delta t} \right)$$

$$+ \frac{y}{(i\Delta y + r_{oj})^2 c_{i,j}} \sum_{n=1}^{i-1} (n\Delta y + r_{oj})^2 \left(c_{xn,j} \right.$$

$$\left. \frac{x_{n,j+1} - x_{n,j}}{\Delta t} \right.$$

$$+ c_{Tn,j} \frac{T_{n,j+1} - T_{n,j}}{\Delta t}\Bigg)\Bigg]\left(\frac{T_{i+1,j} - T_{i-1,j}}{2\Delta y}\right)$$

$$- \underline{A}_{i,j}\underline{F}_{i,j} \frac{x_{i+1,j} - 2x_{i,j} + x_{i-1,j}}{(\Delta y)^2}$$

$$+\Bigg(\underline{G}_{i,j} \frac{x_{i+1,j} - x_{i-1,j}}{2\Delta y} - \underline{B}_{i,j}\underline{F}_{i,j} \frac{T_{i+1,j} - T_{i-1,j}}{2\Delta y}$$

$$- \frac{2}{(i\Delta y + r_{oj})} \underline{A}_{i,j}\underline{F}_{i,j}\Bigg)\left(\frac{x_{i+1,j} - x_{i-1,j}}{2\Delta y}\right) \quad ; \; i = 1,2,\ldots \qquad [3.56]$$

where

$$\underline{X}_{i,j} = \frac{x_{i,j+1} - x_{i,j}}{\Delta t}$$

$$- \frac{x_{i+1,j} - x_{i-1,j}}{2\Delta y} \frac{\Delta y}{2c_{i,j}} \left(c_{xi,j} \frac{x_{i,j+1} - x_{i,j}}{\Delta t}\right.$$

$$\left. + c_{Ti,j} \frac{T_{i,j+1} - T_{i,j}}{\Delta t}\right) \qquad [3.57]$$

$$\underline{T}_{i,j} = \frac{T_{i,j+1} - T_{i,j}}{\Delta t}$$

$$- \frac{T_{i+1,j} - T_{i-1,j}}{2\Delta y} \frac{\Delta y}{2c_{i,j}} \left(c_{xi,j} \frac{x_{i,j+1} - x_{i,j}}{\Delta t}\right.$$

$$\left. + c_{Ti,j} \frac{T_{i,j+1} - T_{i,j}}{\Delta t}\right) \qquad [3.58]$$

$$x = x_A \qquad [3.59]$$

$$c_x = \frac{\partial c}{\partial x_A} \qquad [3.60]$$

$$c_T = \frac{\partial c}{\partial T} \qquad [3.61]$$

and

$$\underline{H}_{i,j} = \frac{r_{oj}^2}{(i\Delta y + r_{oj})^2 c_{i,j}} \frac{\Delta y}{2} \left[c_{xO,j} \left(\frac{\partial x_A}{\partial y}\right)_{O,j} + c_{TO,j} \left(\frac{\partial T}{\partial y}\right)_{O,j} \right] + \frac{1}{c_{i,j}} \frac{\Delta y}{2} \left(c_{xi,j} \frac{x_{i+1,j} - x_{i-1,j}}{2\Delta y} + c_{Ti,j} \frac{T_{i+1,j} - T_{i-1,j}}{2\Delta y} \right) + \frac{\Delta y}{(i\Delta y + r_{oj})^2 c_{i,j}} \sum_{n=1}^{i-1} (n\Delta y + r_{oj})^2 \left(c_{xn,j} \frac{x_{n+1,j} - x_{n-1,j}}{2\Delta y} + c_{Tn,j} \frac{T_{n+1,j} - T_{n-1,j}}{2\Delta y} \right) \qquad ; i = 1,2,... \qquad [3.62]$$

Since at any given time j the temperature and composition profiles in the gaseous film are known, the temperature and composition changes at location i ($i \neq 0$) from $T_{i,j}$ to $T_{i,j+1}$ and from $x_{i,j}$ to $x_{i,j+1}$, respectively, may be readily found by solving simultaneously Equations [3.57] and [3.58].

The stability criterion for the above difference equations is discussed later.

Because temperature and composition gradients at the droplet surface are very large, the results are markedly affected by using different finite-difference relationships to evaluate these derivatives there, with the same space

increment size. Among various formulas, gradients at the droplet surface were best approximated by a six-point Lagrange polynomial[17], as in

$$\left.\frac{\partial u}{\partial y}\right|_{y=0} = \frac{1}{5!\,\Delta y} \sum_{m=0}^{5} L_m u_{m,j} \qquad [3.63]$$

where $L_0 = -274$, $L_1 = 600$, $L_2 = -600$, $L_3 = 400$, $L_4 = -150$, and $L_5 = 24$.

The partial derivatives of the thermodynamic and transport properties which appear in the equations of change were determined by using forward differences.

Since the ambient conditions are approached asymptotically, the numerical integration was carried out to a certain radial distance where the profiles did not change appreciably. At this point, of the order of ten initial droplet radii, the following quasi-steady asymptotic equations were used:

$$\frac{d^2\tilde{T}}{dy^2} + \frac{2}{y+r_o}\frac{d\tilde{T}}{dy} = 0 \quad , \; y \geq y^* \qquad [3.64]$$

and

$$\frac{d^2\tilde{x}_A}{dy^2} + \frac{2}{y+r_o}\frac{d\tilde{x}_A}{dy} = 0 \quad , \; y \geq y^* \qquad [3.65]$$

where $\tilde{T}$ and $\tilde{x}_A$ are used to indicate that they hold only for $y \geq y^*$. The assumptions involved in these simplified quasi-steady equations may be deduced from [3.29] and [3.30]. Since

most of the non-ideal and variable properties effects occur in the vicinity of the droplet surface, and the velocity of the mixture is inversely proportional to the square of the radial distance, the approximation in matching the temperature and composition profiles is numerically justifiable. One commonly used approximation to determine numerically the boundary conditions near the edge of the boundary layers is to fix in time the profiles there. However, this approach was discarded, for it affects the shape of the profiles due to the continuous variation of the boundary layer thicknesses.

In order to test the entire numerical technique, the temperature response of a carbon dioxide, 1000-micron-radius, porous sphere vaporizing in nitrogen at 815°K and 72.9 atmospheres was calculated using different mesh sizes. Since the steady state temperatures presented in the previous section were obtained with a more accurate numerical technique which evaluates the functions at intermediate positions within a space increment, a comparison can be made to assess the accuracy of the results. The steady state temperature predicted with a space increment of $0.4r_o$ was found to be 280°K, whereas for a $0.2r_o$ increment the steady state temperature was found to be 277°K. Previous steady state calculations with a space increment of $0.025r_o$ near the droplet surface show a steady state temperature of 275°K. Thus, the larger the mesh size the larger the error introduced in the calculations, and

as a consequence of this error, the computations tend to predict consistently higher energy rates into the droplet. The discrepancy in the results is primarily caused by the inability of the finite-difference equations with relatively large mesh sizes to portray accurately the large temperature and composition gradients at the droplet surface. Unfortunately, the numerical technique does not allow one to alter the space increment size during the integration, and the computing time using uniform small mesh sizes is prohibitively long due to the enormous amount of calculations. The technique is numerically stable if Fourier's modulus, based on the difference values of time and space at the ambient conditions, is equal to or less than 0.5. Although no formal mathematical proof is given, violation of the above rule leads to instability. A simple physical argument on stability criteria is given in Reference 1.

Under those conditions where there is no thermodynamic equilibrium between phases in a binary system, the mole fraction at the droplet surface may be computed via an overall conservation equation in the system as[3.45]. However, since the mathematical process to compute the mole fraction is an iterative one, the technique is time consuming. Thus, the following scheme was used. In order to determine the mole fraction at the droplet surface at time j+1, a relationship is sought at time j between a change in the mole fraction at

the surface, δx, and the corresponding change that would be obtained in the mass of the droplet, δm. From Figure 3.2, it is observed that the change $-\delta m$ is directly proportional to δx at a given time j. Hence, when $\delta m = -w\Delta t$, $\delta x = (x_{0,j+1} - x_{0,j})$. In equation form

$$-\delta m = w\Delta t = b_1(x_{0,j+1} - x_{0,j}) + b_2 \qquad [3.66]$$

where b_1 and b_2 are determined at time j. Since Equation [3.66] is an approximation, for only the mole fraction at the droplet surface is changed, the accuracy of the technique was always monitored through Equation [3.45].

Applications to a CO_2-N_2 System

Vaporization histories were calculated for carbon dioxide (component A) droplets vaporizing in nitrogen (component B) under critical and supercritical pressure conditions. The critical temperature of pure CO_2 is 304.2°K and its critical pressure 72.9 atmospheres.

Figure 3.3 illustrates the vaporization history for a carbon dioxide droplet, of 1000-micron initial radius, $0.8T_{cA}$ initial temperature, vaporizing in nitrogen under constant ambient conditions of 1400°K and 72.9 atmospheres (P_{cA}). This history is carried out in time until 80 percent of the droplet mass has been vaporized. It is observed that the droplet temperature rises rapidly from its initial temperature to approach asymptotically its corresponding steady state temperature

which is slightly higher than the corresponding temperature computed without inclusion of the droplet surface regression. It is also observed that most of the droplet's lifetime is spent in the heating-up period. The droplet radius initially increases for a short time after the initial conditions due to the thermal expansion of the liquid, since most of the energy arriving at the droplet surface is utilized to heat-up the droplet. The initial slope of the percent-mass-vaporized curve is initially small, forming an inflection point thereafter. The small initial slope reflects the fact that the mass vaporization rates are relatively small in the early part of the vaporization process. However, the initial value for the mass vaporization rate, at $t = 0$, not only depends upon the initial droplet temperature, which partially fixes the potential for mass transfer, but also depends upon the ambient temperature, for the same pressure conditions, i.e., the higher the ambient temperature, the higher the initial vaporization rate, for the same liquid temperature and pressure. Thus, the excess energy arriving at the droplet surface, since the droplet is not under steady state conditions for that value of ambient temperature, is not totally used for heating up, but it is also used to increase the rate of vaporization. Hence, the initial value for the vaporization rate is substantially larger had the droplet been under steady state conditions at the initial liquid temperature, e.g., for this particular history, the initial vaporization rate

is higher than the corresponding steady state vaporization rate at the initial droplet temperature by a factor of 2. This clearly points out the importance of the coupling between heat and mass transfer phenomena, as well as the sensitivity of the vaporization rates. The slope in the percent-mass-vaporized curve is also small at the end of the vaporization process because of the decrease in the surface area. Instantaneous vaporization rates as well as the variation of the surface regression rate with time for the same CO_2 droplet are shown in Figure 3.4. The mass vaporization rate increases after the initial conditions because of the rapid increase in the droplet temperature, reaches a maximum which is substantially higher than the initial value, to decrease thereafter. Similarly, it is observed that the rate of surface regression is positive for a short period of time due to thermal expansion of the liquid, then becomes gradually negative for some time and grows progressively more negative (not completely noticeable in this figure) tending toward an infinite value at the end of the vaporization process because of the decrease in the surface area.

Figure 3.5 shows a complete vaporization history for a carbon dioxide droplet, of 1000-micron initial radius, $0.8T_{cA}$ initial temperature, vaporizing in nitrogen under constant ambient conditions of $815^{\circ}K$ and 72.9 atmospheres (P_{cA}). The only difference between this history and the

preceding one is that the ambient nitrogen temperature is lower in this case. Thus, for the conditions illustrated in Figure 3.5, the droplet is closer to its steady state at all times, and the liquid temperature does not rise very rapidly after the initial conditions, for most of the energy conducted to the droplet is utilized to evaporate the liquid. The droplet approaches asymptotically its steady state temperature up to a point where the surface-to-volume ratio becomes appreciable. At this inflection point, the liquid temperature increases until the vaporization process is completed, with the temperature increase being markedly rapid at the end of the droplet's lifetime. The radius does not exhibit any increase due to thermal expansion in the early part of the vaporization process, even though the liquid temperature is the same as in Figure 3.3, for the same reasons outlined above. After approximately the first 1/4 of the droplet's lifetime, the radius approaches asymptotically a relationship of the form

$$(t_v - t) \alpha \ r_o \ (t)^{1.81} \qquad [3.67]$$

which is close to r_o^2.

Figure 3.6 shows the corresponding instantaneous values for the mass vaporization rate and change of droplet radius with time. The initial value for the rate of vaporization is lower than the corresponding value given in Figure 3.4,

for the same initial liquid temperature. Furthermore, it is noticed that the mass vaporization rate increases from its initial value and reaches a maximum which is considerably lower than the one shown in Figure 3.4, to decrease thereafter. Thus, the closer the initial droplet temperature to the steady state temperature, the less pronounced the maximum in the vaporization rate curve. Under steady state conditions, the rate of vaporization decreases monotonically with time. The instantaneous values for the mass vaporization rate were found to approach asymptotically a relationship of the form

$$w \alpha\ r_o(t)^{1.183} \qquad [3.68]$$

which is close to the previously determined value of $r_o^{1.0}$. The rate of change of droplet radius with time becomes progressively negative, changes curvature as the radius decreases, and approaches asymptotically an infinite value at the end of the droplet's lifetime because of the decrease in surface area. Reference 26 reports a similar calculated behavior in the rate of change of radius with time for 50/50 Aerozine droplets in the combustion chamber of a rocket motor.

Figure 3.7 shows graphically the variation with time of the heat transfer by conduction at the droplet surface. The evolution with time of the one-dimensional composition and temperature profiles in the film is shown in Figures 3.8 and 3.9 respectively. Thermal and concentration boundary layer

thicknesses increase with time first and then decrease. Temperature and composition gradients at the droplet surface are of the order of 10^3-10^4 $^oK/cm.$ and 10^1 g-mole A/g-mole cm., respectively.

Thus far only ambient conditions where steady state solutions exist (Figure 2.13) have been considered. Supercritical pressure conditions where a droplet may approach or exceed its thermodynamic critical temperature by an unsteady process will be considered next.

Figures 3.10, 3.11, and 3.12 show the vaporization history for a carbon dioxide droplet, of 1000-micron initial radius, 0.9 T_{cA} initial temperature, vaporizing in nitrogen under constant ambient conditions of 1184^oK and 112 atmospheres ($1.53P_{cA}$). For these supercritical pressure conditions a carbon dioxide droplet vaporizing in nitrogen continuously heats up from its initial conditions until disappearance, crossing in the process a critical mixing point when the liquid temperature is equal to $0.95T_{cA}$, namely point D in Figure 2.2. The vaporization history is carried out in time until the droplet has slightly exceeded its thermodynamic critical temperature. It is observed from Figure 3.10 that the droplet reaches its critical temperature very rapidly with little vaporization taking place, thus becoming a dense mass of vapor. Therefore, the underlying assumption in Spalding's point source theory and Rosner's distributed source

theory, i.e., that the droplet rapidly becomes a dense vapor, is understood by taking into consideration the high temperatures prevailing in the combustion chamber of a rocket motor. No noticeable effect is exhibited by the liquid temperature, which varies almost linearly in the region of the critical temperature, as the droplet crosses critical mixing point D. Although the percent-mass-vaporized and droplet radius curves exhibit essentially the same behavior as in the previous histories shown, their corresponding instantaneous values for the rate of vaporization and rate of change of radius with time do exhibit a discontinuity at the critical mixing point. For these particular ambient and initial conditions, the rate of vaporization increases from its initial value until the critical mixing point is reached, decreasing thereafter by a different unsteady mechanism. The droplet radius does not exhibit any observable thermal expansion in the early part of the vaporization process. The rate of change of droplet radius with time shows a discontinuity at the critical mixing point, reflecting the one in the mass vaporization rate.

Figure 3.13 illustrates the vaporization history for a carbon dioxide droplet, of 1000-micron initial radius, $0.8T_{cA}$ initial temperature, vaporizing in nitrogen under constant ambient conditions of $646^{o}K$, and 112 atmospheres ($1.53P_{cA}$). As in the previous history the droplet crosses critical mixing point D during the vaporization process. The history is

carried out in time until the critical temperature has been reached, where approximately 98 percent of the droplet mass has been vaporized. Under these relatively low ambient temperature conditions most of the droplet's lifetime is spent in subcritical temperature states. Surface-to-volume effects are observed in the temperature response during the latter part of the vaporization process. Instantaneous values for the rate of vaporization and rate of change of droplet radius with time are shown in Figure 3.14. Since the critical mixing point, D, is crossed after the mass vaporization rate has reached its maximum, the discontinuity in the rate of vaporization is barely observable. Both of these discontinuities in the rate of vaporization and rate of change of droplet radius with time cannot be detected through the data of Figure 3.13.

A supercritical vaporization history, where steady state conditions exist and the droplet does not cross any critical mixing point during its vaporization, is shown in Figure 3.15 for a carbon dioxide droplet, of 1000-micron initial radius, $0.8T_{cA}$ initial temperature, vaporizing in nitrogen under constant ambient conditions of 374°K, and 112 atmospheres ($1.53P_{cA}$). It is observed that the vaporization process is similar to the one depicted in Figure 3.5 where the initial droplet conditions are close to steady state. The droplet only approaches its steady state conditions. The rate of convergence in the temperature response

is very slow with a maximum value in the rate of change of liquid temperature with time equal to 0.9°K/sec., reflecting the fact that most of the energy conducted to the droplet is utilized to evaporate the liquid. From Figure 3.16 it is noted that the rate of surface regression is negative during the entire vaporization process.

It is observed from Figures 3.11, 3.12, and 3.14 that the rate of vaporization decreases as a critical mixing point is crossed and the rate of change of droplet radius with time exhibits a discontinuity. Although a simple physical explanation cannot be given due to the coupling between heat and mass transfer phenomena, the mole fraction of carbon dioxide at the droplet surface was found to decrease after a critical mixing point was crossed, thus decreasing the potential for mass transfer. Accordingly, the thermal conductivity and density of the CO_2-N_2 gaseous mixture surrounding the droplet decrease also, modifying the heat transfer conducted to the surface.

Comparisons with a Low Pressure Unsteady Model

It is of interest to compare the foregoing unsteady results with those predicted by the low pressure semi-empirical theory of Reference 10 for the case of zero relative velocity. The purpose of this comparison is threefold:

a. Because the semi-empirical theory of Reference 10 was developed for droplet vaporization under low pressure environmental conditions, the effects associated with dense mixtures, the effects of pressure upon the physical properties, and the variation of the properties through the vapor film are not taken into account. Thus, the overall effect of these corrections can be estimated by simple means.

b. Because the results presented in this work are difficult to reproduce for another binary system which may be of interest, or experimental verification of the CO_2-N_2 results may not be feasible, the trends predicted by the above unsteady calculations may be compared through a third vaporization theory which is simple, and only requires average low pressure properties.

c. The applicability range of the semi-empirical theory can be estimated.

Reference 10 shows in detail the derivation of the equations involved in the analysis. Therefore, only the final expressions used in the calculations are reproduced here for convenient reference.

The molar vaporization rate is given by

$$w = \frac{4\pi r_o P D_{AB}}{R T_{av}} \ln \frac{P}{P - p_v} \qquad [3.69]$$

$$= - 4\pi r_o^2 c_A^{\ell} \frac{dr_o}{dt} - \frac{4}{3}\pi r_o^3 \frac{dc_A^{\ell}}{dt} \qquad [3.70]$$

The rate of change of droplet temperature with time is computed by the following expression ($T^{\ell} \leq T_{cA}$):

$$\frac{dT^{\ell}}{dt} = \frac{w c_{pA} (T_\infty - T^{\ell})}{m_d c_{pA}^{\ell} \left(\exp \frac{w c_{pA}}{4\pi k r_o} - 1 \right)} - \frac{\lambda w}{m_d c_{pA}^{\ell}} \qquad [3.71]$$

where

$$T_{av} = \frac{T_\infty + T^{\ell}}{2} \qquad [3.72]$$

$$k = \frac{p_v}{2P} k_A + \left(1 - \frac{p_v}{2P}\right) k_B \qquad [3.73]$$

In the calculations which follow, low pressure values for D_{AB}, k_A, k_B, and c_{pA} were used. these properties were evaluated at the average temperature T_{av}. Similarly, p_v, λ, c_A^{ℓ}, and c_{pA}^{ℓ} were taken at the pure liquid saturation conditions corresponding to T^{ℓ}. Property correlations were determined from References 19, 23, and 31. Vaporization histories were computed numerically be a recursive formula of the third category due to Heun[8].

Before discussing the results it is of interest to note that, for the case of steady state conditions, Equation [3.71]

reduces identically to Equation [1.18] derived by making use of the equations of change and assuming constant mean low pressure properties throughout the film, namely k, and c_{pA}. However, the rate of vaporization expression,[3.69],does not reduce to[1.14]. Equation [3.69] may be derived using the equations of change and assuming a constant mean value for the ratio (D_{AB}/T) throughout the postulated mixture of ideal gases surrounding the droplet.

As it was discussed above, the initial values for the rate of vaporization are largely enhanced by the ambient temperature through the coupling in the temperature and composition profiles, for the same liquid temperature. Inspection of Equation [3.69] indicates that the initial values for the vaporization rate can only be enhanced through the ratio $(D_{AB}/T)_{av}$.

Figures 3.17 and 3.18 show a comparison between the vaporization histories previously presented in Figures 3.3 and 3.5 and those predicted by the low pressure semi-empirical theory (Equations [3.69] and [3.71]). Under these near critical conditions the agreement between these calculated results is very reasonable considering the simplicity in the latter calculations. The percent-mass-vaporized curves, which are important in the determination of the droplet's lifetime, agree with no substantial difference between them. This is not to say that the instantaneous vaporization rates also agree

with each other, as illustrated graphically in Figures 3.19 and 3.20. The initial values for the mass vaporization rate differ approximately by a factor of 2. Agreement in vaporization rates within approximately 20 percent is usually regarded as quite good.

A comparison between supercritical vaporization histories is shown in Figures 3.21 through 3.24. It is observed from Figures 3.21 and 3.22 that the droplet also reaches its critical temperature by an unsteady process in the latter calculations, although without physical reason. As it was shown graphically in Figure 2.14, Equations [3.69] through [3.71] do not yield either steady state solutions for these particular nitrogen conditions, therefore, the unsteady mathematical process is carried out until the critical temperature is reached. Initial values for the mass vaporization rate are lower in the latter calculations by a factor greater than 2. Figures 3.23 and 3.24 show a substantial disagreement between calculated results under high density conditions, namely high pressures and low ambient temperatures. The droplet's lifetime differs by a factor of approximately 1.5 in this case. High density conditions are important in high pressure sprays, as those encountered in operating diesel engines. Since the effects of total pressure on vapor pressure and enthalpy of vaporization are considerable under these conditions (Figures 2.2 and 2.3), the results predicted by the simplified vaporization theory can

be greatly improved by taking into account these effects. Figures 3.25 and 3.26 show a comparison between calculated results at high densities by taking into account the effects of total pressure on vapor pressure and enthalpy of vaporization. It is observed that the agreement between vaporization times is excellent and the instantaneous vaporization rates agree with no substantial difference between them. Therefore, vaporization times under high density conditions may be estimated by the simple theory of Reference 10 provided the vapor pressure and enthalpy of vaporization are properly corrected. Unfortunately, the simplified theory ceases to be useful as soon as the critical mixing line is reached.

Concluding Remarks

The following conclusions may be drawn from the above unsteady analysis:

i. The unsteady heating-up period is most important in the vaporization process of single droplets under high pressure environmental conditions. Its importance may be estimated qualitatively if one considers that the time required by a solid sphere to reach a steady state temperature is related to the thermal diffusivity by Fourier's modulus, i.e., $t = r_o^2/\alpha$. Furthermore, making use of Equations [2.24] and [2.25] it is observed that the ratio of heating-up to steady state periods is directly proportional to the ratio $(c_{pA}/k)^{\ell}$. Although the specific heat as well as the thermal conductivity of a pure substance increase with pressure, the specific heat increases much faster in the critical region than the thermal conductivity[25]. Hence, the unsteady heating-up period is most important at high pressures.

ii. A vaporizing droplet can indeed reach and exceed its thermodynamic critical temperature, thus becoming a dense mass of vapor, at supercritical pressures by an intrinsically unsteady process. Under high enough ambient temperatures and a supercritical pressure, a droplet reaches very rapidly its critical temperature.

iii. Initial values for the mass vaporization rate are largely enhanced as the ambient temperature increases, for the same initial droplet conditions.

iv. Inclusion of the effects associated with dense mixtures, the effect of total pressure on vapor pressure and enthalpy of vaporization, as well as the pressure effect upon the thermophysical properties, cannot be disregarded in high pressure vaporization analyses.

v. Large density variations are exhibited in a small radial distance surrounding a vaporizing droplet. Temperature and composition gradients at the droplet surface are appreciable.

vi. Slight departures from the square law dependence in the variation of the droplet's lifetime with radius were found.

vii. Vaporization times may be estimated by the quasi-steady theory of Reference 10 over a wide range of temperatures and pressures, provided the vapor pressure and enthalpy of vaporization are properly corrected under high density conditions. Without corrections, the theory of the reference predicts too long vaporization times under high pressures and low ambient temperature conditions.

viii. None of the major assumptions introduced in the analysis, namely, essentially infinite liquid thermal conductivity, a continual formation of completely

fresh liquid surface, and thermodynamic equilibrium at the droplet interface preclude a droplet from reaching its critical temperature under supercritical pressure conditions by an unsteady process.

ix. As the critical temperature of the liquid is approached the absorption rate of nitrogen into carbon dioxide may become important. Therefore, the accuracy of the absolute values reported may become debatable. However, the limiting case considered is a necessary one for the absence of diffusion data.

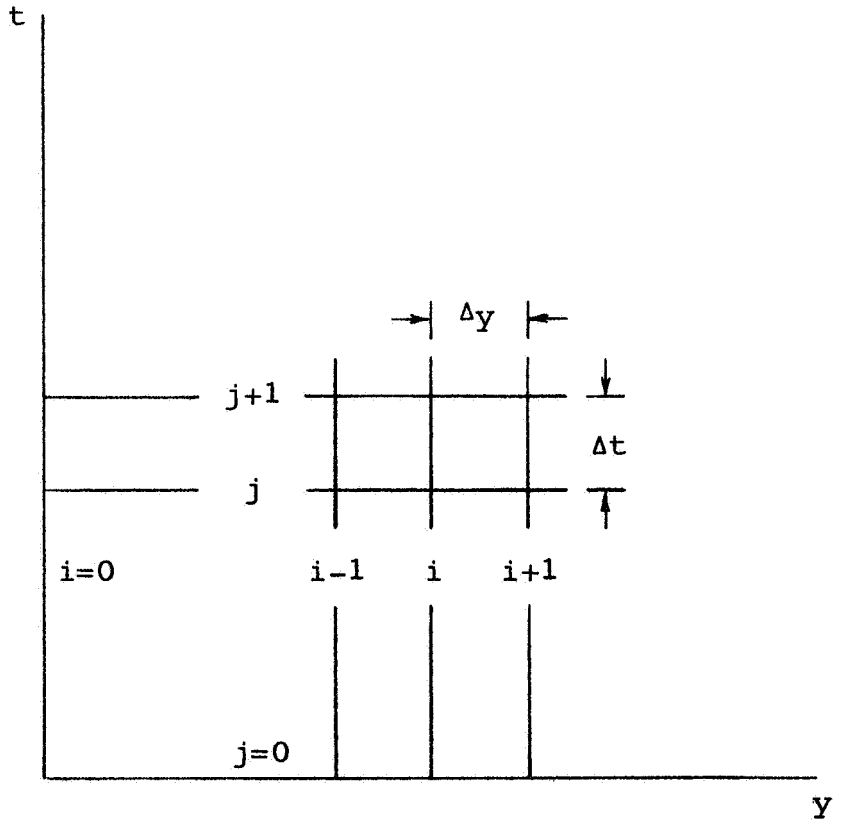

Figure 3.1. Finite-difference grid.

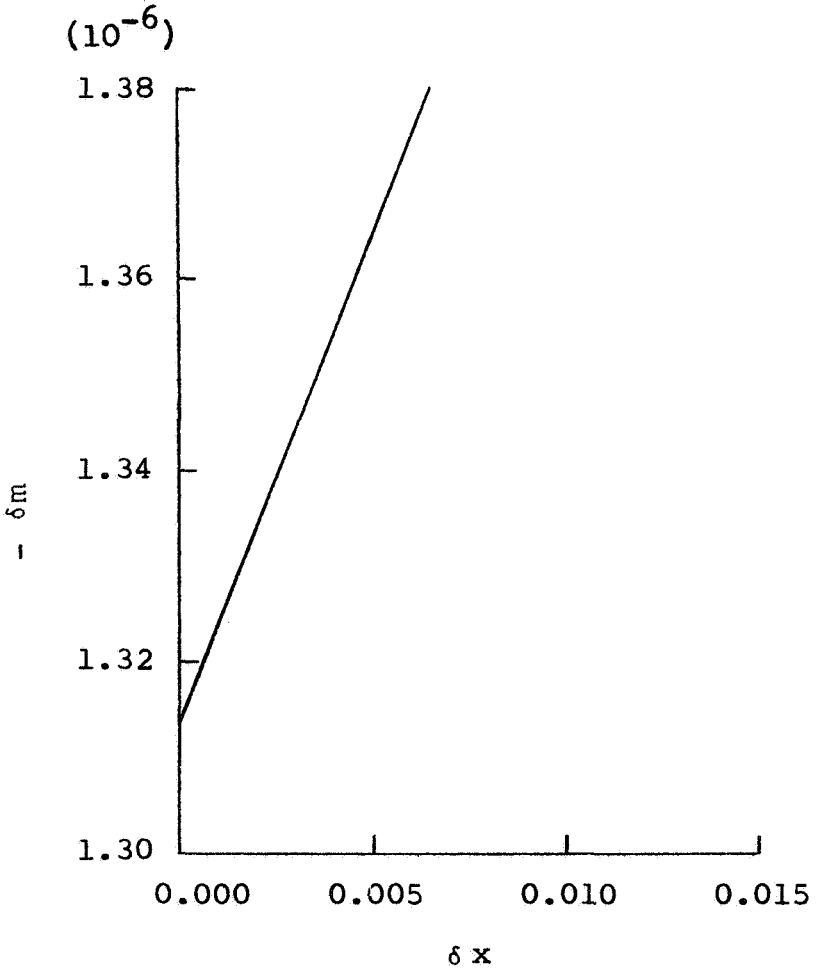

Figure 3.2. Relationship between a change in the mole fraction at the surface and the corresponding change that would be obtained in the mass of the droplet.

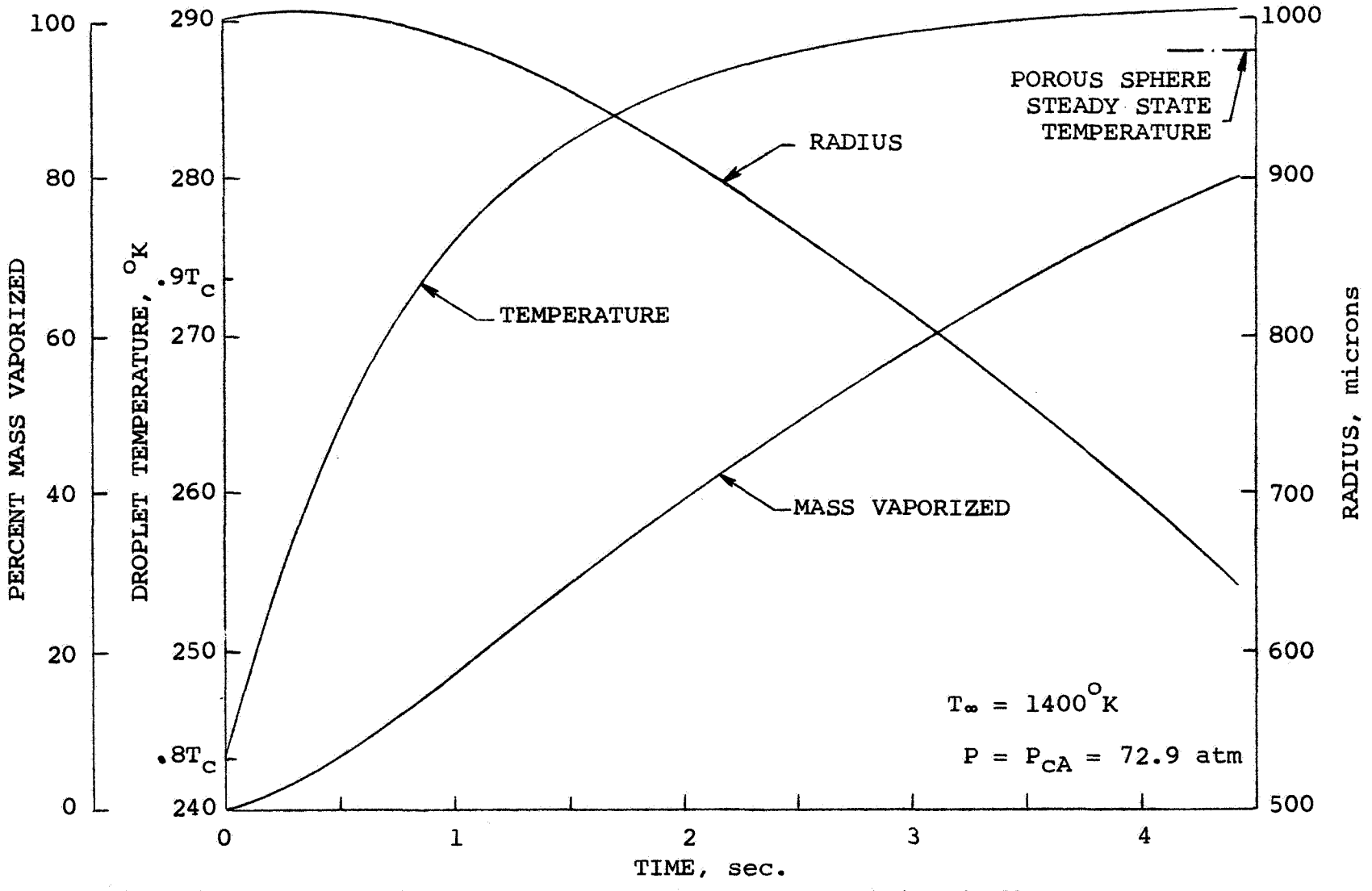

Figure 3.3. Vaporization history of a CO_2 droplet vaporizing in N_2.

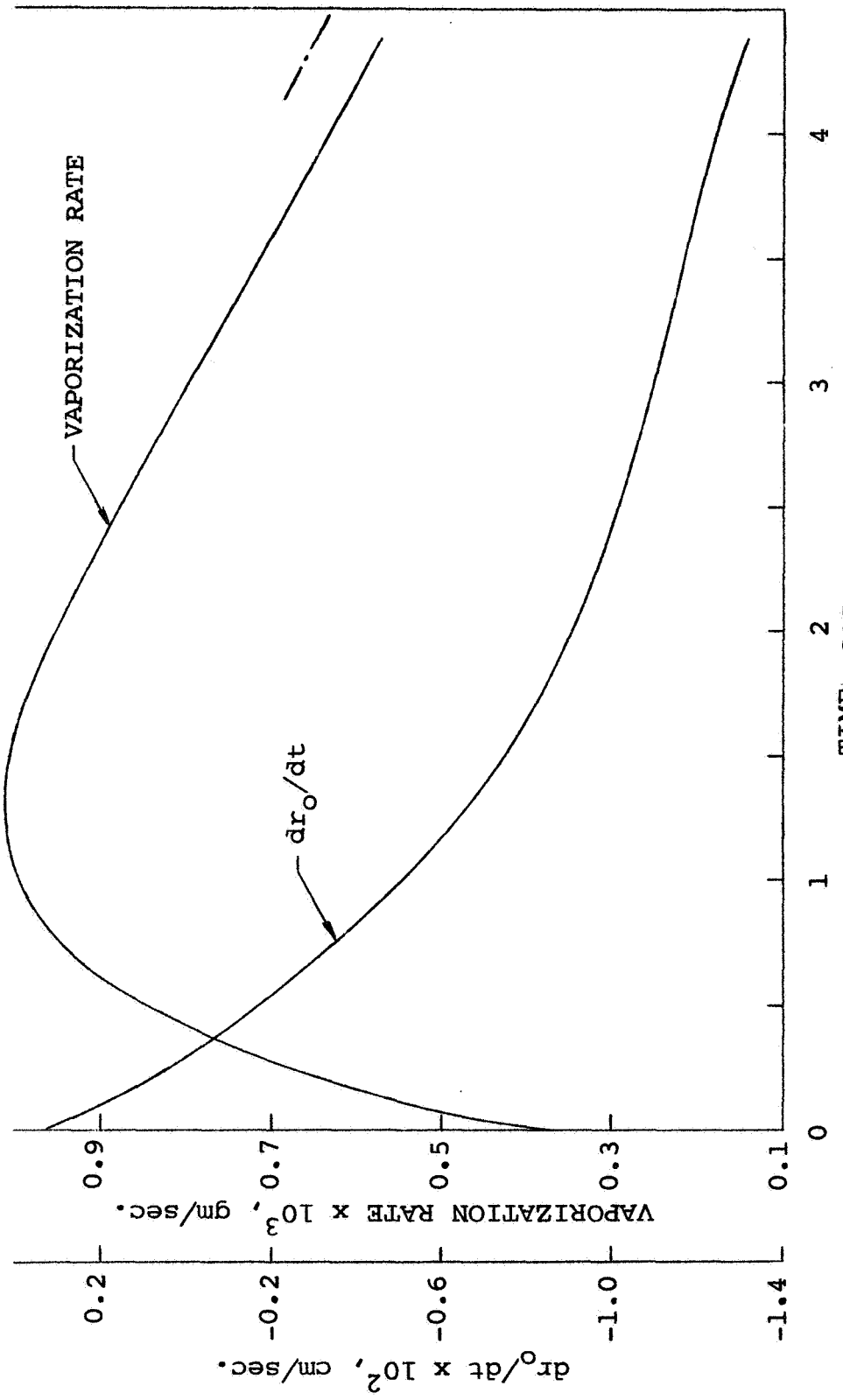

Figure 3.4. Instantaneous vaporization rates and variation of surface regression rate for the same CO_2 droplet of Fig. 3.3.

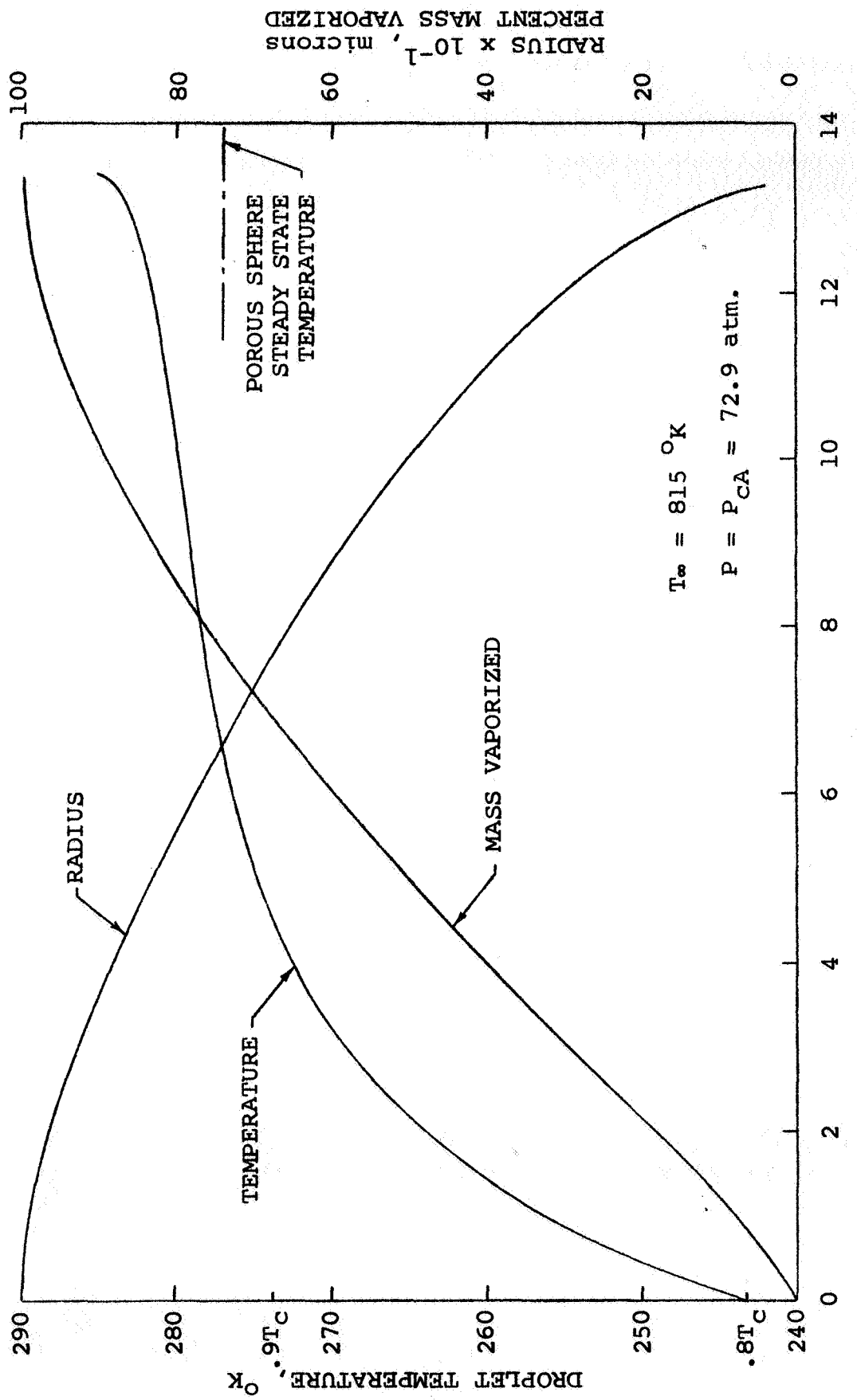

Figure 3.5. Vaporization history of a CO_2 droplet vaporizing in N_2.

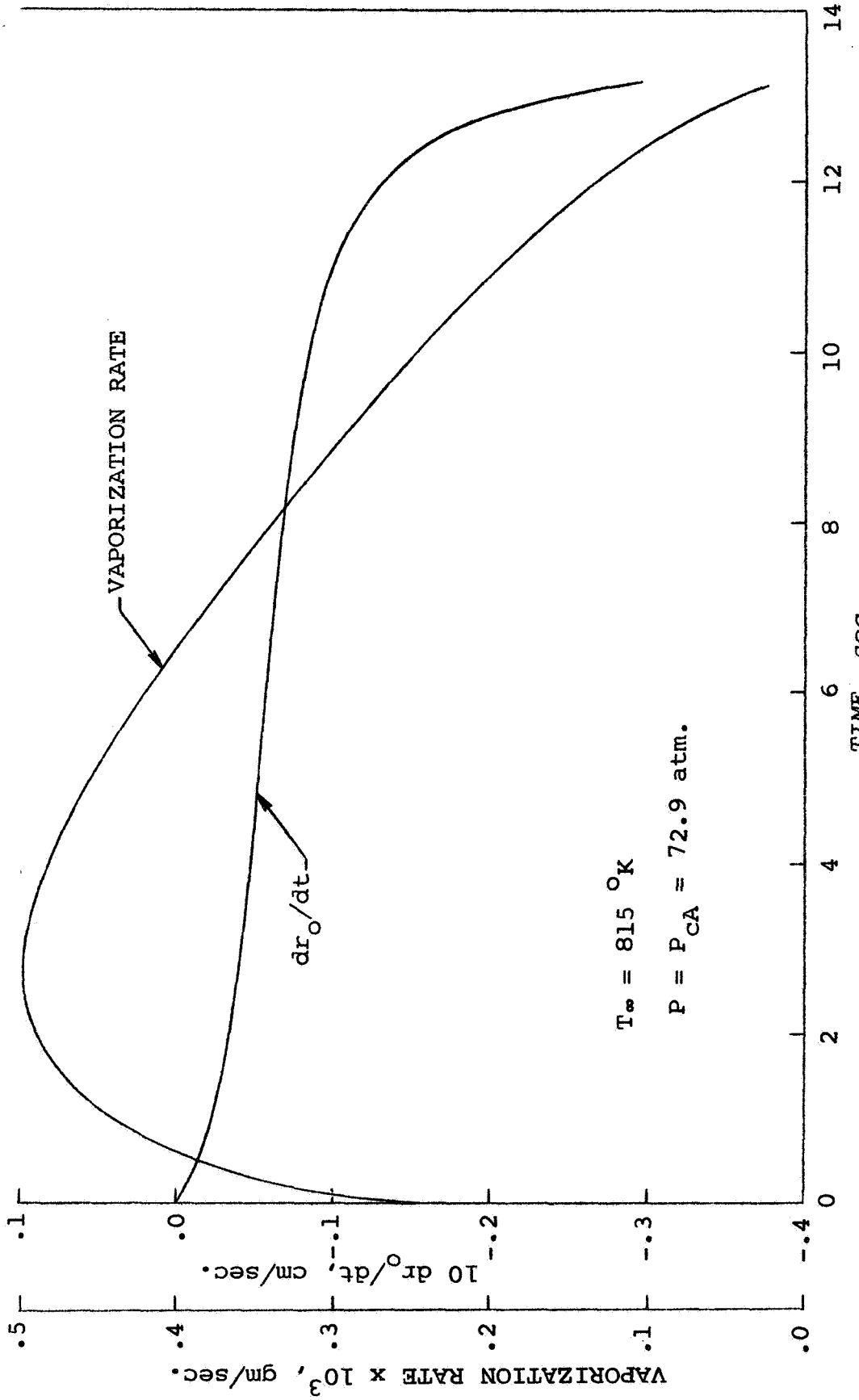

Figure 3.6. Instantaneous values for the mass vaporization rate and variation of surface regression rate.

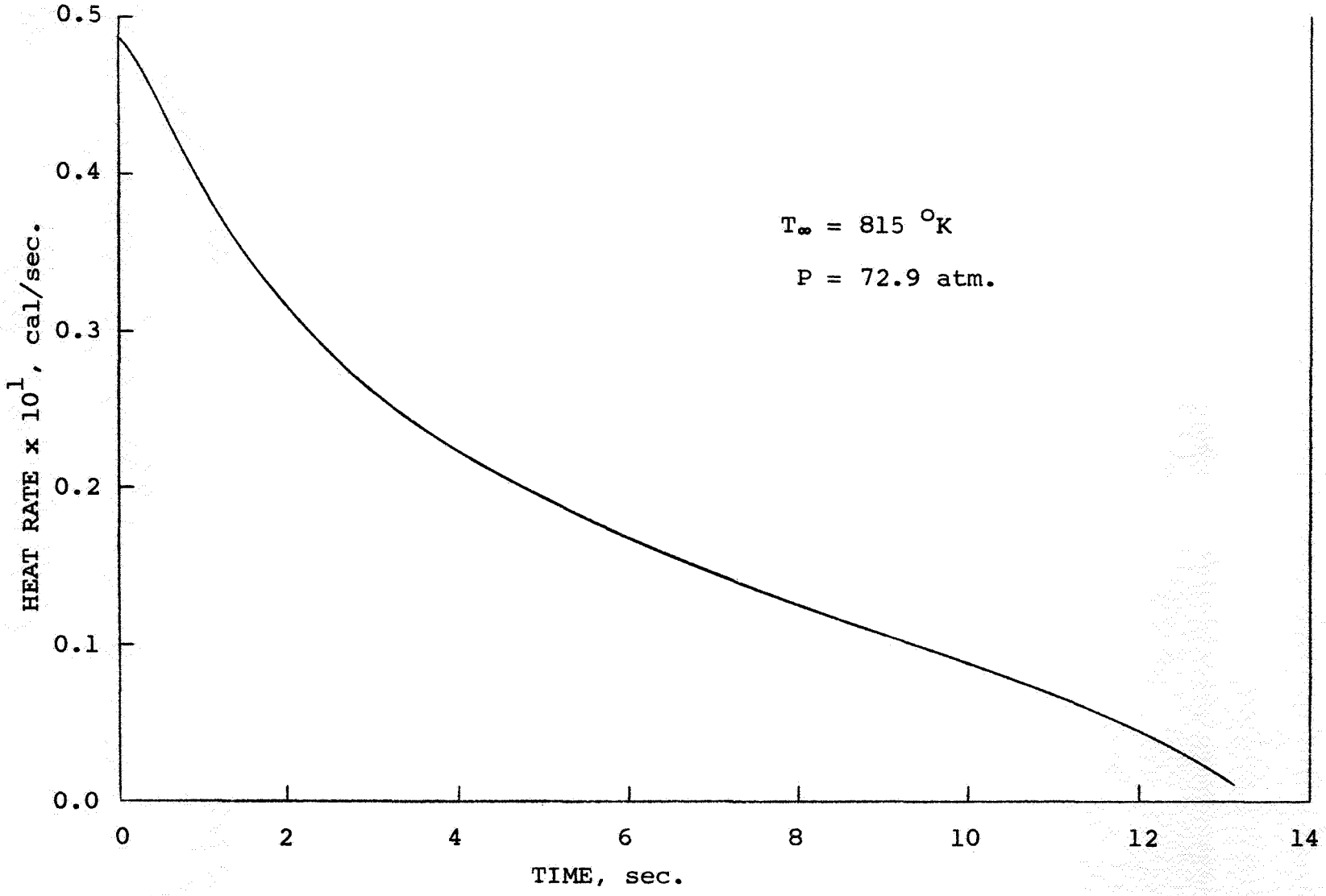

Figure 3.7. Variation with time of the heat transfer by conduction at the droplet surface.

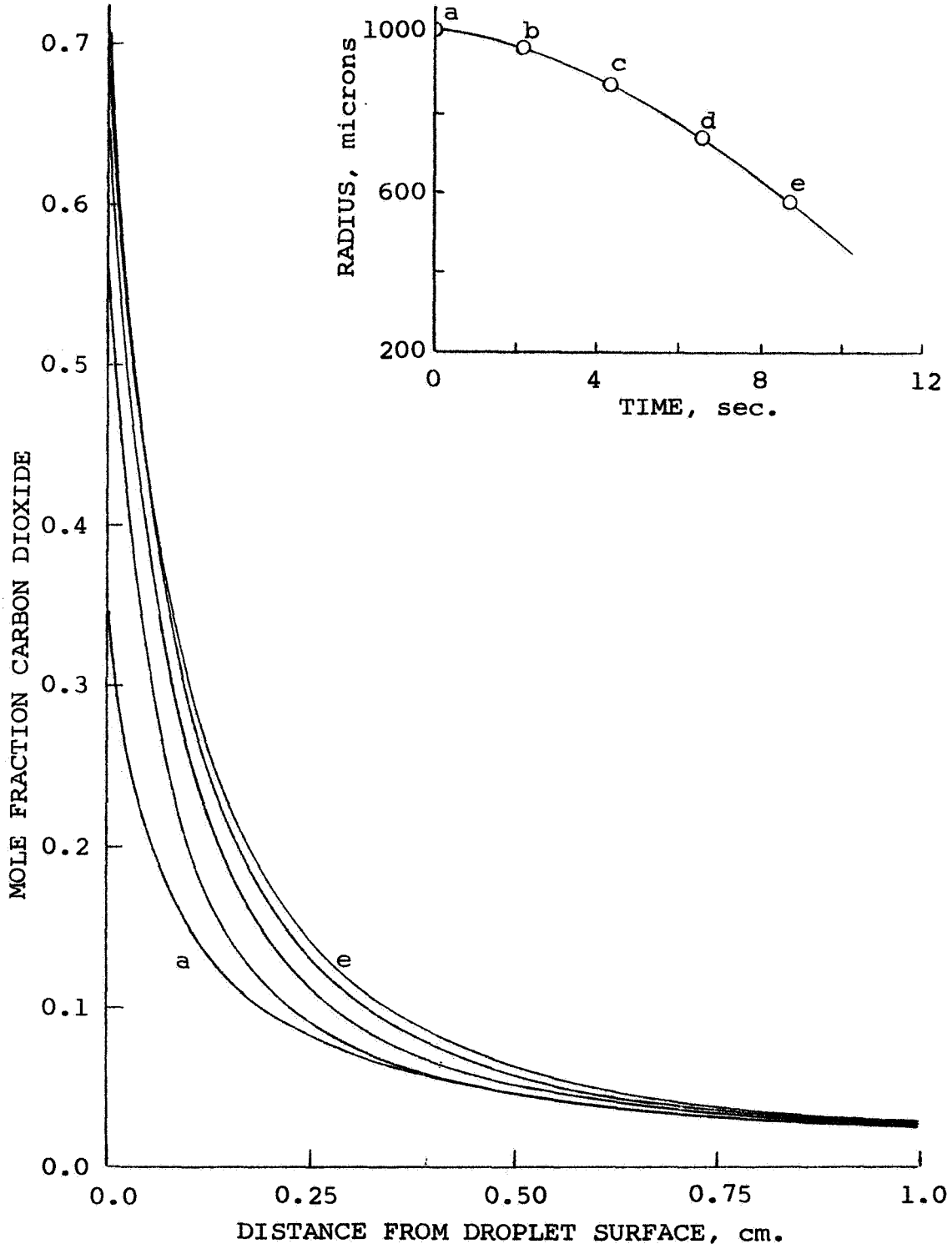

Figure 3.8. Evolution with time of the one-dimensional composition profiles in the film surrounding a vaporizing droplet. Vaporization conditions equal to those of Fig. 3.5.

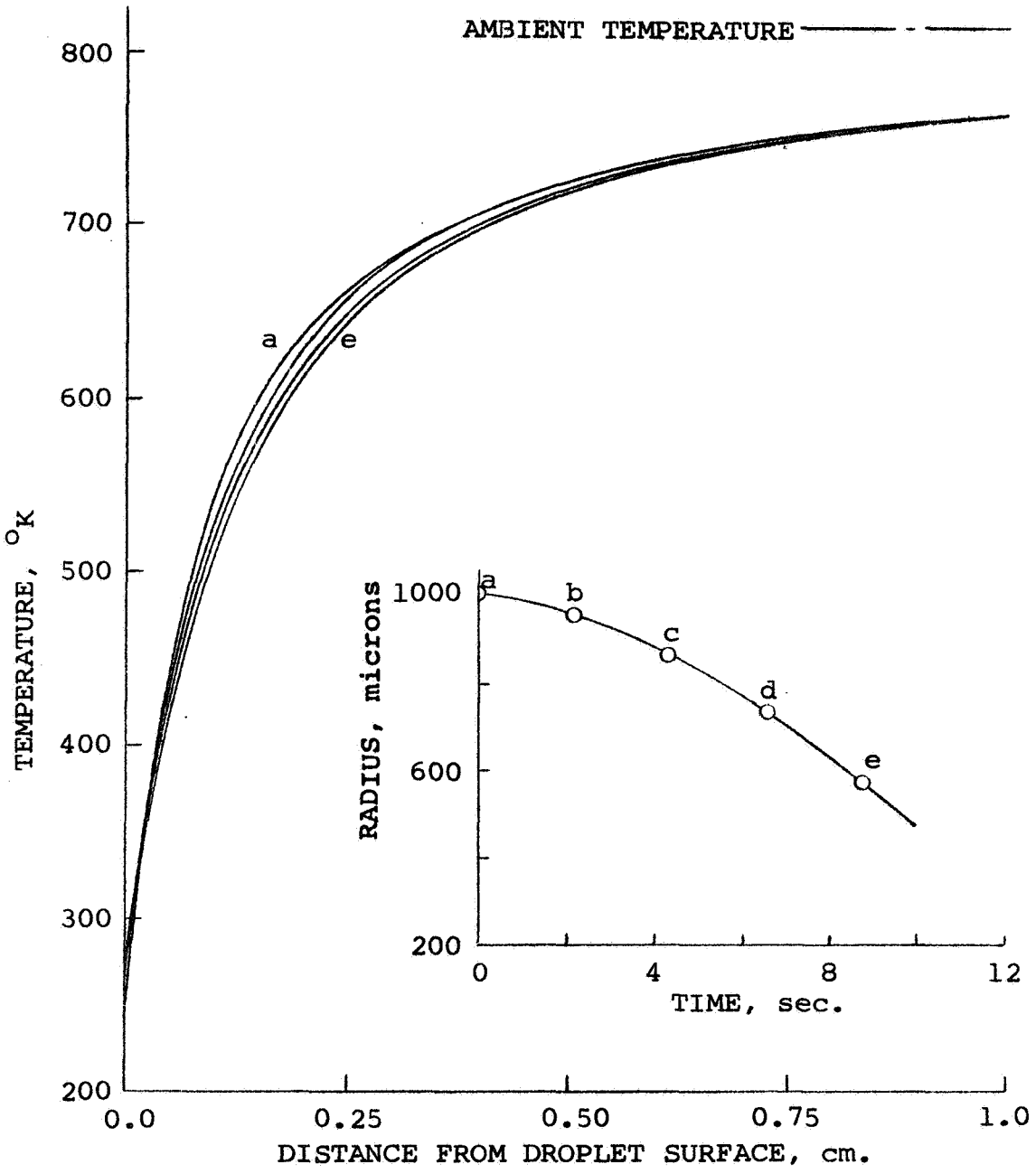

Figure 3.9. Evolution with time of the one-dimensional temperature profiles in the film surrounding a vaporizing droplet. Vaporization conditions equal to those of Fig. 3.5.

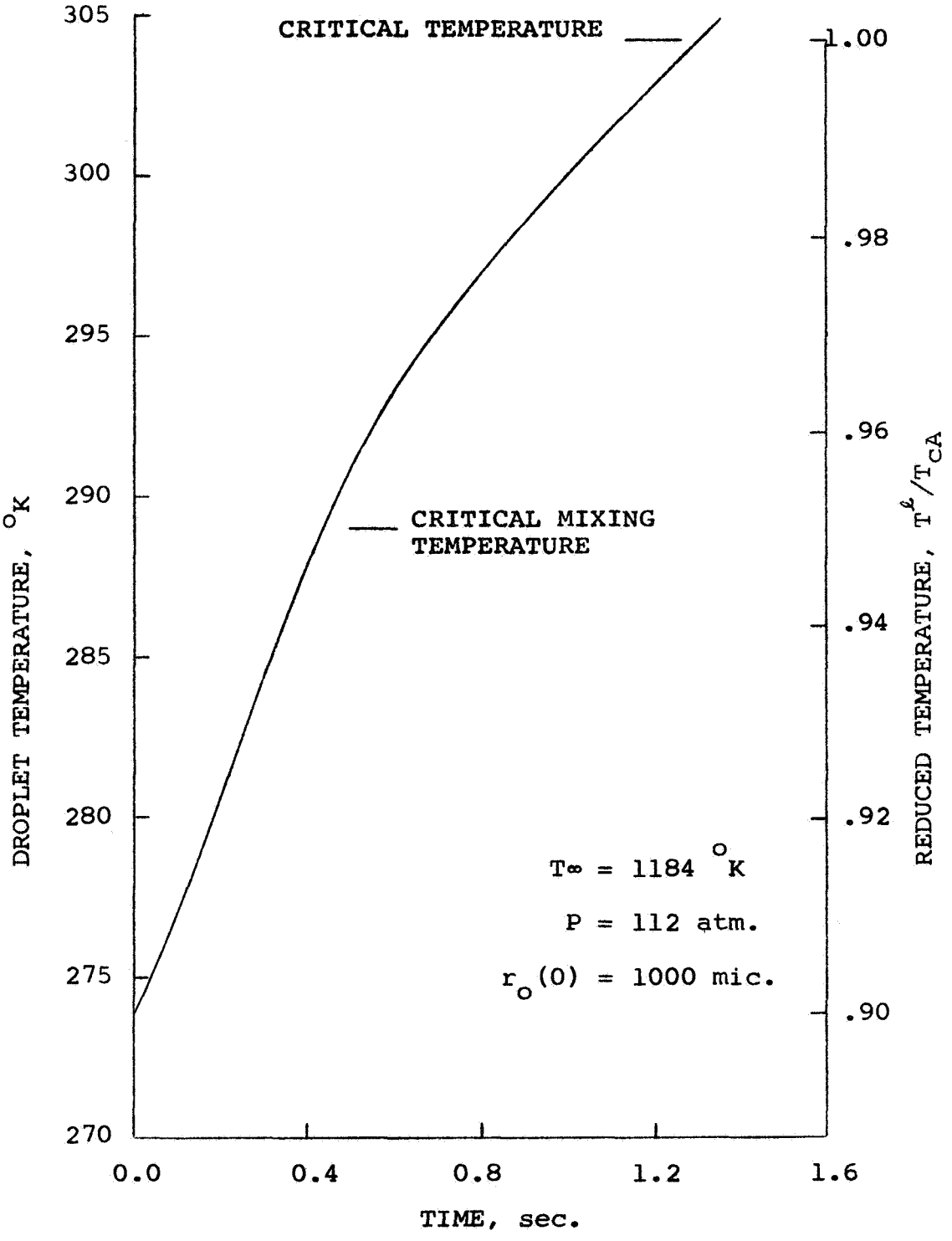

Figure 3.10. Temperature response of a CO_2 droplet vaporizing in N_2.

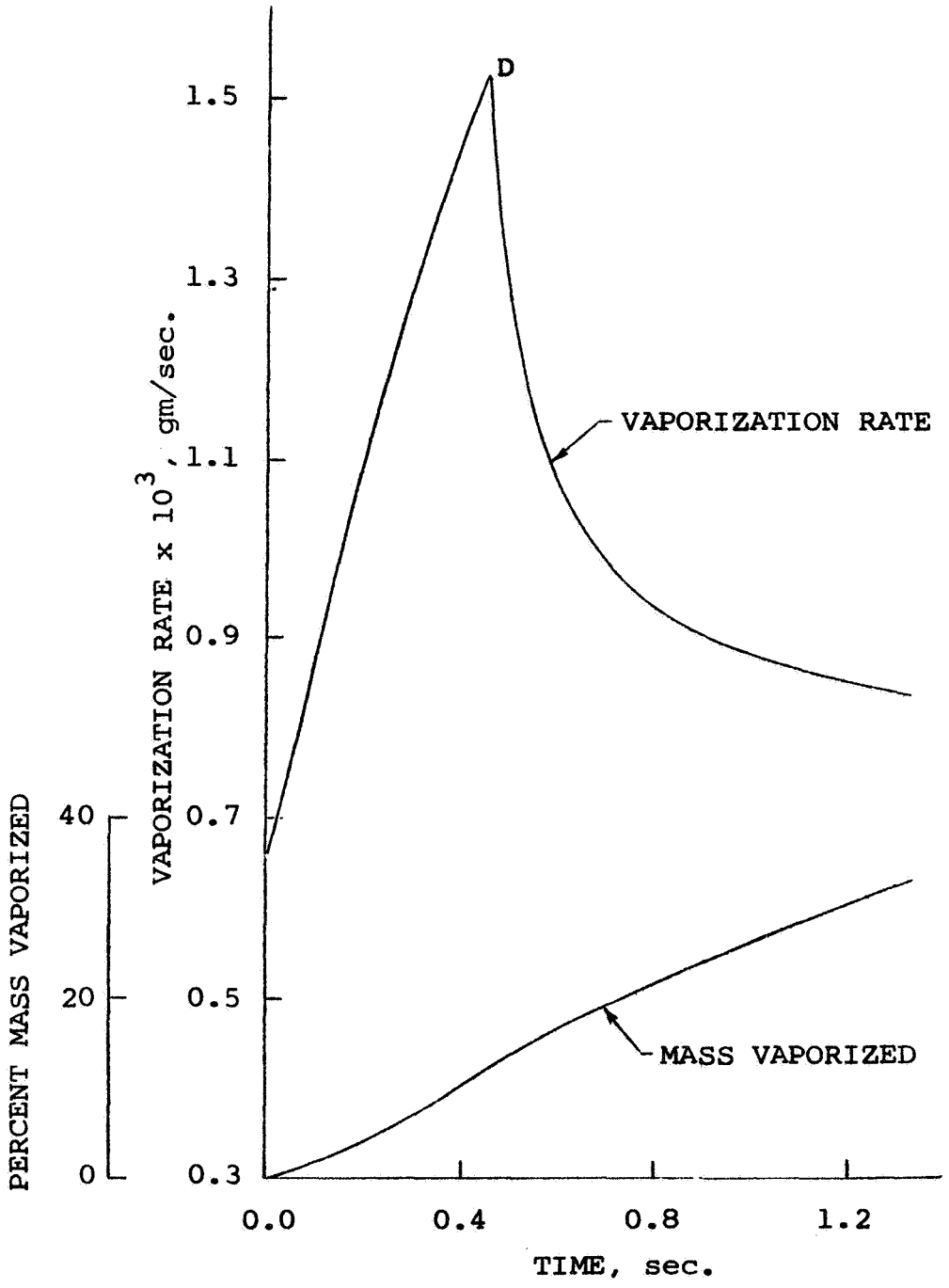

Figure 3.11. Mass vaporization rate and percent-mass-vaporized curves for the same vaporizing droplet of Fig. 3.10.

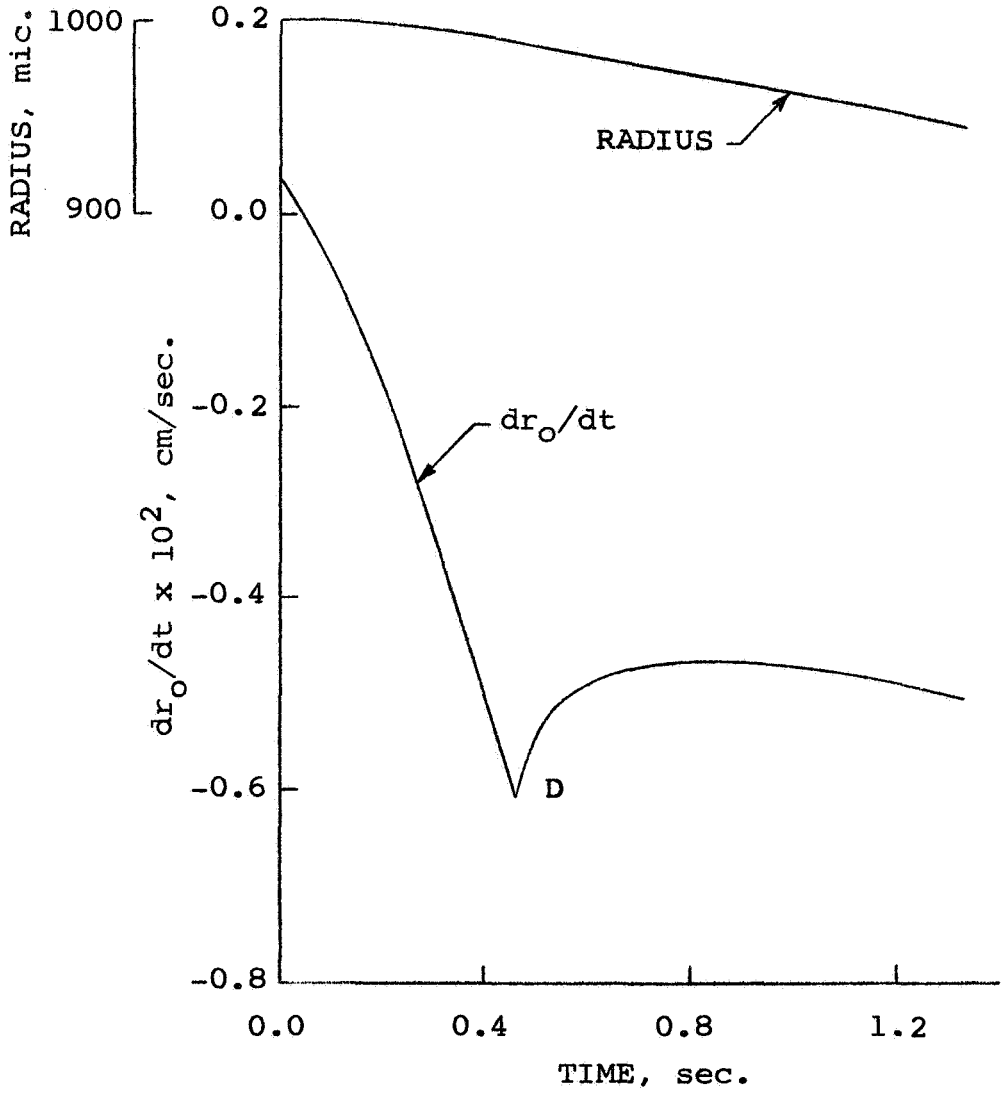

Figure 3.12. Variation and rate of change of droplet radius with time for the vaporizing droplet of Fig. 3.10.

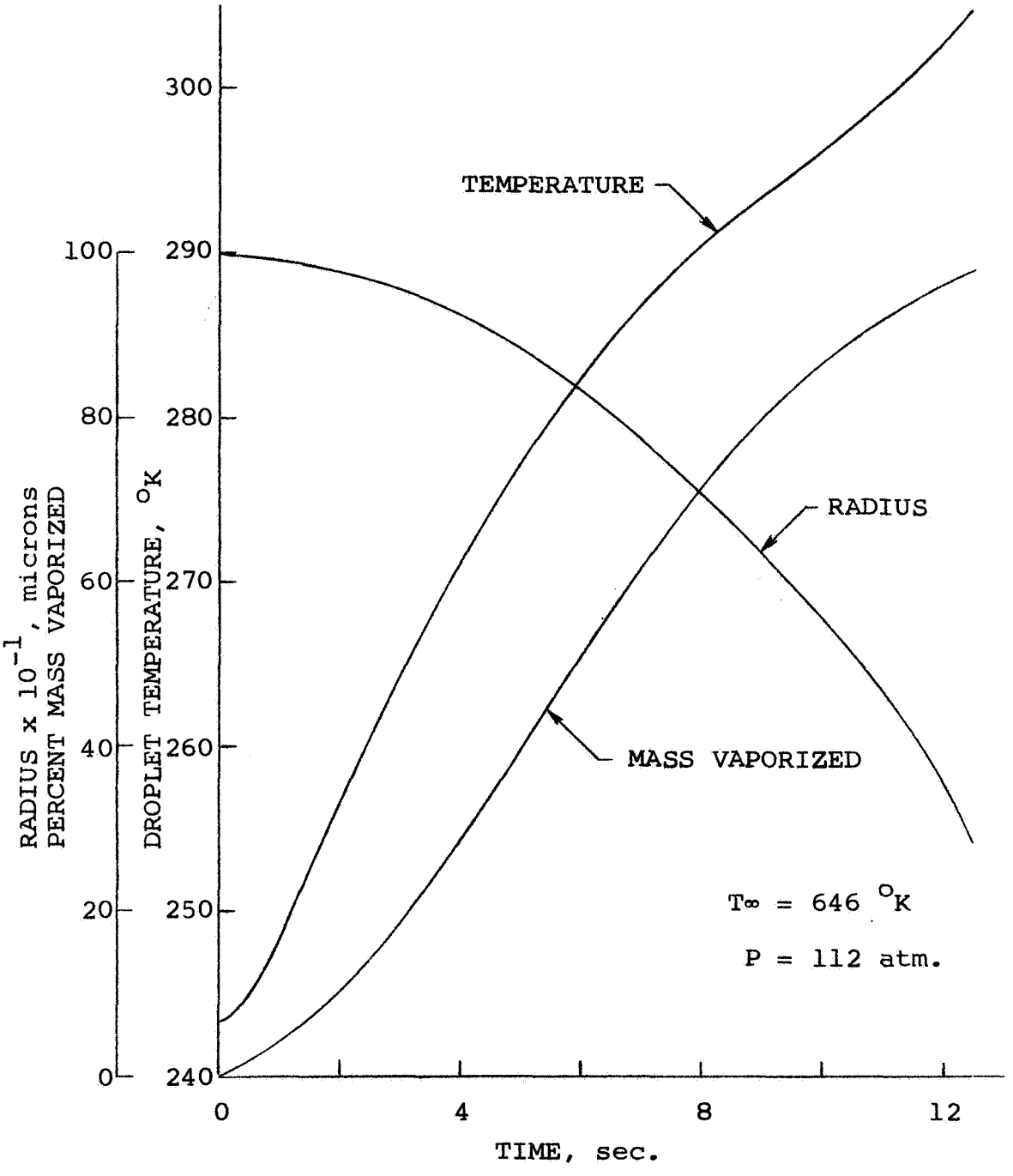

Figure 3.13. Vaporization history of a CO_2 droplet vaporizing in N_2.

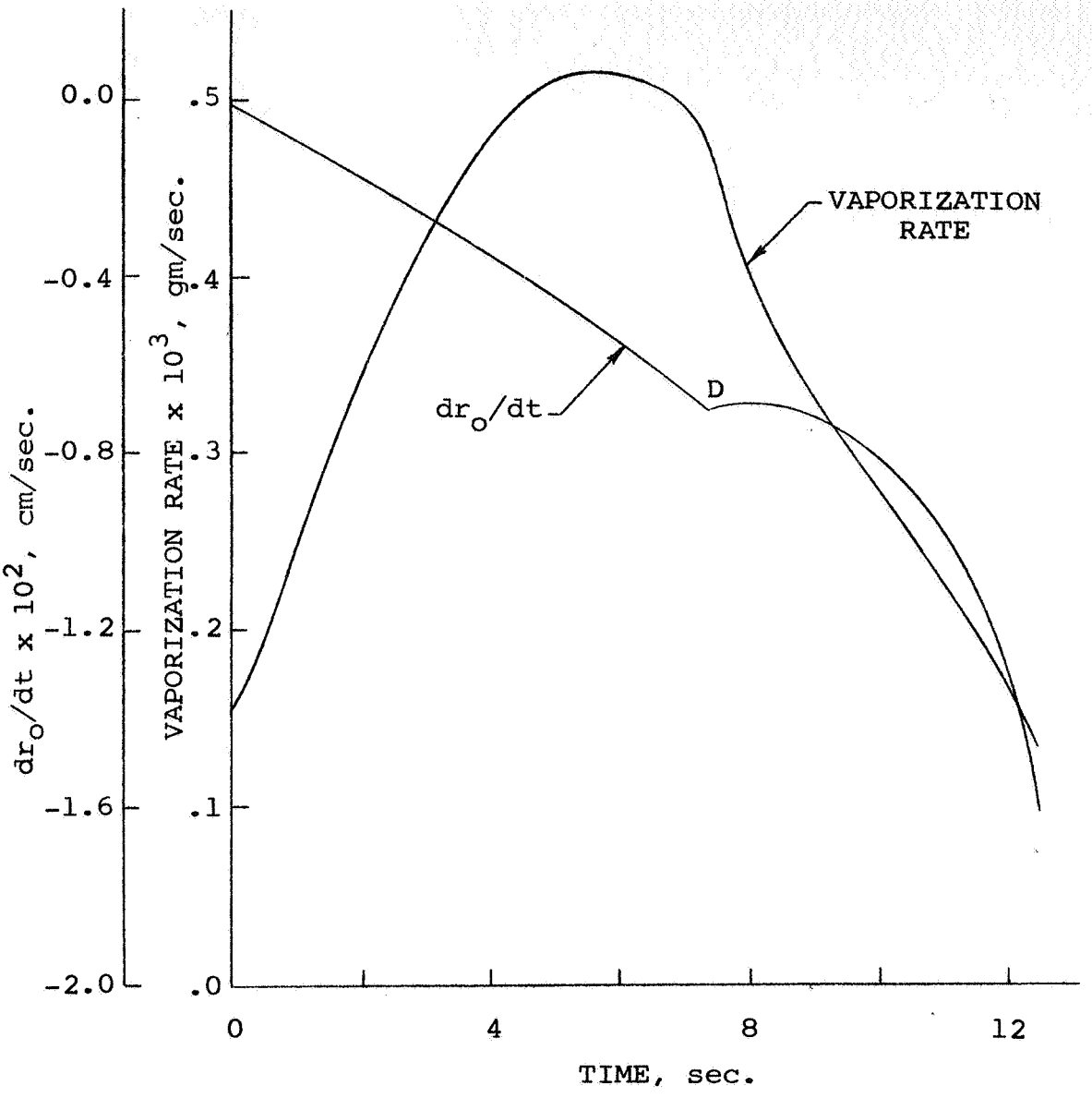

Figure 3.14. Instantaneous values for the mass vaporization rate and variation of surface regression rate.

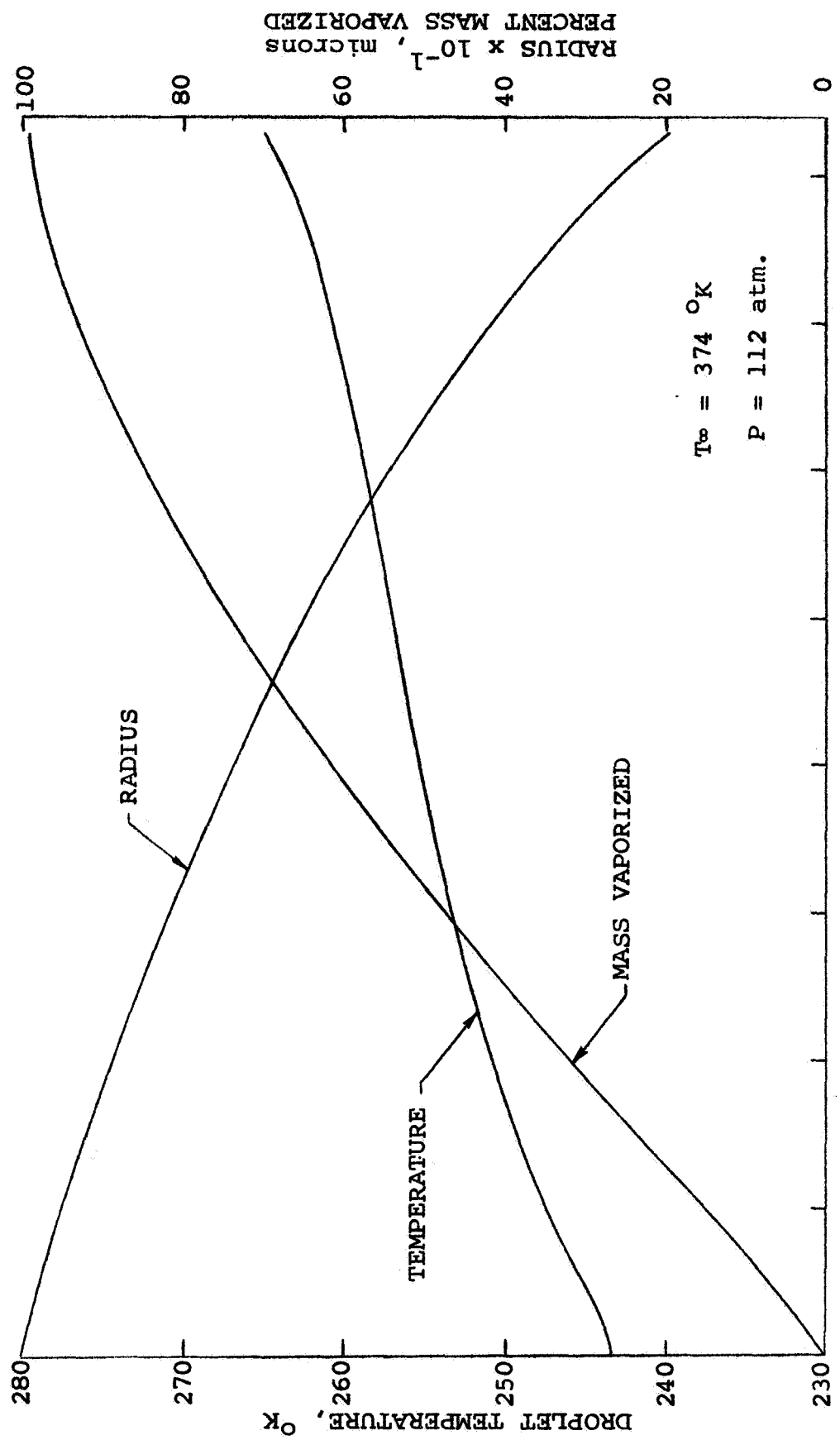

Figure 3.15. Vaporization history of a CO_2 droplet vaporizing in N_2.

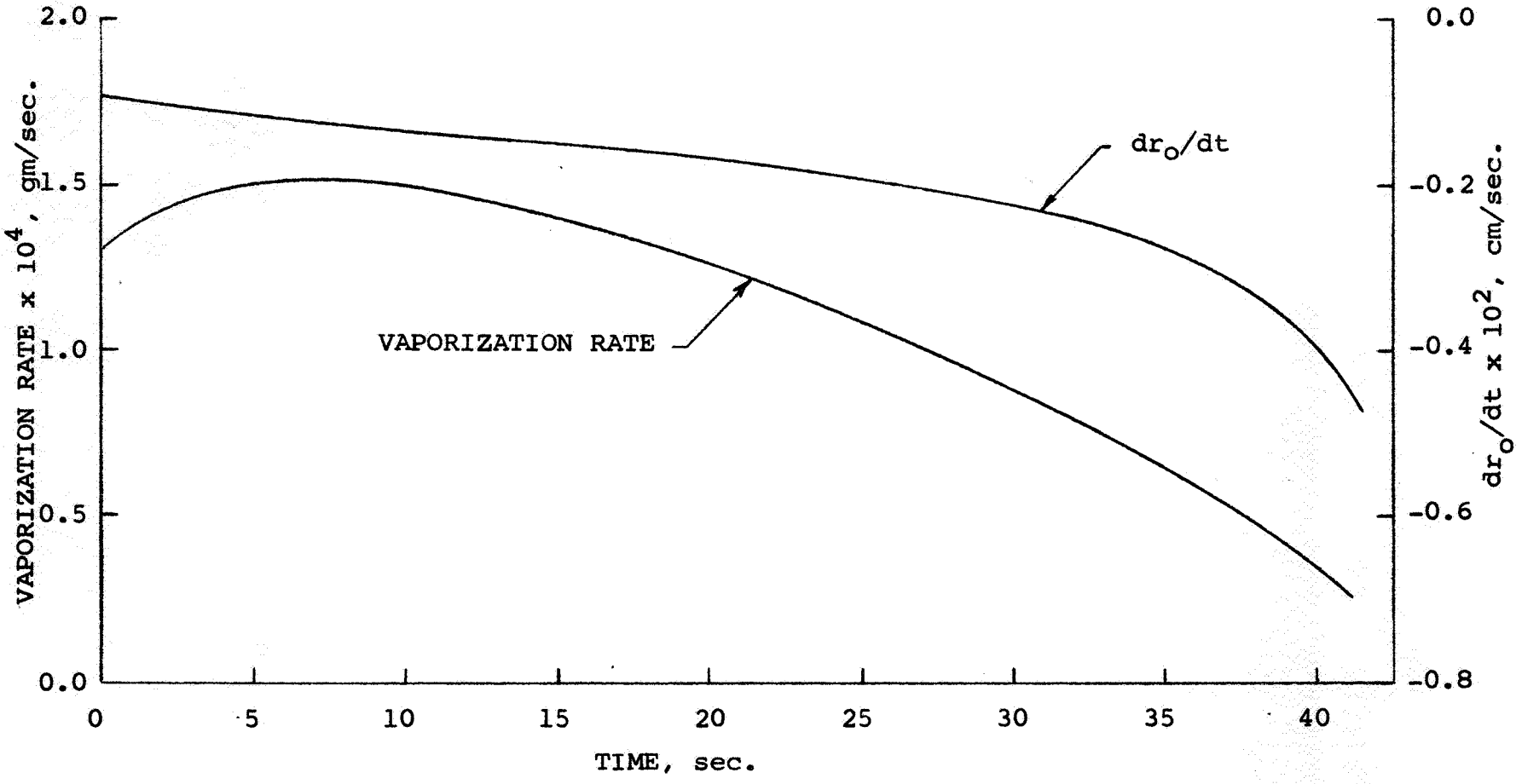

Figure 3.16. Instantaneous values for the rate of vaporization and rate of change of droplet radius with time for the same CO_2 droplet of Fig. 3.15

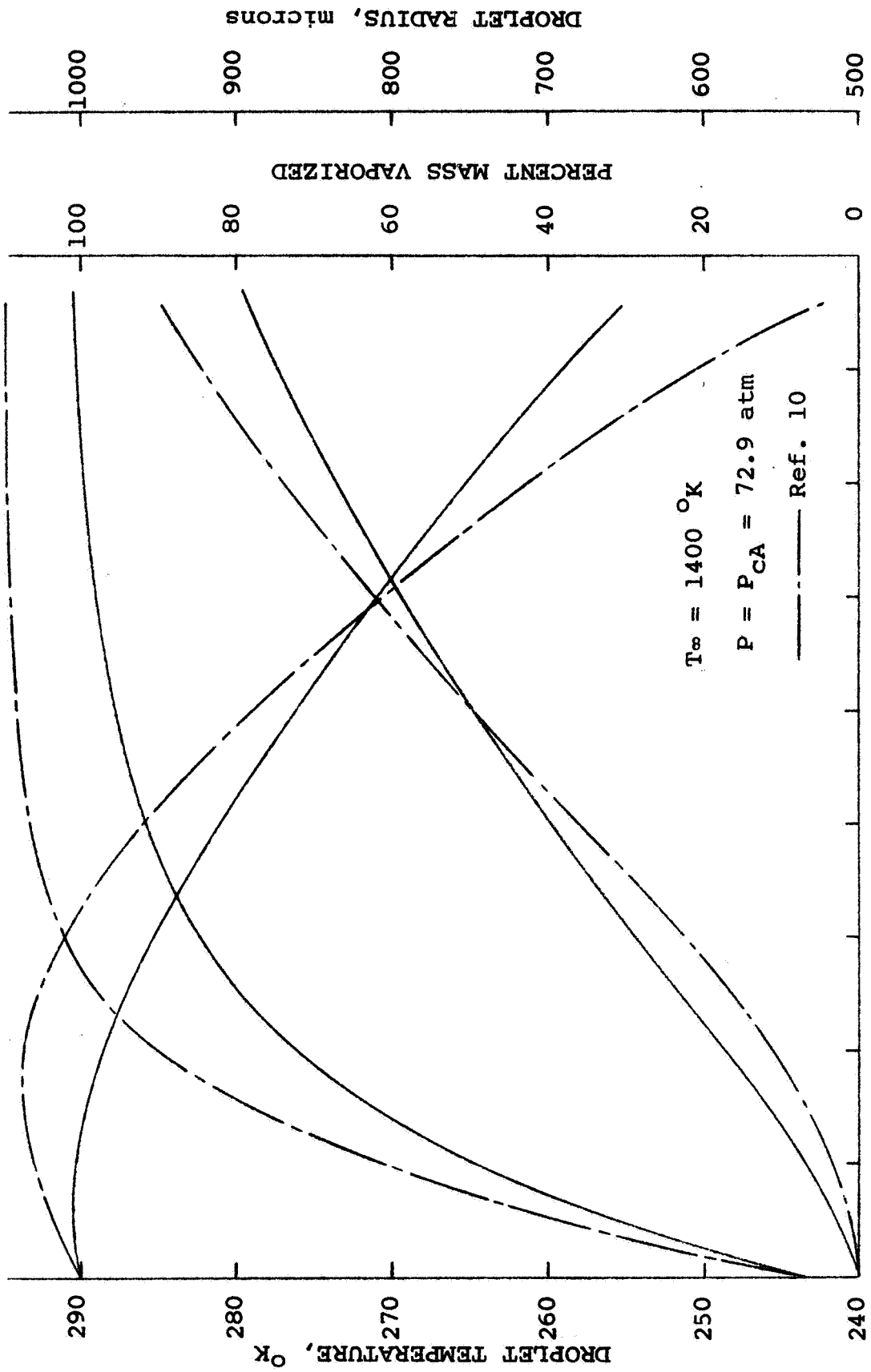

Figure 3.17. Comparison between vaporization histories.

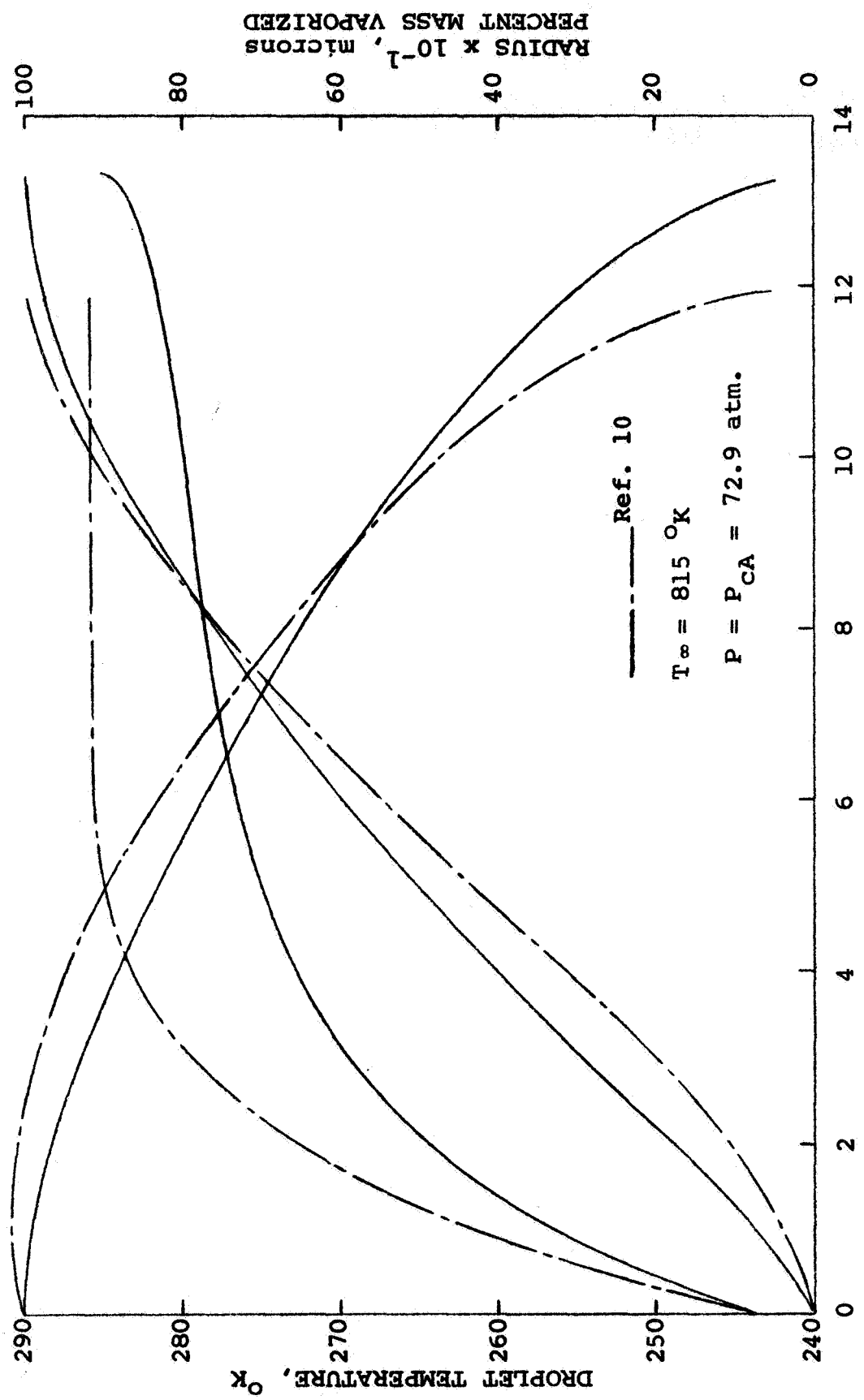

Figure 3.18. Comparison between vaporization histories.

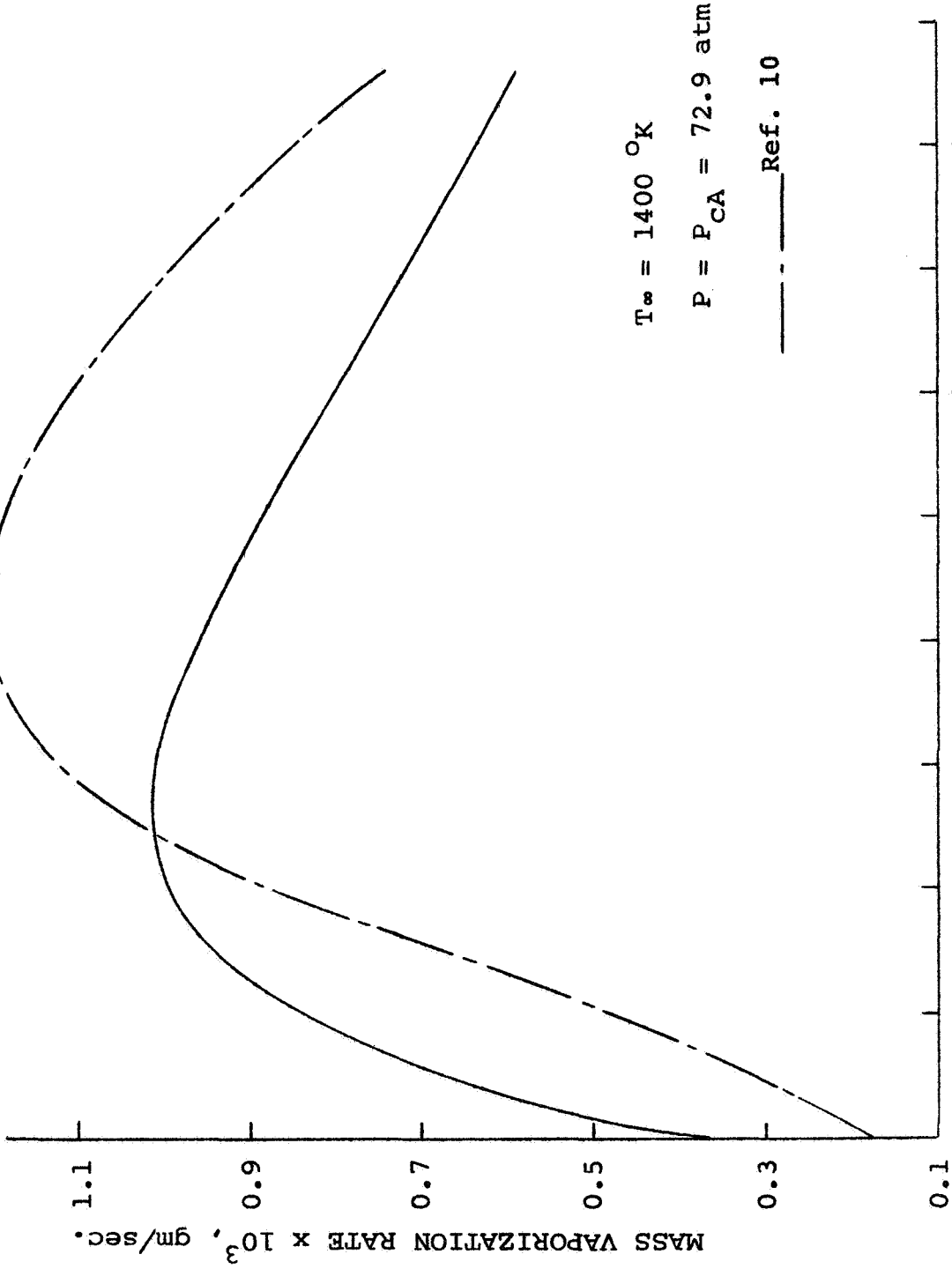

Figure 3.19. Comparison between mass vaporization rates.

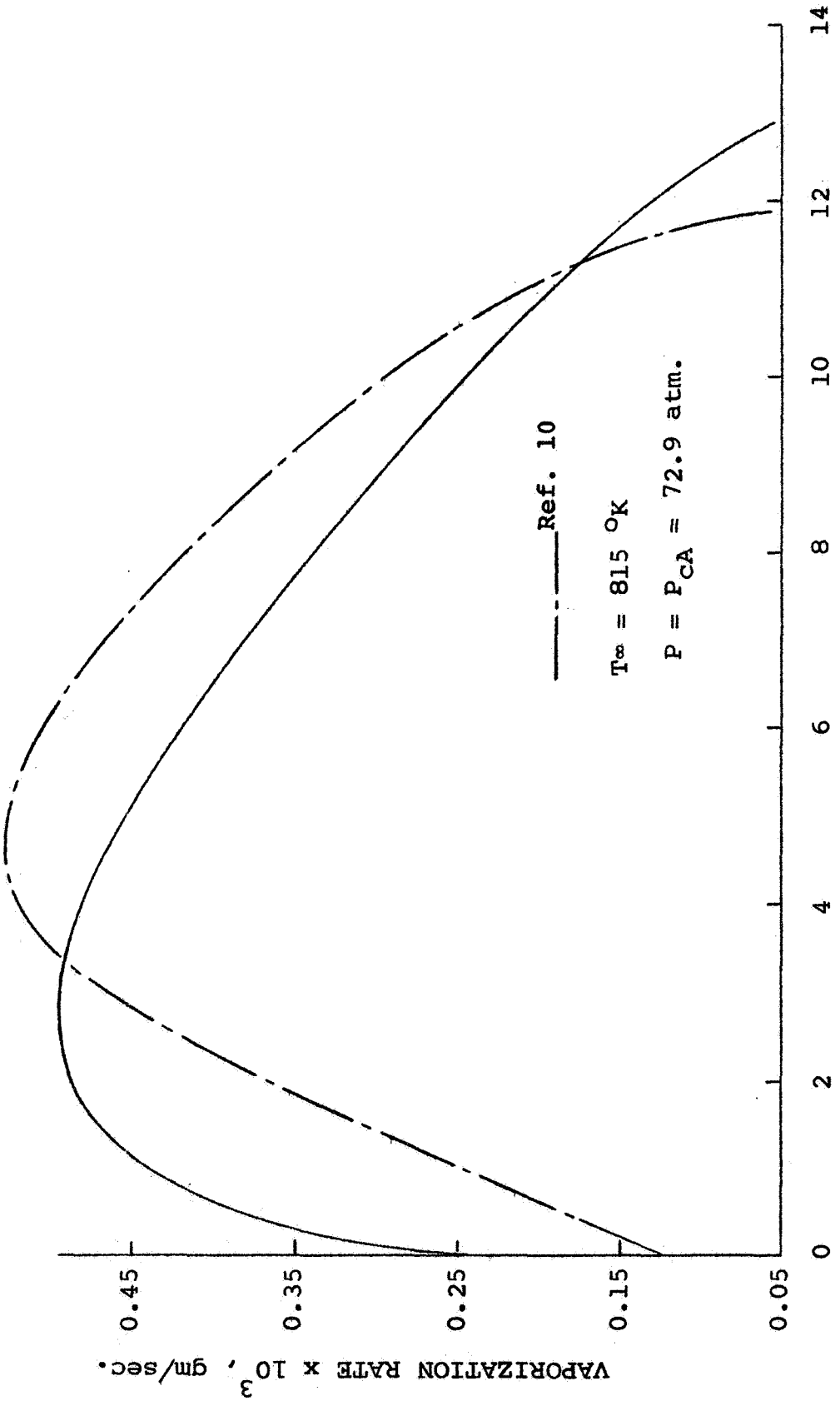

Figure 3.20. Comparison between mass vaporization rates.

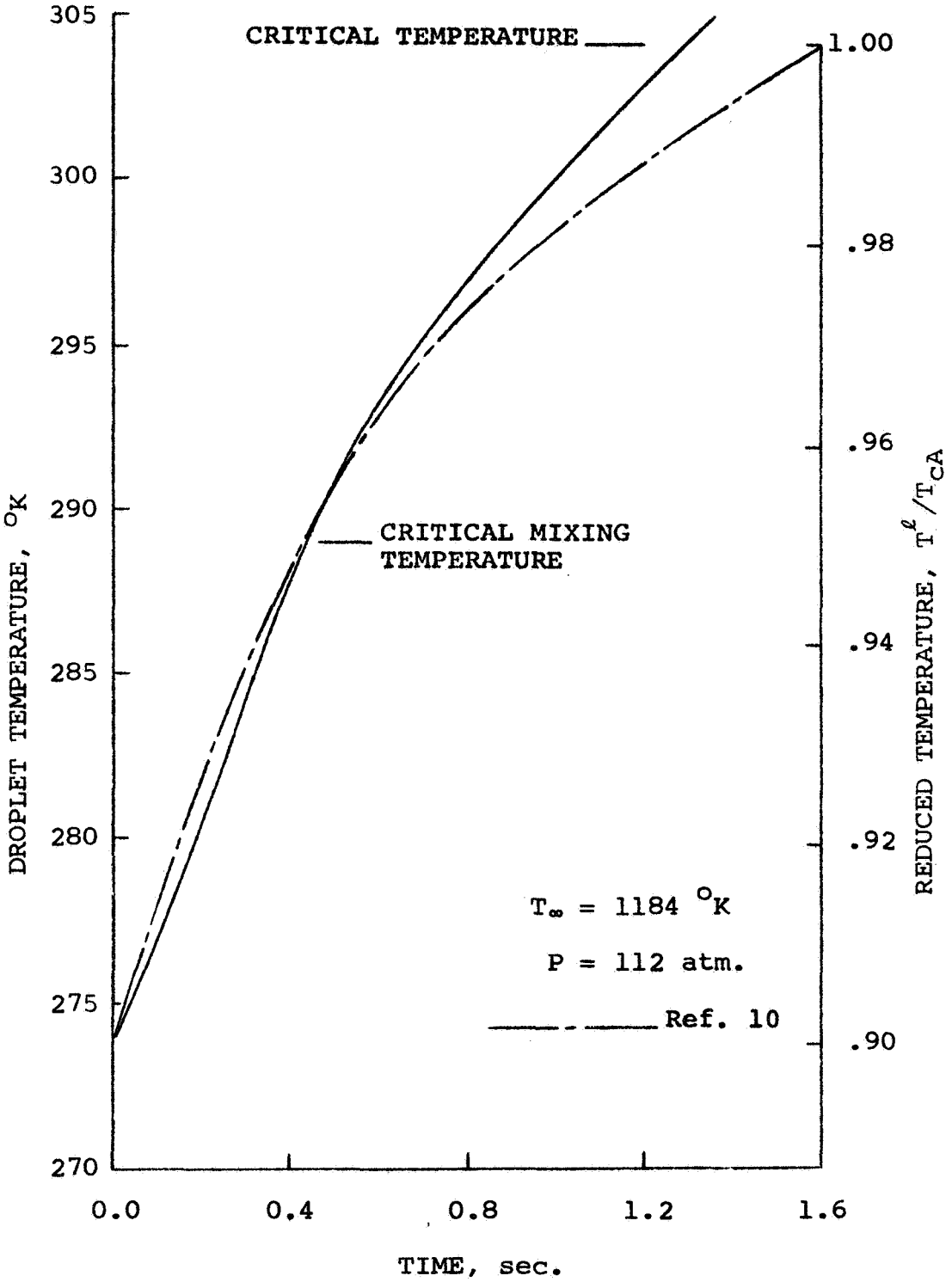

Figure 3.21. Comparison between droplet temperature responses.

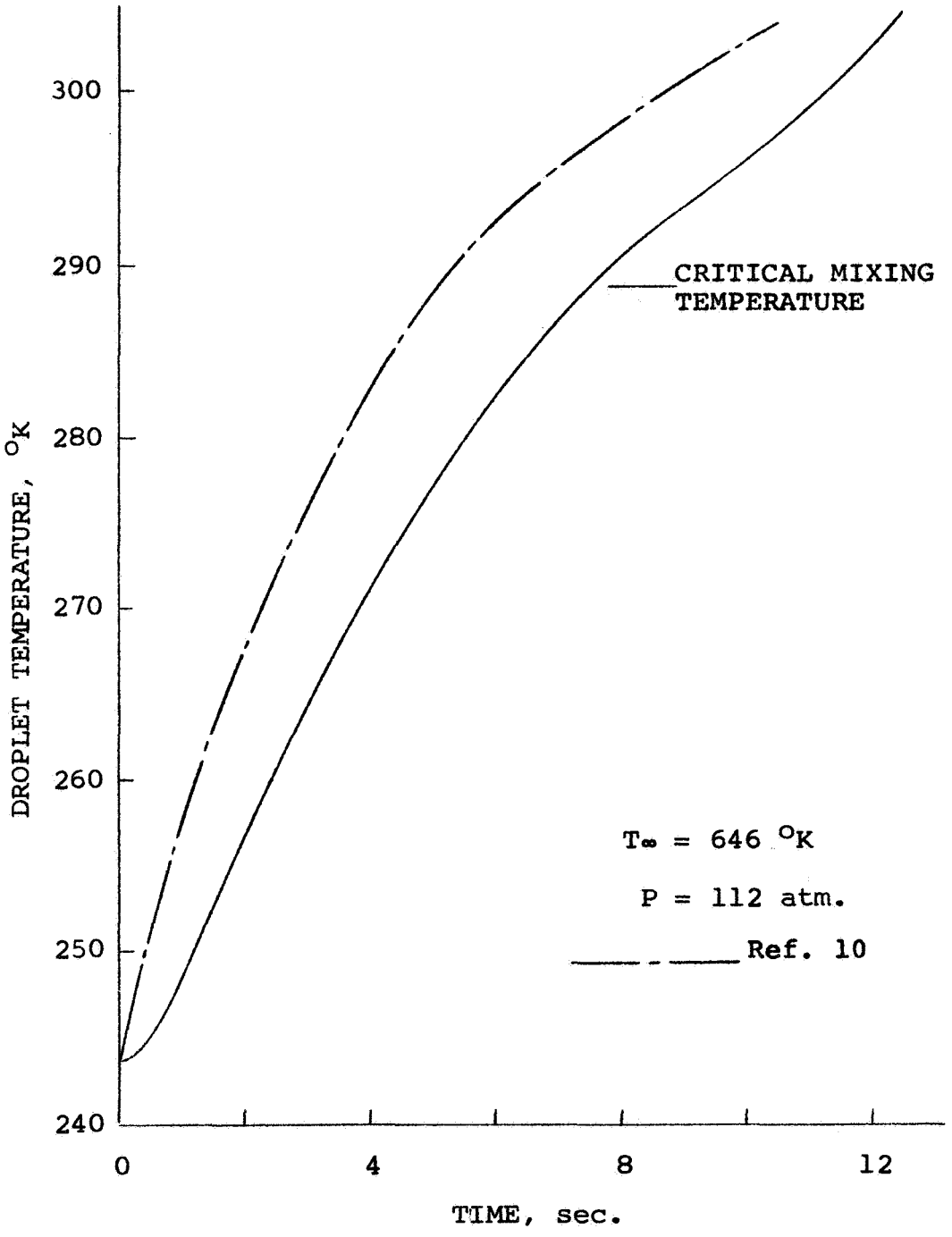

Figure 3.22. Comparison between droplet temperature responses.

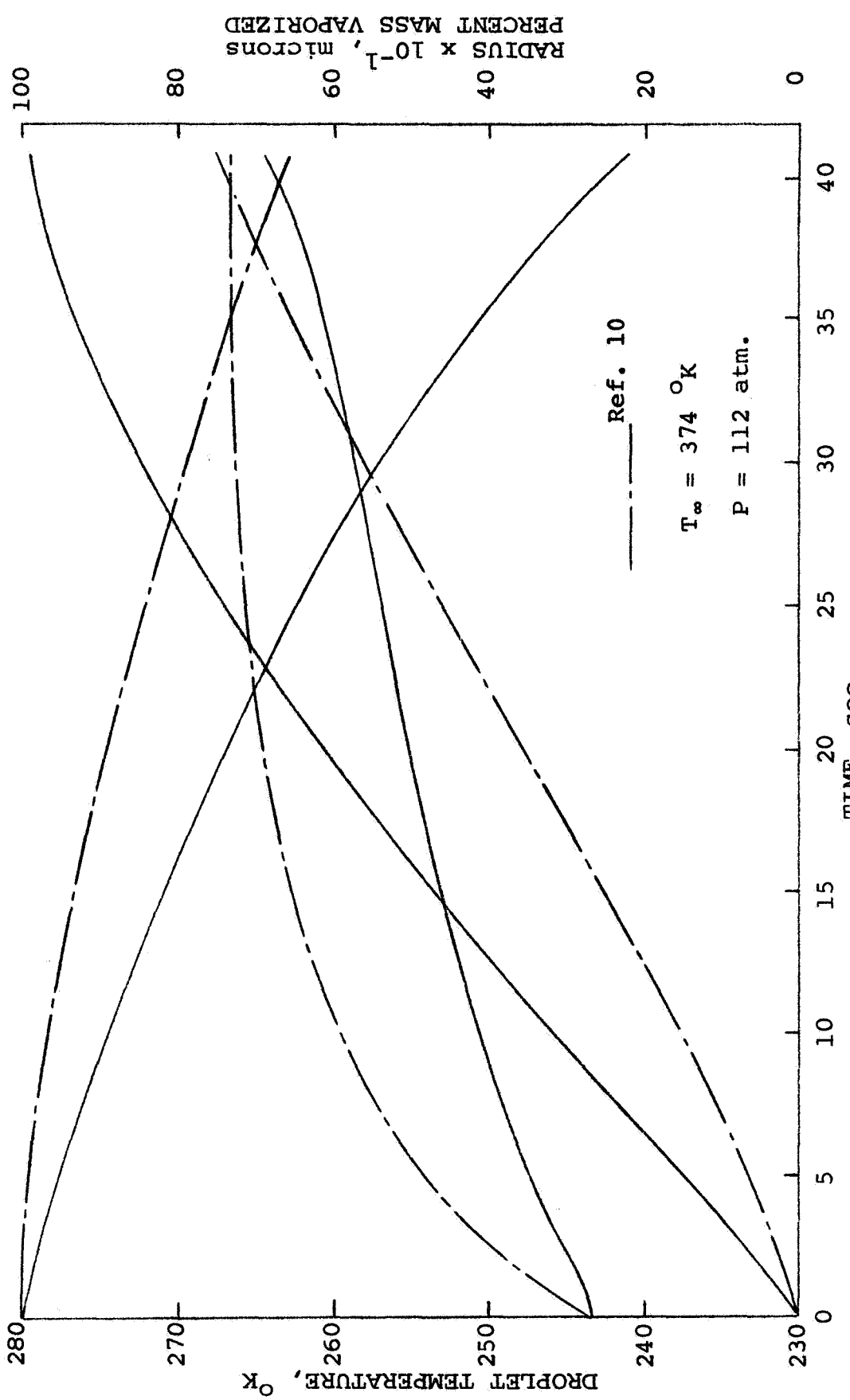

Figure 3.23. Comparison between vaporization histories.

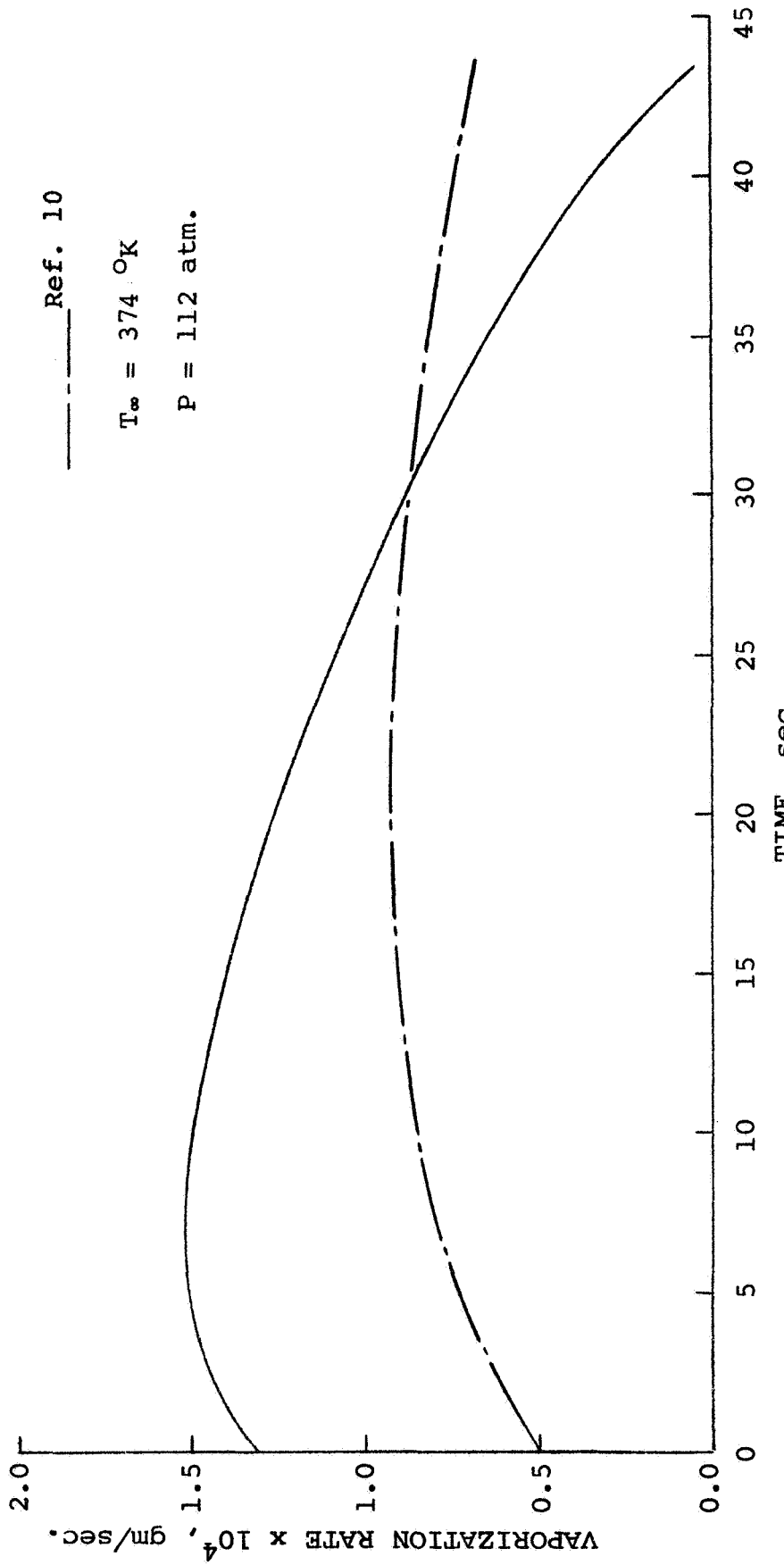

Figure 3.24. Comparison between mass vaporization rates.

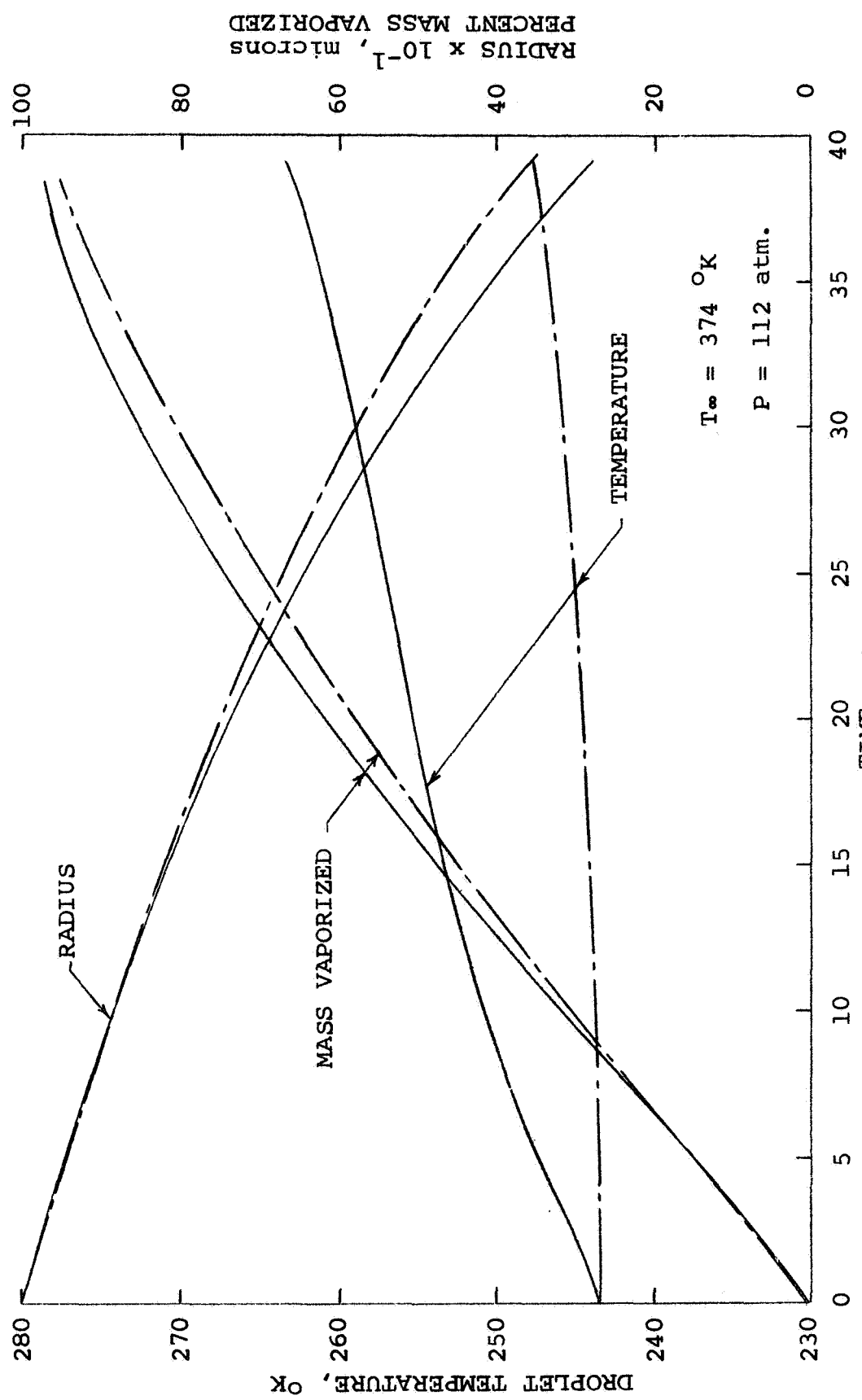

Figure 3.25. Comparison between vaporization histories. Effects of total pressure on vapor pressure and enthalpy of vaporization are included in the film theory of Ref. 10.

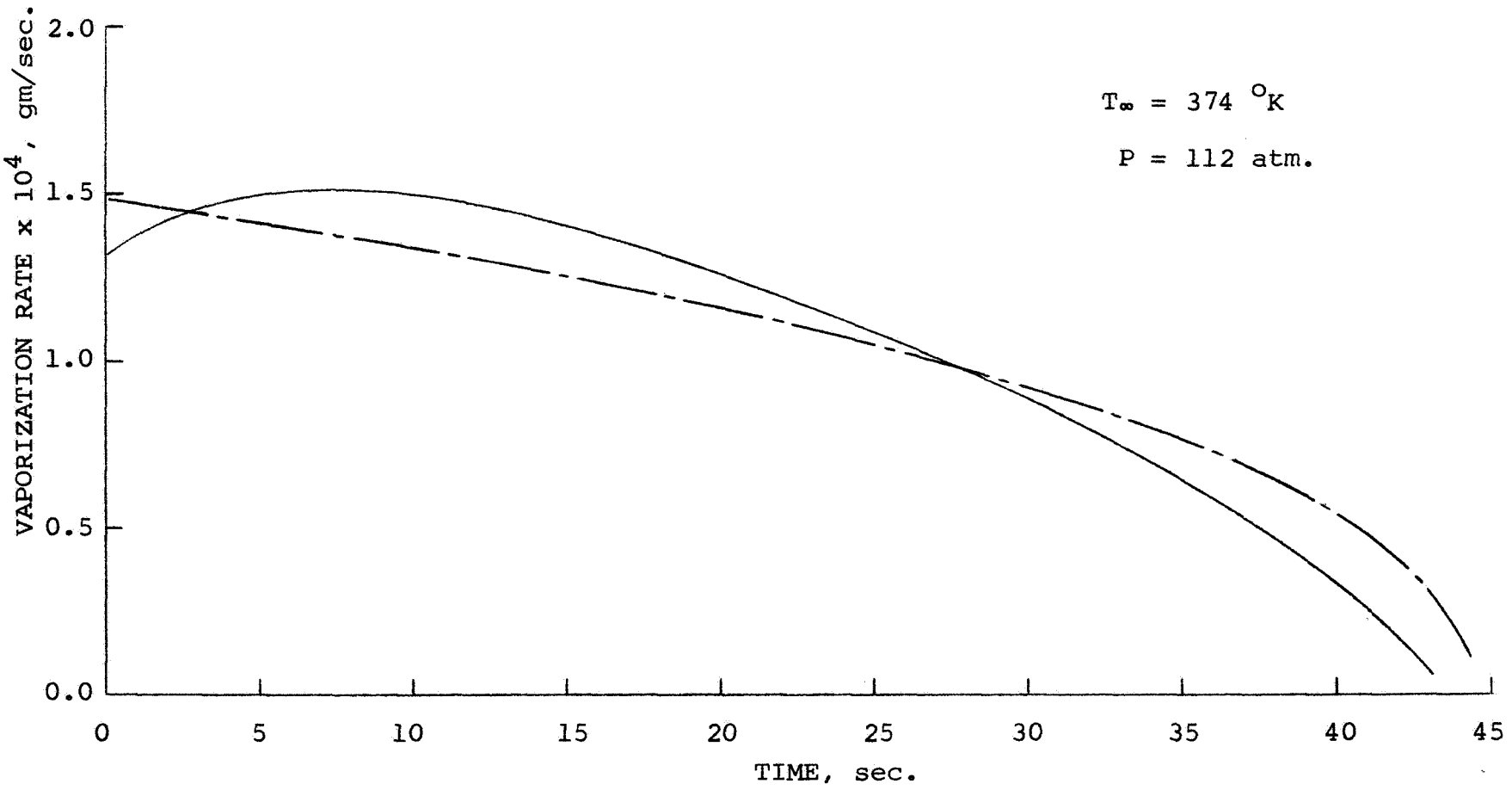

Figure 3.26. Comparison between mass vaporization rates. Effects of total pressure on vapor pressure and enthalpy of vaporization are included in the film theory of Ref. 10.

IV. UNSTEADY VAPORIZATION WITH PRESSURE OSCILLATIONS

The vaporization process is recognized as a fundamental factor in determining combustion instability. Numerous studies carried out in the past have indicated that pressure oscillations in a combustor often amplify with the result of engine destruction.

Heidmann and Wieber[12,13] investigated the vaporization process in unstable combustors with traveling transverse oscillations by analyzing the frequency response of the droplet vaporization process to oscillations in pressure under a wide range of conditions. They indicated that if the mass vaporization rate and total pressure are both simultaneously above or below their average values there is a potential for combustion instability in the overall dynamic analysis of a combustion system. Conversely, if the mass vaporization rate variation is out of phase with respect to the oscillation in pressure,damping is introduced into the system.

The analysis which follows does not attempt to describe the entire dynamic frequency response of the droplet vaporization process subjected to radial pressure oscillations, nor to establish a criterion for combustion instability. The calculations provide a measure of the

sensitivity of the vaporization process to superimposed pressure oscillations as well as the driving or damping potential to instability as postulated above. Making use of the analysis the assumption of essentially infinite liquid thermal conductivity is evaluated by comparing the liquid temperature response under the assumption of finite thermal conductivity. Relaxation times in the gas phase under high density conditions are discussed.

The basic relationships in the analysis are first derived for a binary system of components A-B. These relationships are then applied to carbon dioxide droplets vaporizing in nitrogen under high pressure conditions with superimposed pressure oscillations. It is assumed that, for relatively small pressure oscillations, the total pressure in the system is only a function of time, and the liquid properties, as well as the vapor pressure and enthalpy of vaporization are not significantly affected by the oscillations in pressure. Moreover, the variation in nitrogen temperature associated with the pressure oscillations is assumed to be isentropic.

Theoretical Model

Most of the governing equations and boundary conditions presented in the last section require only slight modifications in order to take into account the superimposed pressure oscillations on the vaporization process.

Equation of continuity of species A:

$$c \frac{\partial x_A}{\partial t} + cV_{MO} \frac{\partial x_A}{\partial r} = \frac{1}{r^2} \frac{\partial}{\partial r} (r^2 c D_{AB} \frac{\partial x_A}{\partial r}) \quad [4.1]$$

Equation of continuity of the mixture:

$$\frac{\partial c}{\partial t} + \frac{1}{r^2} \frac{\partial}{\partial r} (r^2 c V_{MO}) = 0 \quad [4.2]$$

Equation of energy:

$$cx_A \frac{\partial \bar{H}_A}{\partial t} + cx_B \frac{\partial \bar{H}_B}{\partial t} + N_A \frac{\partial \bar{H}_A}{\partial r} + N_B \frac{\partial \bar{H}_B}{\partial r}$$

$$= \frac{1}{r^2} \frac{\partial}{\partial r} (r^2 k \frac{\partial T}{\partial r}) + J \frac{dP}{dt} \quad [4.3]$$

Equation of state:

$$c = c(x_A, P, T) \quad [4.4]$$

The partial molal enthalpy of each component, $\bar{H}_A$ and $\bar{H}_B$, the thermal conductivity of the mixture, k, and the

binary diffusivity, D_{AB}, are taken as functions of temperature, pressure, and composition.

Introducing the transformation

$$y = r - r_o(t) \qquad [4.5]$$

and making use of the chain rule in order to take into account the temperature, pressure, and composition dependence upon the thermodynamic and transport properties, the governing equations may be arranged in the independent variables y, and t.

Thus, integrating the equation of continuity for the mixture:

$$V_{My} = \frac{r_o^2}{(y + r_o)^2} \left[V_{My}\,(0,t) + \dot{r}_o\right] \frac{(c)_{y=0}}{c}$$

$$- \dot{r}_o \left[1 - \frac{1}{(y + r_o)^2 c} \int_0^y (y + r_o)^2 \left(\frac{\partial c}{\partial x_A} \frac{\partial x_A}{\partial y} + \frac{\partial c}{\partial T} \frac{\partial T}{\partial y} \right) dy \right]$$

$$- \frac{1}{(y + r_o)^2 c} \int_0^y (y + r_o)^2 \left(\frac{\partial c}{\partial x_A} \frac{\partial x_A}{\partial t} + \frac{\partial c}{\partial T} \frac{\partial T}{\partial t} + \frac{\partial c}{\partial P} \frac{dP}{dt} \right) dy \qquad [4.6]$$

Similarly, the equations of continuity for species A and energy become, in the independent variables y, and t:

$$\frac{\partial x_A}{\partial t} = \underline{A}' \frac{\partial^2 x_A}{\partial y^2} + \left(\underline{B}' \frac{\partial T}{\partial y} + \frac{2\underline{A}'}{y + r_o} - V_{My} \right) \frac{\partial x_A}{\partial y} \qquad [4.7]$$

and

$$\frac{\partial T}{\partial t} = \underline{C}' \frac{\partial^2 T}{\partial y^2} + \left(\underline{D}' \frac{\partial x_A}{\partial y} + \underline{E}' \frac{\partial T}{\partial y} \quad \frac{2\underline{C}'}{y + r_o} - V_{My} \right) \frac{\partial T}{\partial y}$$

$$- \underline{A}' \underline{F}' \frac{\partial^2 x_A}{\partial y^2} + \left(\underline{G}' \frac{\partial x_A}{\partial y} - \underline{B}' \underline{F}' \frac{\partial T}{\partial y} - \frac{2\underline{A}' \underline{F}'}{y + r_o} \right) \frac{\partial x_A}{\partial y}$$

$$+ \underline{H}' \frac{dP}{dT} \qquad [4.8]$$

where

$$\underline{A}' = \frac{(cD_{AB})}{c} \qquad [4.9]$$

$$\underline{B}' = \frac{1}{c} \frac{\partial (cD_{AB})}{\partial T} \qquad [4.10]$$

$$\underline{C}' = \frac{k}{c\, c_p} = \alpha \qquad [4.11]$$

$$\underline{D}' = \frac{1}{c\, c_p} \left[\frac{\partial k}{\partial x_A} + cD_{AB} (\bar{c}_{pA} - \bar{c}_{pB}) \right] \qquad [4.12]$$

$$\underline{E}' = \frac{1}{c\, c_p} \frac{\partial k}{\partial T} \qquad [4.13]$$

$$\underline{F}' = \frac{1}{c\, c_p} \left[x_A \frac{\partial \bar{H}_A}{\partial x_A} + (1 - x_A) \frac{\partial \bar{H}_B}{\partial x_A} \right] \qquad [4.14]$$

$$\underline{G}' = \frac{(cD_{AB})}{c\, c_p} \left(\frac{\partial \bar{H}_A}{\partial x_A} - \frac{\partial \bar{H}_B}{\partial x_A} \right) \qquad [4.15]$$

$$\underline{H}' = \frac{1}{c_p} \left[\frac{J}{c} - x_A \frac{\partial \bar{H}_A}{\partial P} - (1 - x_A) \frac{\partial \bar{H}_B}{\partial P} \right] \qquad [4.16]$$

Under the postulated assumptions the boundary conditions at the droplet surface are the same as those presented in the last section, namely Equations [3.43], [3.44], and [3.47].

Ambient conditions are specified by

$$x_A (\infty, t) = 0 \qquad [4.17]$$

and

$$T (\infty, t) = \bar{T}_\infty (P/\bar{P})^{\frac{\gamma-1}{\gamma}} \qquad [4.18]$$

where $\bar{T}_\infty$ and $\bar{P}$ are respectively the average ambient temperature and pressure. Furthermore,

$$P = \bar{P} + P'\sin(2\pi f' t) \qquad [4.19]$$

where P' and f' are respectively the amplitude and frequency of the sinusoidal pressure oscillation.

Numerical Method of Solution

The equations of change were solved using the same explicit numerical technique described in the last section with minor modifications in order to take into account the additional terms which arise from the superimposed pressure oscillations.

The oscillatory pressure component was initially set equal to zero in the unsteady vaporization process. When evaporation reduced the droplet radius to an arbitrary value or the liquid temperature reached a specified value, a sinusoidal oscillation in pressure of amplitude P' and frequency f' was imposed upon the vaporization process.

Applications to a CO_2-N_2 System

Figure 4.1 shows the response of a CO_2 droplet vaporizing in N_2 at average temperature and pressure conditions of 374°K and 112 atm., to a sinusoidal pressure oscillation, 4 atm. peak to peak, and with a frequency of 500 Hz. The pressure oscillation is imposed on the vaporization history of Figure 3.15 when the droplet radius has been reduced to 697 microns. The cycle time is very small compared to the droplet's lifetime and the liquid temperature (256.18°K) is virtually unchanged throughout one oscillation. It is observed that the gas phase responds immediately to the changing pressure under these high density conditions. The mass vaporization rate is essentially out of phase with respect to the pressure and/or heat waves, where the heat wave represents the variation in the heat transferred by conduction at the droplet surface. Thus, a negative response factor is obtained, where the response factor is defined by[13]

$$N' = \frac{\int_0^{1/f'} w_d P_d \, dt}{\int_0^{1/f'} P_d^2 \, dt} \qquad [4.20]$$

where

$$P_d = \frac{P - \bar{P}}{\bar{P}} \qquad [4.21]$$

$$w_d = \frac{w - \bar{w}}{\bar{w}} \qquad [4.22]$$

The response factor, N',indicates the degree of driving or damping to combustion instability as generally postulated in the dynamic analysis of a combustion system whether it is positive or negative, respectively.

Figure 4.2 shows the same vaporizing droplet of Figure 4.1 except that the frequency of the pressure oscillation is very low, namely 0.5 Hz. For this low frequency case the liquid temperature has enough time to respond to the imposed pressure oscillation, changing the vapor pressure, and a response factor slightly positive is obtained.

The above results agree qualitatively with the frequency response analysis of Heidmann and Wieber for heptane droplets with superimposed transverse oscillations, viz., a positive response factor is obtained at low frequencies where the liquid temperature has enough time to respond, and a negative gain is obtained at high frequencies where the vaporization time is large compared to the oscillation period.

Considering that the average nitrogen temperature is relatively low in the foregoing calculations, higher temperature conditions were analyzed maintaining the average total pressure at the same value, namely 112 atmospheres.

Figures 4.3 and 4.4 show the response of a carbon dioxide droplet vaporizing in nitrogen at average temperature and pressure conditions of 1184°K and 112 atm., to a sinusoidal pressure oscillation, 4 atm. peak to peak, and with a frequency of 1000 Hz. The oscillation in pressure is imposed on the vaporization history of Figure 3.10 when the liquid temperature is 276°K and 287°K, respectively. Under these conditions less than 10 percent of the droplet mass has been vaporized. The cycle time is very small compared to the droplet vaporization time and the liquid temperature remains virtually unchanged (0.03°K/cycle) throughout one oscillation. Contrary to the previous low nitrogen temperature cases, the heat arriving at the droplet surface is substantially larger in this case. Furthermore, the mass vaporization rate is essentially in phase with respect to the pressure and/or heat waves. Thus, a positive response factor is obtained. In order to see if the phase angle between the pressure and the vaporization rate oscillations changes under higher frequency conditions, as one may suspect from the behavior exhibited in Figures 4.1 and 4.2, pressure oscillations with frequencies of 5000 Hz. and 15000 Hz. were imposed upon the same droplet whose response is illustrated in Figure 4.4. It is observed from Figures 4.5 and 4.6 that the mass vaporization rate remains in phase with the pressure and/or heat waves even at these high frequencies. Therefore, one may discard the extremely small liquid

temperature change as the cause for the vaporization rate variation, nevertheless small, to be in phase with the pressure and/or heat waves at high frequencies. However, as discussed in the last section, the initial values for the mass vaporization rate in the unsteady process without pressure oscillations are largely enhanced under high ambient temperature conditions through the coupling in the temperature and composition profiles, for the same liquid temperature. Consequently, one may conjecture that at high frequencies the vaporization rate is in phase with the pressure and/or heat waves during the early stages of the vaporization process provided the energy arriving at the droplet surface is high enough to drive the vaporization response in that direction.

Figure 4.7 illustrates the response of a carbon dioxide droplet vaporizing in nitrogen at average temperature and pressure conditions of 646°K and 112 atm., to a pressure oscillation, 4 atm. peak to peak, and with a frequency of 1000 Hz. imposed during different stages in the vaporization history shown in Figure 3.13. It is observed that the vaporization rate is in phase with the oscillation in pressure during the early part of the vaporization process and reverses its behavior as the process progresses. A similar response to pressure oscillations is observed during the early part of the vaporization process under average nitrogen conditions of 1400°K and 72.9 atmospheres.

Thus far only cases where the droplet temperature is lower than the corresponding critical mixing temperature have been considered. Figure 4.8 shows the response of a carbon dioxide droplet vaporizing in nitrogen at average temperature and pressure conditions of 1184 °K and 112 atm., to a pressure oscillation, 4 atm. peak to peak, and with a frequency of 1000 Hz. The oscillation in pressure is imposed on the vaporization history of Fig. 3.10 when the droplet temperature is slightly higher than the critical mixing temperature for this particular value of average total pressure. It is observed that the vaporization rate tends to increase more rapidly in this case (approximately 0.1 percent per cycle) than in the previous ones considered.

In order to observe the overall effect of the pressure oscillations upon the entire vaporization process including supercritical mixing conditions, pressure oscillations, 4 atm. peak to peak, and with a frequency of 1000 Hz. were imposed on a carbon dioxide droplet of 15-micron initial radius and initial temperature of $0.8T_{cA}$, vaporizing in nitrogen at average temperature and pressure conditions of 646 °K and 112 atmospheres. These vaporization conditions are similar to those of Fig. 3.13. It is observed from Figs. 4.9 and 4.10 that the overall effect of these relatively small amplitude pressure oscillations (of the order of 2 percent of the total pressure) on the

entire vaporization process is negligibly small and the physical significance of the above response factors is uncertain under these conditions. Unfortunately, in order to analyze the overall effects of large pressure oscillations, the momentum equation would have to be included as well as the variations in the liquid properties, complicating enormously the analysis and thus making the computing time prohibitively longer. Nevertheless, the foregoing results indicate that the relaxation times in the gas phase are very short under high density conditions, a major concern in quasi-steady analyses.

In order to evaluate the assumption of essentially infinite liquid thermal conductivity in the above calculations, where the liquid temperature remains virtually unchanged throughout one cycle under high density conditions, the limiting case of a solid sphere, treated as a semi-infinite body, of finite thermal conductivity and subjected to a periodic surface heat flux oscillation is now considered.

It can be shown that the steady periodic temperature distribution, $T(Z,t)$, in a semi-infinite body subjected to a periodic surface heat flux $Q = Q'\sin(2\pi f't)$, and with an initial temperature, say zero, is given by

$$T(Z,t) = \frac{Q'\exp(-ZN)}{2kN}\left[\sin(2\pi f't - ZN) - \cos(2\pi f't - ZN)\right], \quad Z \geq 0 \quad [4.23]$$

where

$$N = (\pi f' c c_p / k)^{1/2} \qquad [4.24]$$

Thus, the magnitude of the maximum temperature change at the surface is

$$\left| T(0,t) \right|_{max} = \frac{Q'}{(2\pi f' k c c_p)^{1/2}} \qquad [4.25]$$

For the liquid and heat flux conditions illustrated in Fig. 4.1 the maximum droplet temperature change is found to be approximately 0.005 °K, making the assumption of essentially infinite liquid thermal conductivity unimportant.

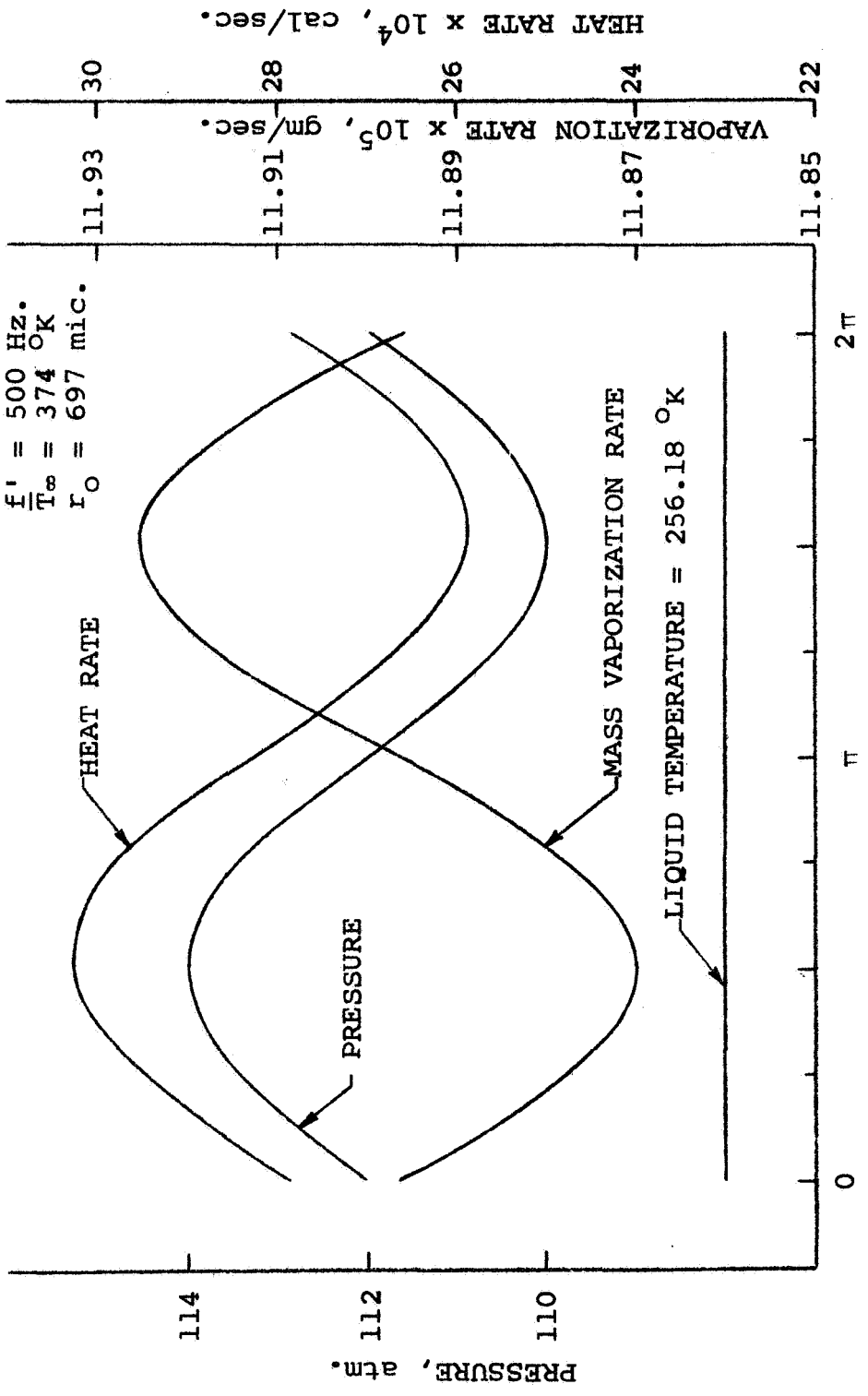

Figure 4.1. Response of a CO_2 droplet vaporizing in N_2.

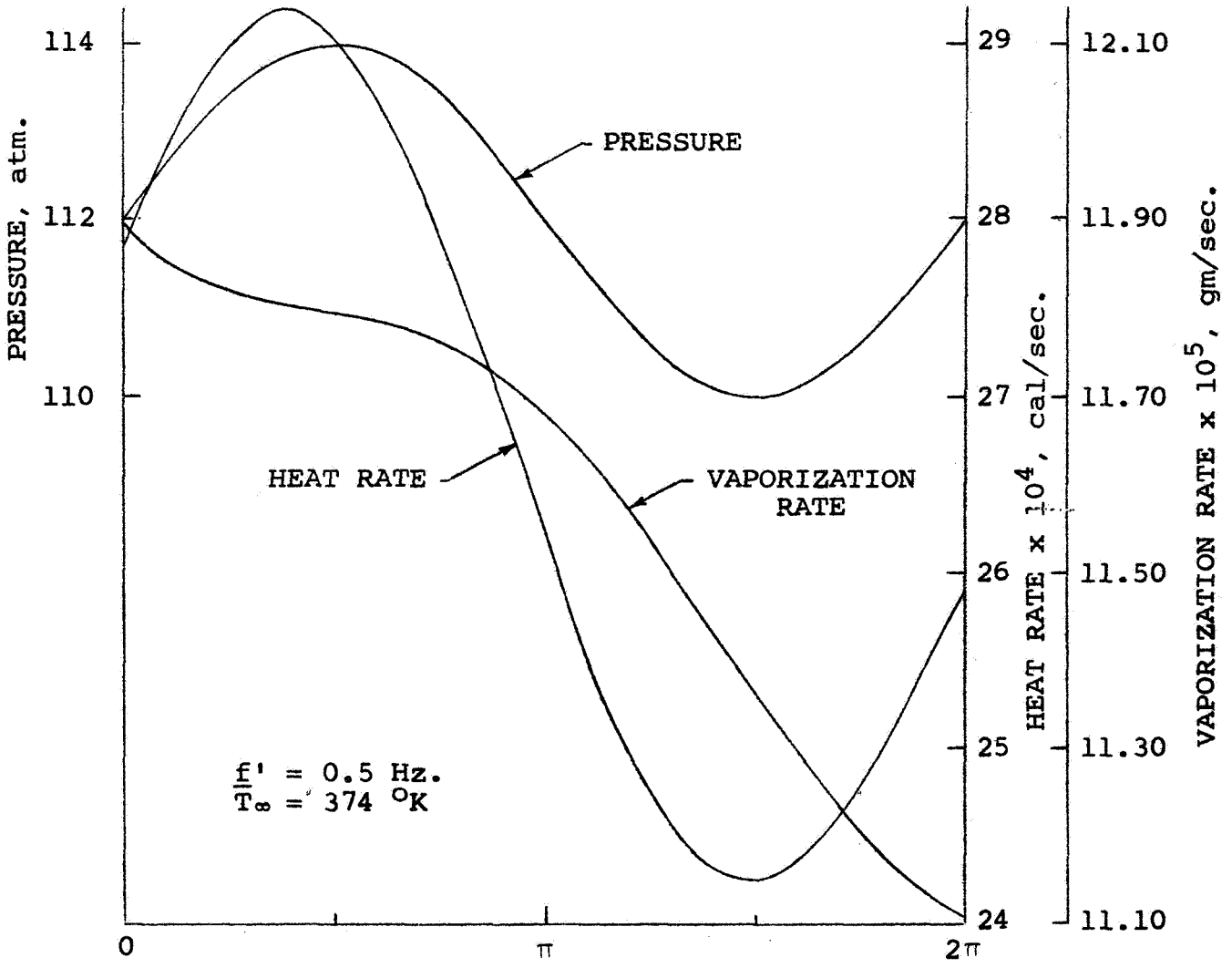

Figure 4.2. Response of a carbon dioxide droplet vaporizing in nitrogen. The pressure oscillation is imposed when the droplet radius and temperature are 697 mic. and 256.2 °K.

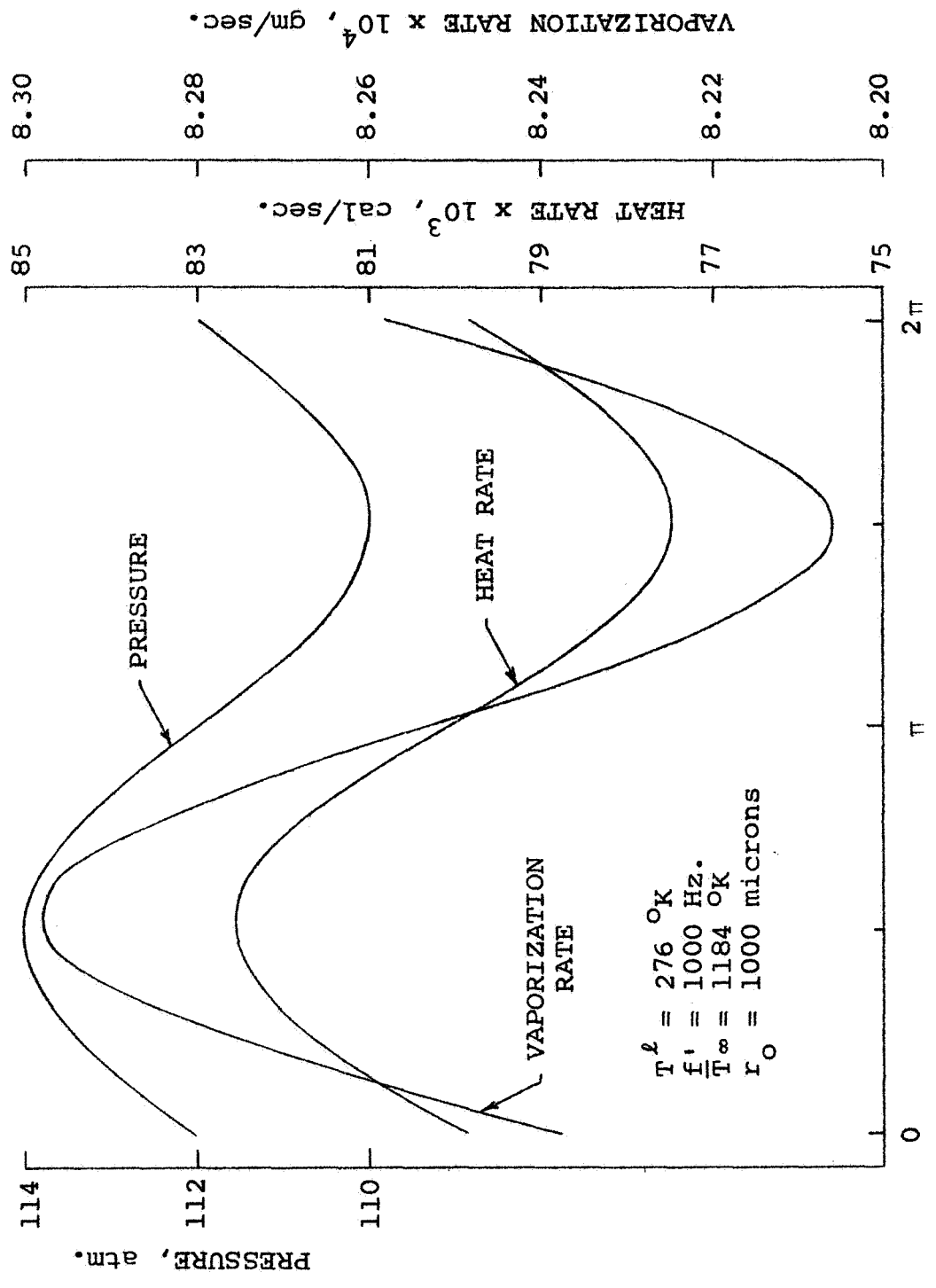

Figure 4.3. Response of a CO_2 droplet vaporizing in N_2.

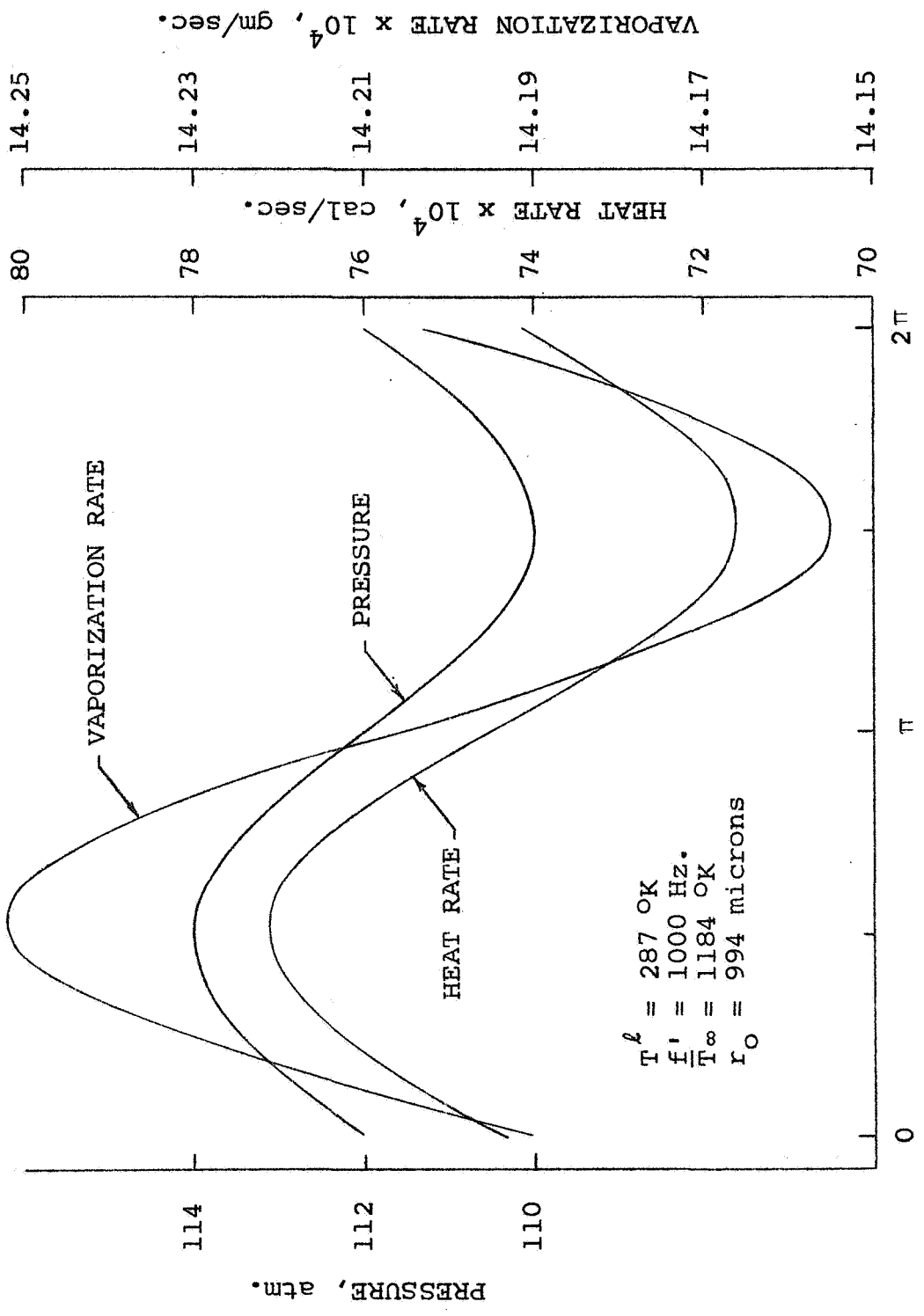

Figure 4.4. Response of a CO_2 droplet vaporizing in N_2.

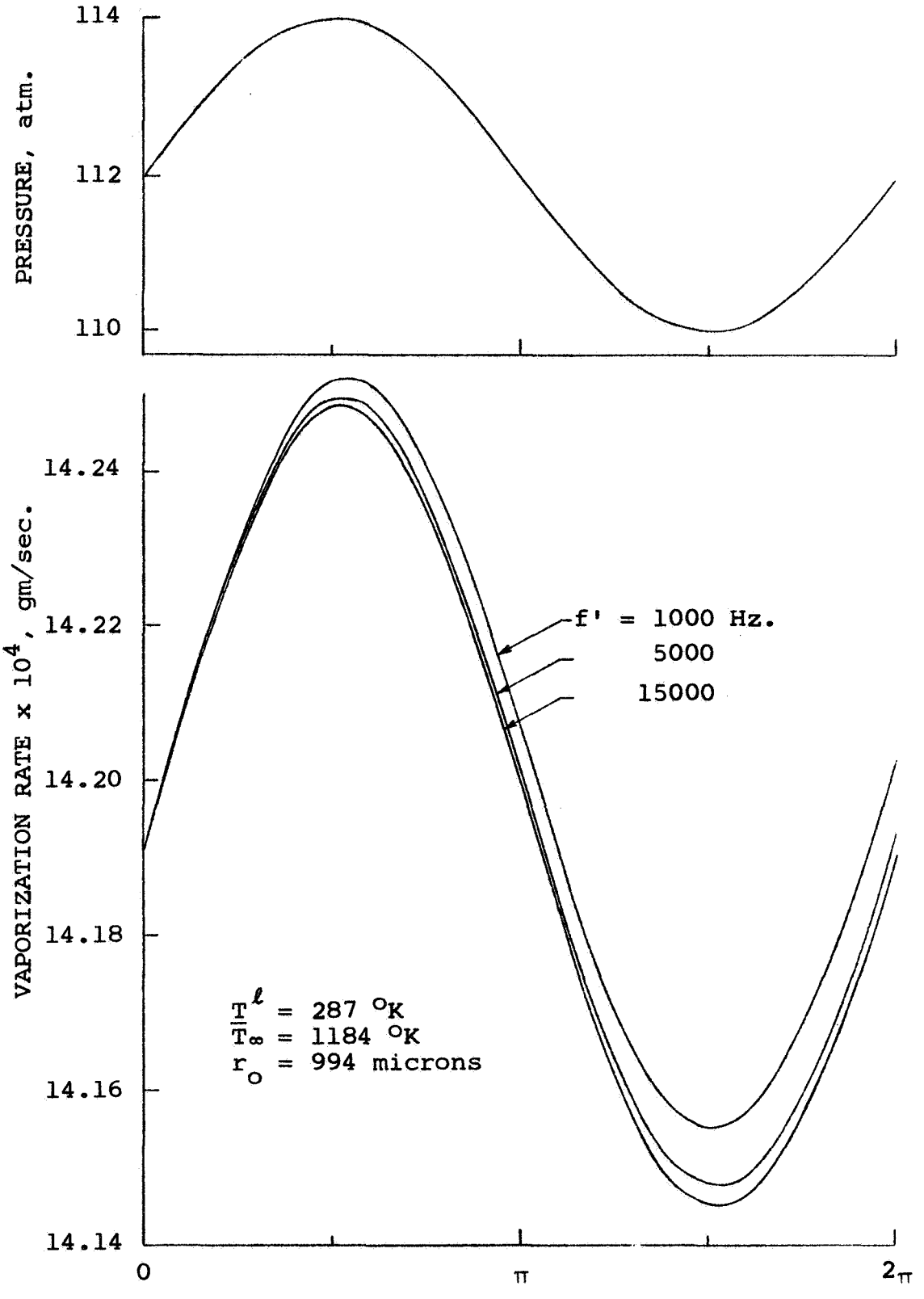

Figure 4.5. Effect of frequency upon the mass vaporization rate.

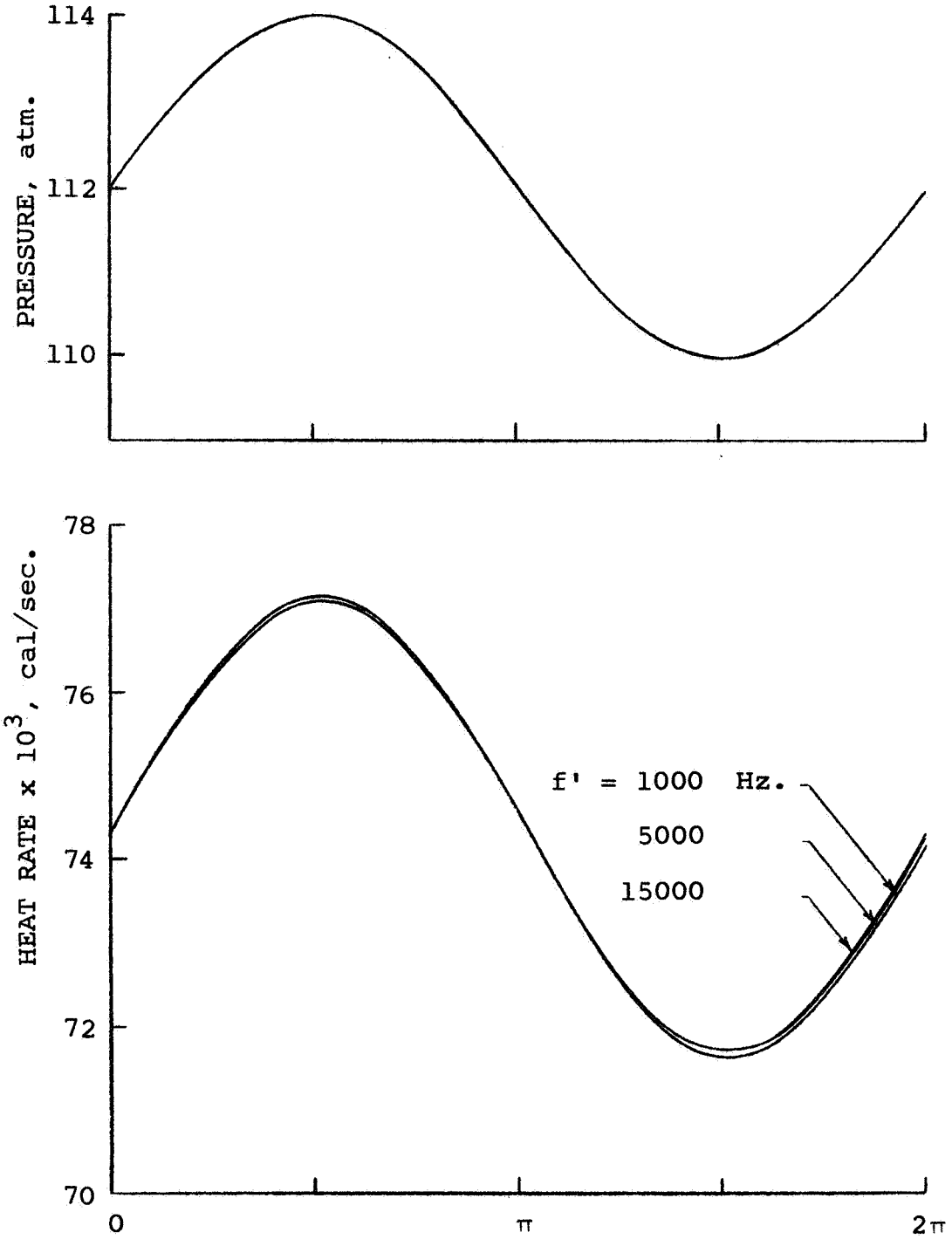

Figure 4.6. Effect of frequency upon the heat arriving at the droplet surface by conduction. Vaporization conditions equal to those of Fig. 4.5.

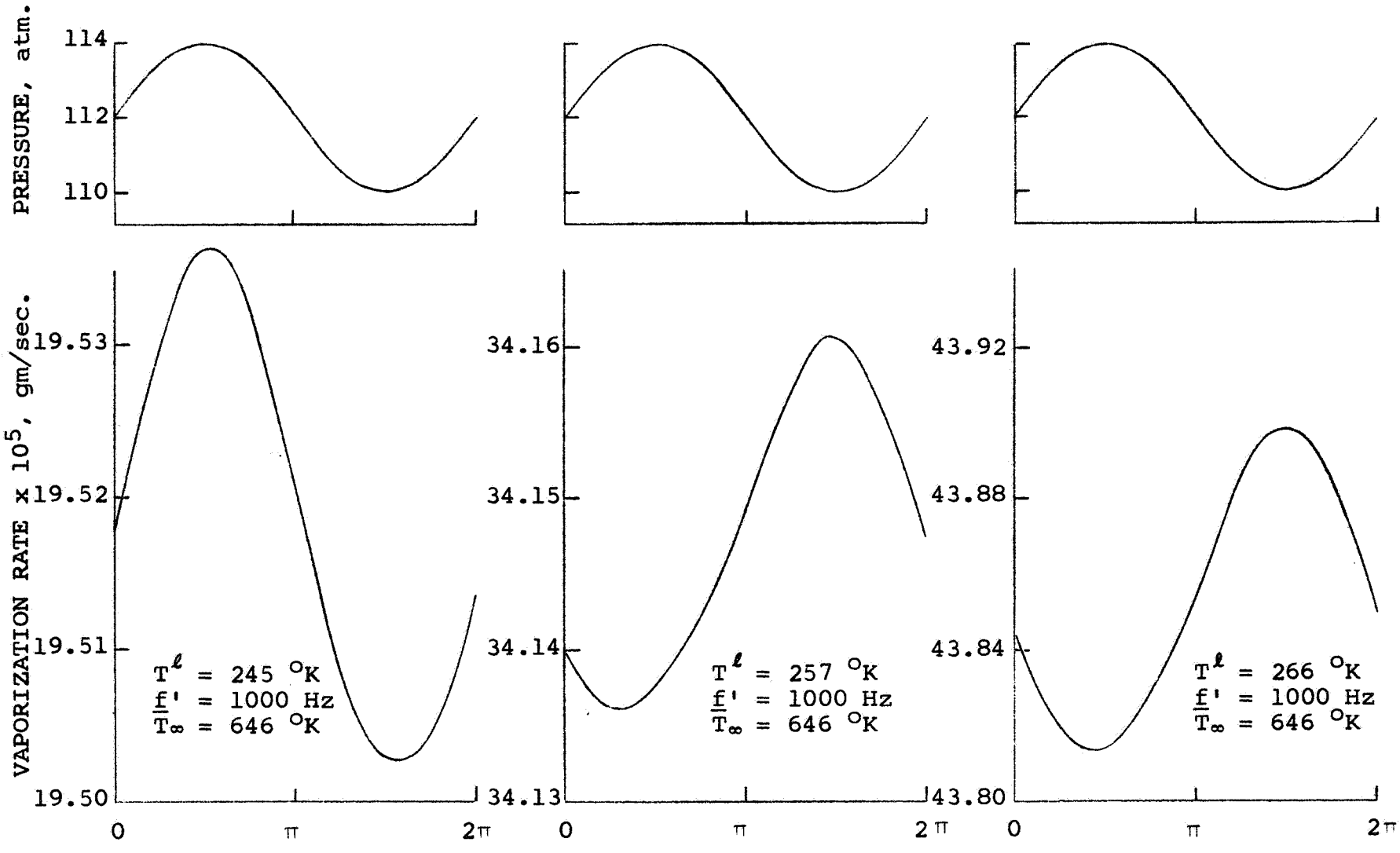

Figure 4.7. Pressure oscillations imposed during different stages in the vaporization process.

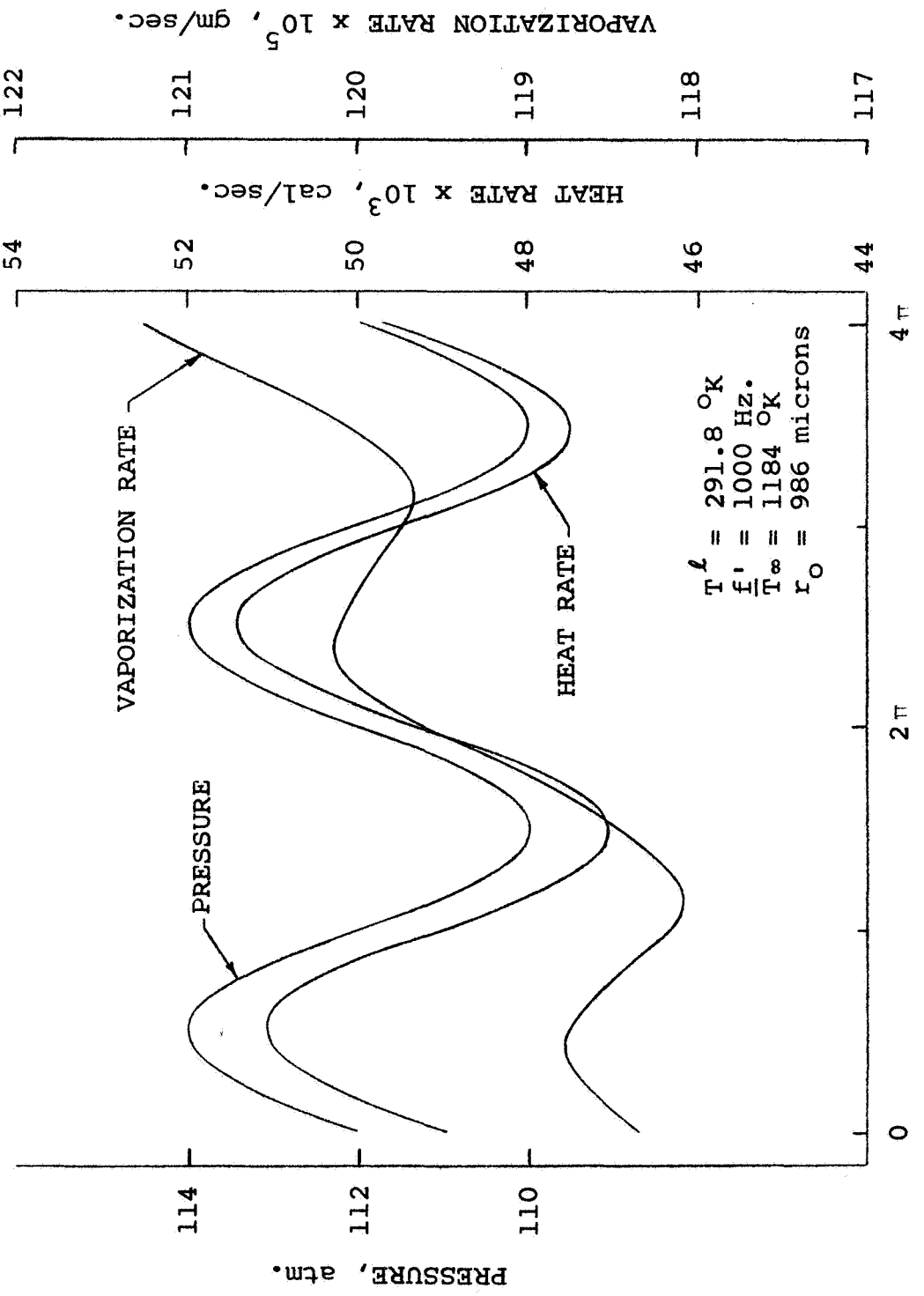

Figure 4.8. Response of a CO_2 droplet vaporizing in N_2.

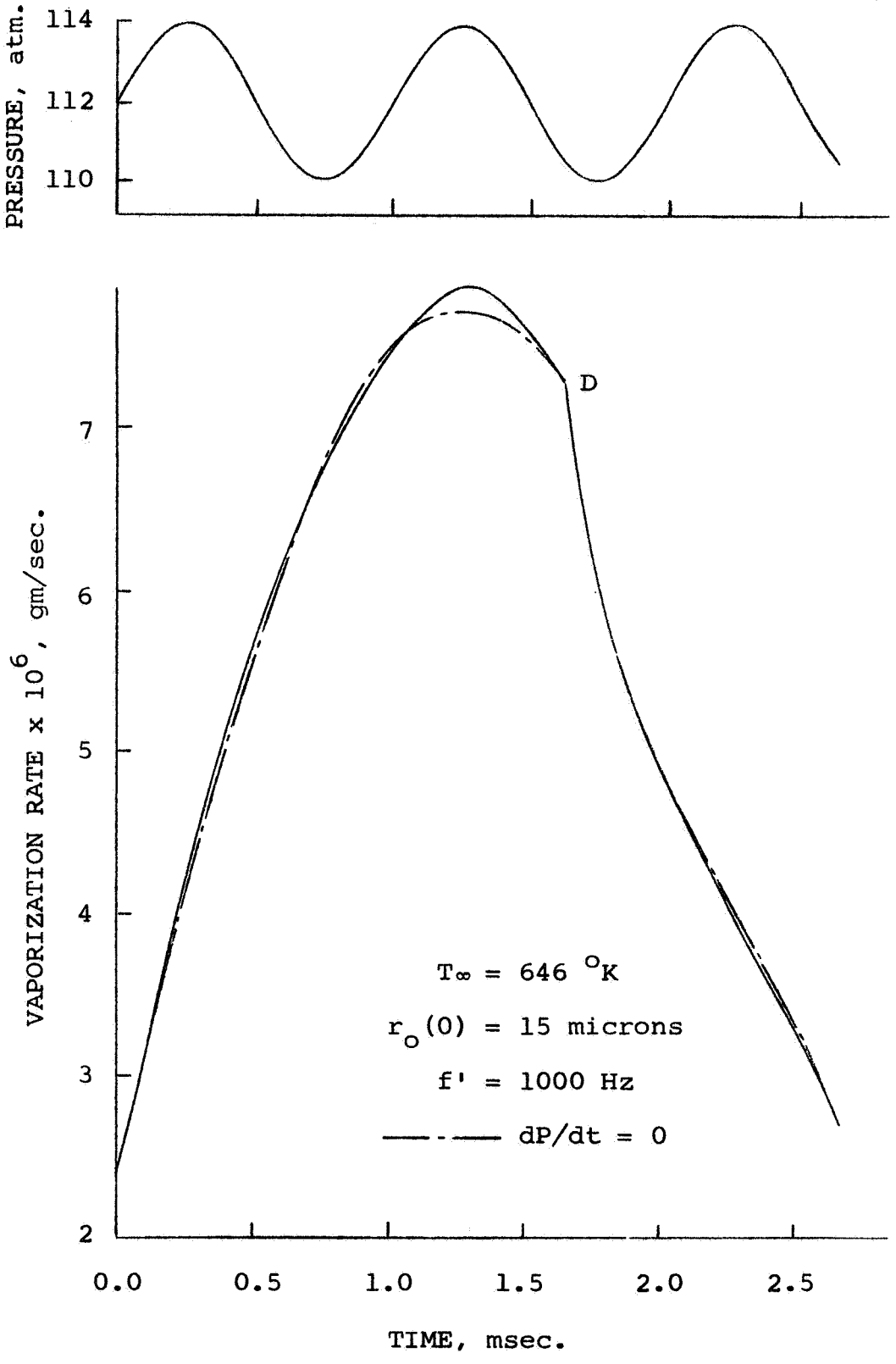

Figure 4.9. Mass vaporization rate of a carbon dioxide droplet with and without pressure oscillations.

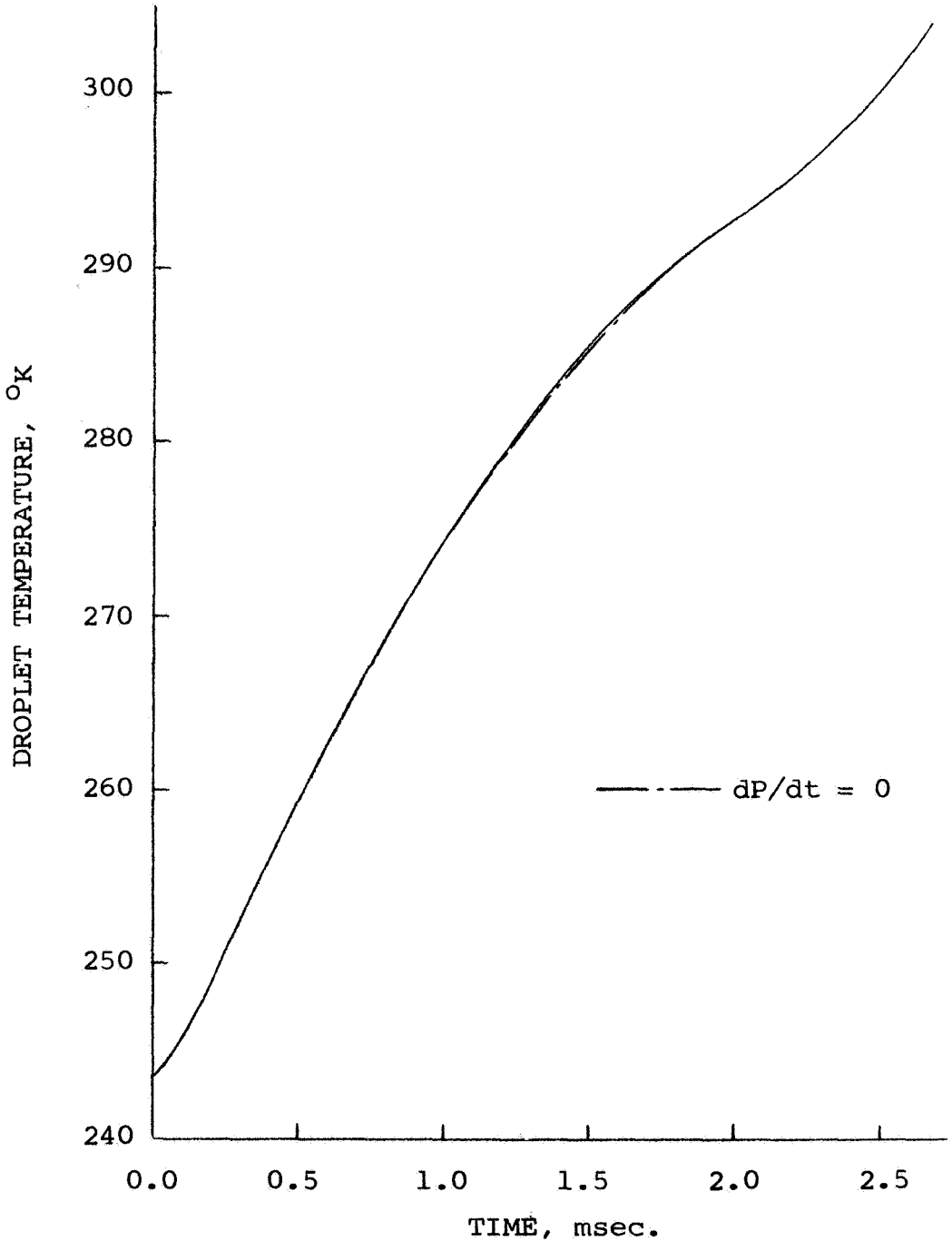

Figure 4.10. Droplet temperature response with and without pressure oscillations. Vaporization conditions equal to those of Fig. 4.9.

V. CONCLUSIONS

This investigation has shown that at supercritical pressures a droplet may reach and exceed its thermodynamic critical temperature, thus becoming a dense mass of vapor, by an intrinsically unsteady process. Under supercritical pressure and high ambient temperature conditions, such as those encountered in the combustion chamber of a rocket motor, a liquid droplet rapidly reaches its critical temperature with little vaporization taking place. On the other hand, under supercritical pressure and low or moderate ambient temperature conditions, such as those of high pressure sprays encountered in diesel engines, a liquid droplet may pass through the critical mixing line but it may not reach its thermodynamic critical temperature.

It has been shown that for a given value of ambient temperature there is an upper limit in the total pressure of the system above which steady state conditions cannot be obtained in the vaporization process. Furthermore, at high pressures most of the droplet's lifetime is spent under unsteady conditions.

The non-ideal effects associated with dense mixtures, hitherto neglected, cannot be ignored in vaporization analyses at high ambient pressures. The effect of the inert gas pressure on the vapor pressure is appreciable at high

pressures and the enthalpy of vaporization is drastically modified.

High density gradients are exhibited in the vicinity of the vaporizing droplet. Similarly, temperature and composition gradients at the droplet surface are very large.

The mass vaporization rate increases with increased pressure and/or ambient temperature. Initial values for the rate of vaporization are largely enhanced by an increase in the ambient temperature, for the same value of liquid temperature and pressure.

The entire droplet vaporization time follows closely the square law dependence on the variation of the droplet radius.

Vaporization times can be predicted with reasonable accuracy by the quasi-steady theory of Reference 10 over a wide range of temperature and pressures, provided the vapor pressure and enthalpy of vaporization are properly corrected under high density conditions. Without corrections, the theory of Reference 10 predicts too long vaporization times under high pressure and low ambient temperature conditions. Conversely, it predicts shorter vaporization times under moderate pressures and high ambient temperatures.

Sinusoidal pressure oscillations of relatively small amplitude have a negligibly small overall effect upon the entire vaporization process.

Relaxation times in the gas phase are very short and

thus the gaseous phase may be treated by a quasi-steady analysis. This is to say that the profiles in the gas phase accommodate very rapidly to a new position after a disturbance has been imposed.

The theory presented is limited in scope to those cases where gravitational and hydrodynamic effects can be neglected. Absorption rates of the inert gas into the liquid phase are assumed to be negligible and the liquid phase is assumed to have a uniform temperature. The theory does not account for any radiant energy exchange nor chemical reactions in the boundary layer. Coupled effects associated with transport processes, i.e., the Soret and Dufour effects, are neglected. Although the validity of this assumption may be debatable due to the high composition and temperature gradients in the vicinity of the droplet surface, the assumption is a necessary one because of the lack of data.

The stagnation point of a liquid droplet immersed in a gas stream contains many of the features of unsteady vaporization and thus an analysis similar to the one presented here may be carried out.

Although numerous research studies on the thermodynamics of high pressure mixtures are being conducted, most of them are applicable only to nonpolar mixtures with little knowledge on the liquid phase behavior. Therefore, systematic investigations on a wide variety of mixtures, such as those encountered in an operating engine, may greatly enhance the possi-

bilities to describe a system analytically.

Visual investigations of interfaces in transport processes may largely illuminate the present fundamental knowledge on thermodynamic equilibrium, absorption rates, and thermal gradients in the liquid phase.

It is hoped that this investigation has illuminated some of the fundamental aspects of the single droplet vaporization process at high pressures and will stimulate further research studies, so that eventually the vaporization process in an operating engine can be analytically simulated.

APPENDIX A

A. Thermodynamic Properties

The Redlich-Kwong equation of state is

$$P = \frac{RT}{(v - b)} - \frac{a}{T^{0.5}v(v + b)} \qquad [A.1]$$

In order to apply Equation [A.1] to mixtures several mixing rules are possible.

In terms of the gaseous mixture compressibility factor, Equation [A.1] was arranged in the following form[22]:

$$z = \frac{1}{(1 - h)} - \frac{A^2}{B}\frac{h}{(1 + h)} \qquad [A.2]$$

where

$$A = \sum_i x_i(0.4278T_{ci}^{2.5}/P_{ci}T^{2.5})^{1/2} \qquad [A.3]$$

$$B = \sum_i x_i(0.0867T_{ci}/P_{ci}T) \qquad [A.4]$$

$$h = BP/z \qquad [A.5]$$

Inspection of Equations [A.1] and [A.2] shows that solving for v or z (given T, P, and x_i) involves trial-and-error calculations. Hence, for digital computer programming it is convenient to rewrite Equation [A.2] as

$$z^3 - z^2 + (A^2 - B - B^2P)Pz - A^2BP^2 = 0 \qquad [A.6]$$

The compressibility factor of the vapor phase was determined at each point through the boundary layer from Equation [A.6] by the Newton-Raphson method. The pure component critical constants were determined from Reference 23.

The partial molal enthalpy of component i in the gaseous mixture was determined by the following thermodynamic relation

$$\frac{H_i^o - \bar{H}_i}{RT^2} = \frac{\partial}{\partial T}\left(\ln \frac{f_i}{x_i P}\right) \qquad [A.7]$$

where, in the gas phase[22]

$$\ln \frac{f_i}{x_i P} = \frac{B_i}{B}(z - 1) - \ln (z - BP) - \frac{A^2}{B}\left(\frac{2A_i}{A} - \frac{B_i}{B}\right)\ln\left(1 + \frac{BP}{z}\right) \qquad [A.8]$$

Thus, differentiating Equation [A.8] with respect to temperature, the following expression is obtained:

$$\frac{H_i^o - \bar{H}_i}{RT^2} = \left[\frac{B_i}{B} - \frac{1}{z - BP} + \frac{A^2}{B}\left(\frac{2A_i}{A} - \frac{B_i}{B}\right)\frac{PB}{z(z + BP)}\right] C' + \frac{B}{T}\left[\frac{A^2}{B}\left(\frac{2A_i}{A} - \frac{B_i}{B}\right)\frac{P}{z + BP} - \frac{P}{z - BP}\right] + \frac{3}{2T}\left[\ln\left(1 + \frac{BP}{z}\right)\left(\frac{2A_i}{A} - \frac{B_i}{B}\right)\frac{A^2}{B}\right] \qquad [A.9]$$

where

$$C' = \frac{-\frac{7P^2A^2B}{2T} + \frac{P}{T}\left(\frac{5}{2}A^2 - B - 2PB^2\right)z}{3z^2 - 2z + P(A^2 - B - B^2P)}$$

From the above equation

$$\lim_{\substack{P \to 0 \\ z \to 1}} \bar{H}_i = H_i^o \qquad [A.10]$$

In order to determine the vapor-liquid equilibrium conditions at the interface, as well as the enthalpy of vaporization, Equation [A.1] may be arranged as

$$z^3 - z^2 + \left(\frac{a}{T^{0.5}} - bRT - b^2P\right)\frac{Pz}{(RT)^2} - \frac{abP^2}{R^3T^{3.5}} = 0 \qquad [A.11]$$

with the following mixing rules slightly modified from Reference 7:

$$a = \sum_i \sum_j x_i x_j a_{ij} \qquad [A.12]$$

$$b = \sum_i x_i b_i \qquad [A.13]$$

$$a_{ii} = \Omega_{ai} R^2 T_{ci}^{2.5}/P_{ci} \qquad [A.14]$$

$$a_{ij} = 0.5(\Omega_{ai} + \Omega_{aj})RT_{cij}^{1.5} v_{cij}/[0.291-0.04(\omega_i + \omega_j)] \qquad [A.15]$$

$$b_i = \Omega_{bi} RT_{ci}/P_{ci} \qquad [A.16]$$

$$v_{cij}^{1/3} = (v_{ci}^{1/3} + v_{cj}^{1/3})/2 \qquad [A.17]$$

$$T_{cij} = (T_{ci}T_{cj})^{1/2} \qquad [A.18]$$

Pure component constants were determined from References 5 and 23.

The fugacity of each component was determined by[7]

$$\ln \frac{f_i}{x_i P} = \ln \frac{v}{v-b} + \frac{b_i}{v-b} - \frac{2\sum_j x_j a_{ij}}{RT^{1.5}b} \ln \frac{v+b}{v}$$

$$+ \frac{ab_i}{RT^{1.5}b^2}\left(\ln \frac{v+b}{v} - \frac{b}{v+b}\right) - \ln \frac{Pv}{RT} \qquad [A.19]$$

where the molar volume was determined via Equation [A.11]. The heat of vaporization was determined via Equation [A.7].

B. Transport Properties

Thermal Conductivity

Painstaking experimental investigations seem to confirm a considerable enhancement in the thermal conductivity of some pure substances in the immediate vicinity of their thermodynamic critical point[35]. However, contrary to this behavior in the case of a pure substance, the thermal conductivity of some binary mixtures investigated[25] does not exhibit

any pronounced anomaly near the critical mixing point. The absence of this anomaly seems to be established.

Very few experimental data on the thermal conductivity of CO_2-N_2 mixtures at high pressures are available to be correlated. In the absence of this information, the thermal conductivity of the gaseous mixture was calculated by using the Stiel and Thodos pure component correlation[29] treating the mixture as a hypothetical pure substance with pseudo-critical properties:

$$(k - k^o)\bar{g}\bar{z}_c = 14\times10^{-8}(\exp 0.535\bar{c}_r - 1) \ , \ \bar{c}_r < 0.5$$

$$(k - k^o)\bar{g}\bar{z}_c = 13.1\times10^{-8}(\exp 0.67\bar{c}_r - 1.069) \ , \quad 0.5 < \bar{c}_r < 2.0 \qquad [A.20]$$

$$(k - k^o)\bar{g}\bar{z}_c = 2.976\times10^{-8}(\exp 1.155\bar{c}_r + 2.016) \ , \quad 2.0 < \bar{c}r < 2.8$$

where

$$\bar{g} = \bar{T}_c^{\,1/6}\bar{M}^{1/2} / \bar{P}_c^{\,2/3} \qquad [A.21]$$

$$\bar{c}_r = \bar{v}_c/v \qquad [A.22]$$

The pseudocritical constants were determined by using the Prausnitz and Gunn's modified rules[23]:

$$\bar{v}_c = x_A v_{cA} + (1-x_A)v_{cB} \qquad [A.23]$$

$$\bar{z}_c = x_A z_{cA} + (1-x_A)z_{cB} \qquad [A.24]$$

$$\bar{T}_c = x_A T_{cA} + (1-x_A) T_{cB} \qquad [A.25]$$

$$\bar{P}_c = R\bar{z}_c \bar{T}_c / \bar{v}_c \qquad [A.26]$$

$$\bar{M} = x_A M_A + (1-x_A) M_B \qquad [A.27]$$

The molar volume of the mixture was computed via Equation [A.6]. Estimation of the mixture thermal conductivity at low pressures is required. Since it is not in general a linear mole fraction average of the pure component thermal conductivities, Brokaw's method[4] was used:

$$k^o = qk_L + (1-q)k_R \qquad [A.28]$$

where

$$k_L = x_A k_A^o + (1-x_A) k_B^o \qquad [A.29]$$

$$1/k_R = x_A/k_A^o + (1-x_A)/k_B^o \qquad [A.30]$$

$$q = 0.3171300 + 0.2878377(1-x_A) - 0.2380630(1-x_A)^2 + 0.4273880(1-x_A)^3$$

$$= q(\text{mole fraction of light component}) \qquad [A.31]$$

Pure component properties were obtained from References 19, 20, and 23.

The correlation and its computer subroutine were tested against one experimental point[15] at T = 323.2 °K, P = 81 atm., and x_A = 0.659. Although the calculated thermal conductivity

value was found to agree within 1.5 percent of the experimental value, less accuracy may be expected in general under the conditions prevailing in the gaseous film surrounding the vaporizing droplets studied.

Diffusivity D_{AB}

Experimental data on the coefficient of binary diffusion D_{AB} for high pressure mixtures are very scarce. The product cD_{AB} was estimated from a corresponding-states chart for non-polar substances based on self-diffusion measurements[28,30]. Accurate results are obtained at low densities. At high densities the method is regarded as provisional, for very few data are available for comparison.

APPENDIX B

A. STEADY STATE VAPORIZATION AT HIGH PRESSURES

```
C
C     THIS PROGRAM COMPUTES TEMPERATURE AND COMPOSITION
C     PROFILES, AMBIENT TEMPERATURE, AND RATE OF VAPORIZATION
C     FOR SOME GIVEN STEADY STATE CONDITIONS. IT ALSO
C     COMPUTES INITIAL CONDITIONS FOR UNSTEADY VAPORIZATION.
C
C     INPUT DATA
C     R(1) IS THE DROPLET RADIUS
C     T(1) IS THE LIQUID TEMPERATURE
C     XA(1) IS THE MOLE FRACTION AT THE INTERFACE
C     DIFH IS THE ENTHALPY OF VAPORIZATION
C     P IS THE TOTAL PRESSURE
C     Q IS THE ENERGY GOING INTO THE DROPLET, CAL/SEC. UNDER
C     STEADY STATE CONDITIONS SET Q=0. FOR INITIAL CONDITIONS
C     IN UNSTEADY VAPORIZATION Q IS NOT EQUAL TO ZERO.
C     WGM IS A CLOSE GUESS VALUE TO THE VAPORIZATION
C     RATE, GMS/SEC.
C     DELTA IS THE SPACE INCREMENT IN NUMERICAL TECHNIQUE
C
C     OUTPUT DATA
C     TEMPERATURE AND COMPOSITION PROFILES IN THE GAS
C     PHASE, AMBIENT TEMPERATURE, AND RATE OF VAPORIZATION.
C
      DIMENSION T(1000), XA(1000), R(1000), DXA(1000),
     1Y(1000), DY(1000)
      COMMON TL,P,XL,CONL,ZL,HAL
      DEFINE CDRF(T)= 1.14*(T/TC)**(9./10.)
      PRINT 15
   15 FORMAT (1H1,9X,6HRADIUS,14X,4HTEMP,14X,4HMOLE)
      ITER= 0
      DELW= 1.0E-5
      WGM= 0.2E-3
      DELTA= 0.0025
      ML= 300
      PI= 3.14159265
      P= 112.0
      Q= 1.5E-2
    7 ITER= ITER+1
      R(1)= 0.1
      T(1)= 243.36
      XA(1)= 0.335
      DIFH= 1212.
      TCA= 304.2
      TCB= 126.2
      WA= 44.01
      WB= 28.016
      PCA= 72.9
```

```
      PCB= 33.5
      CDABC= 3.05E-6*(1./WA+1./WB)**(1./2.)*(PCA*PCB)
     1**(1./3.)/((TCA*TCB)**(1./12.))
      TC= SQRT(TCA*TCB)
      W= WGM/WA
      DT= 0.001
      DX= 0.001
      TL= T(1)
      XL= XA(1)
      CALL COND
      CON= CONL
      Y(1)= (W*DIFH+Q)/(4.*PI*CON*R(1)**2)
      N= 1
  101 CDAB= CDRF(T(N))*CDABC
      DXA(N)= -W*(1.-XA(N))/(4.*PI*CDAB*R(N)**2)
      TN2= T(N)+DT
      TN1= T(N)-DT
      TL= TN2
      XL= XA(N)
      CALL COND
      CALL ENTH
      CT2= CONL
      HAT2= HAL
      TL= TN1
      CALL COND
      CALL ENTH
      CT1= CONL
      HAT1= HAL
      CONT= (CT2-CT1)/(2.*DT)
      HAT= (HAT2-HAT1)/(2.*DT)
      XN2= XA(N)+DX
      XN1= XA(N)-DX
      TL= T(N)
      XL= XN2
      CALL COND
      CALL ENTH
      CX2= CONL
      HAX2= HAL
      XL= XN1
      CALL COND
      CALL ENTH
      CX1= CONL
      HAX1= HAL
      CONX= (CX2-CX1)/(2.*DX)
      HAX= (HAX2-HAX1)/(2.*DX)
      DY(N)= W*HAX*DXA(N)/(4.*PI*CON*R(N)**2)- (2./R(N) + CONX*
     1DXA(N)/CON + CONT*Y(N)/CON - W*HAT/(4.*PI*CON*R(N)**2))
     2*Y(N)
      HEUN METHOD
      R1= R(N)+(1./3.)*DELTA
      XA1= XA(N)+(1./3.)*DELTA*DXA(N)
      Y1= Y(N)+(1./3.)*DELTA*DY(N)
```

```
      T1= T(N)+(1./3.)*DELTA*Y(N)
      CDAB1= CDRF(T1)*CDABC
      DXA1= -W*(1.-XA1)/(4.*PI*CDAB1*R1**2)
      TL= T1
      XL= XA1
      CALL COND
      CON1= CONL
      TN21= T1+DT
      TN11= T1-DT
      TL= TN21
      CALL COND
      CALL ENTH
      CT21= CONL
      HAT21= HAL
      TL= TN11
      CT11= CONL
      HAT11= HAL
      CONT1= (CT21-CT11)/(2.*DT)
      HAT1= (HAT21-HAT11)/(2.*DT)
      XN21= XA1+DX
      XN11= XA1-DX
      TL= T1
      XL= XN21
      CALL COND
      CALL ENTH
      CX21= CONL
      HAX21= HAL
      XL= XN11
      CALL COND
      CALL ENTH
      CX11= CONL
      HAX11= HAL
      CONX1= (CX21-CX11)/(2.*DX)
      HAX1= (HAX21-HAX11)/(2.*DX)
      DY1= W*HAX1*DXA1/(4.*PI*CON1*R1**2) - (2./R1 + CONX1*
     1DXA1/CON1 + CONT1*Y1/CON1 - W*HAT1/(4.*PI*CON1*R1**2))
     2*Y1
      R2= R(N)+(2./3.)*DELTA
      XA2= XA(N)+(2./3.)*DELTA*DXA1
      Y2= Y(N)+(2./3.)*DELTA*DY1
      T2= T(N)+(2./3.)*DELTA*Y1
      CDAB2= CDRF(T2)*CDABC
      DXA2= -W*(1.-XA2)/(4.*PI*CDAB2*R2**2)
      TL= T2
      XL= XA2
      CALL COND
      CON2= CONL
      TN22= T2+DT
      TN12= T2-DT
      TL= TN22
      CALL COND
      CALL ENTH
```

```
      CT22= CONL
      HAT22= HAL
      TL= TN12
      CALL COND
      CALL ENTH
      CT12= CONL
      HAT12= HAL
      CONT2= (CT22-CT12)/(2.*DT)
      HAT2= (HAT22-HAT12)/(2.*DT)
      XN22= XA2+DX
      XN12= XA2-DX
      TL= T2
      XL= XN22
      CALL COND
      CALL ENTH
      CX22= CONL
      HAX22= HAL
      XL= XN12
      CALL COND
      CALL ENTH
      CX12= CONL
      HAX12= HAL
      CONX2= (CX22-CX12)/(2.*DX)
      HAX2= (HAX22-HAX12)/(2.*DX)
      DY2= W*HAX2*DXA2/(4.*PI*CON2*R2**2) - (2./R2 + CONX2*
     1DXA2/CON2 + CONT2*Y2/CON2 - W*HAT2/(4.*PI*CON2*R2**2))
     2*Y2
      M= N+1
      R(M)= R(N)+DELTA
      XA(M)= XA(N)+DELTA*((1./4.)*DXA(N)+(3./4.)*DXA2)
      Y(M)= Y(N)+DELTA*((1./4.)*DY(N)+(3./4.)*DY2)
      T(M)= T(N)+DELTA*((1./4.)*Y(N)+(3./4.)*Y2)
      IF (ML-M) 104,104,103
  103 N=M
      IF(49-N) 111,111,112
  111 DELTA= 0.01
  112 CONTINUE
      K= N-1
      EPST= T(N)-T(K)
      IF(EPST-0.3) 108,108,107
  108 CONTINUE
      SWITCH TO ASYMPTOTIC SOLUTION
      CPA= HAT
      XAID= 1. - EXP(-W/(4.*PI*CDAB*R(K)))
      TINID= T(K) + 4.*PI*CON*Y(K)*R(K)**2*(EXP(W*CPA/(4.*
     1PI*CON*R(K)))-1.)/(W*CPA)
      EPSXA= XA(K)-XAID
      IF (2-ITER) 12,11,10
   10 EPSXAP= EPSXA
      WGP= WGM
      WGM= WGM+DELW
      GO TO 7
```

```
   11 WGM= WGP+EPSXAP*DELW/(EPSXAP-EPSXA)
      GO TO 7
   12 DO 8 IND= 1,N
    8 PRINT 9, R(IND),T(IND),XA(IND)
    9 FORMAT (1HO, 3E20.6)
      PRINT 13
   13 FORMAT (1HO,9X,11HTEMPERATURE,15X,4HFLOW)
      PRINT 14, TINID, WGM
   14 FORMAT (1HO, 2E20.6)
      STOP
  107 CONTINUE
      TL= T(N)
      XL= XA(N)
      CALL COND
      CON= CONL
      GO TO 101
  104 STOP
      END


      SUBROUTINE PVTX
      COMMON TL,P,XL,CONL,ZL,HAL
      REDLICH-KWONG EQUATION OF STATE
      TCA= 304.2
      TCB= 126.2
      PCA= 72.9
      PCB= 33.5
      T= TL
      XA= XL
      TRA= T/TCA
      TRB= T/TCB
      ASA= SQRT(0.4278/(TRA**(5./2.)*PCA))
      ASB= SQRT(0.4278/(TRB**(5./2.)*PCB))
      BSA= 0.0867/(TRA*PCA)
      BSB= 0.0867/(TRB*PCB)
      ASM= XA*ASA + (1. - XA)*ASB
      BSM= XA*BSA + (1. - XA)*BSB
      ASMS= ASM**2
      NEWTON RAPHSON METHOD
      C3= 1.0
      C2= -1.0
      C1= P*(ASMS - BSM - P*BSM**2)
      C0= - ASMS*BSM*P**2
      Z0= 1.0
      ZM= Z0
      ITN= 0
   42 B= C3
      C= B
      B= C2 + ZM*B
      C= B + ZM*C
      B= C1 + ZM*B
      C= B + ZM*C
```

```
      B= CO + ZM*B
      ZNEW= ZM - B/C
      IF (ABS((ZM - ZNEW)/ZNEW) - 0.01) 43,44,44
   44 ITN= ITN + 1
      IF (ITN - 20) 45,46,46
   45 ZM= ZNEW
      GO TO 42
   46 PRINT 3
    3 FORMAT (1X, 34HFAILS TO CONVERGE IN 20 ITERATIONS)
      PRINT 64, ZM
   64 FORMAT (E10.3)
      STOP
   43 ZM= ZNEW
      Z= ZM
      ZL= Z
      RETURN
      END


      SUBROUTINE COND
      COMMON TL,P,XL,CONL,ZL,HAL
      THERMAL CONDUCTIVITY OF THE MIXTURE
      TCA= 304.2
      TCB= 126.2
      WA= 44.01
      WB= 28.016
      SIGA= 3.941
      SIGB= 3.798
      TBA= 195.2
      TBB= 71.4
      R= 1.98588
      ZCA= 0.274
      ZCB= 0.291
      VCA= 94.0
      VCB= 90.1
      T= TL
      XA= XL
      TRA= T/TCA
      TRB= T/TCB
      VISCOSITIES AT LOW PRESSURE, POISES
      TSA= T/TBA
      TSB= T/TBB
      OMAR= 0.697*(1. + 0.323*LOG(TSA))
      OMBR= 0.697*(1. + 0.323*LOG(TSB))
      VISA= 2.669E-5*OMAR*SQRT(WA*T)/(SIGA**2)
      VISB= 2.669E-5*OMBR*SQRT(WB*T)/(SIG3**2)
      SPECIFIC HEATS AT LOW PRESSURE, CAL/GMOLE K
      IF (T - 240.) 20,21,21
   20 PRINT 22
   22 FORMAT (1X, 25HHEAT CAPACITY IS EXCEEDED)
      STOP
   21 CONTINUE
```

```
      IF (1500. - T) 20,23,23
   23 CONTINUE
      CVA= 5.10709 + 15.42195E-3*T - 9.92626E-6*T**2 +
     12.40272E-9*T**3 - R
      CVB= 7.08396 - 1.28565E-3*T + 3.21241E-6*T**2 -
     11.20800E-9*T**3 - R
      THERMAL CONDUCTIVITY AT LOW PRESSURE
      CONA= (VISA/WA)*(1.30*CVA + 3.40 - 0.70/TRA)
      CONB= (VISB/WB)*(1.30*CVB + 3.40 - 0.70/TRB)
      BROKAW METHOD
      Q= 0.31713 + 0.28784*(1. - XA) - 0.23806*(1. - XA)**2
     1+0.42739*(1. - XA)**3
      CML= XA*CONA + (1. - XA)*CONB
      CMRR= XA/CONA + (1. - XA)/CONB
      CMR= 1./CMRR
      CONO= Q*CML + (1. - Q)*CMR
      THERMAL CONDUCTIVITY AT HIGH PRESSURE
      TCM= XA*TCA + (1. - XA)*TCB
      ZCM= XA*ZCA + (1. - XA)*ZCB
      W= XA*WA + (1. - XA)*WB
      VCM= XA*VCA + (1. - XA)*VCB
      PCM= 82.0544*ZCM*TCM/VCM
      CALL PVTX
      Z= ZL
      V= 82.0544*Z*T/P
      ROR= VCM/V
      GAM= TCM**(1./6.)*SQRT(W)/(PCM**(2./3.))
      F= GAM*ZCM**5
      IF (0.5 - ROR) 11,10,10
   11 IF (2.0 - ROR) 12,13,13
   12 IF (2.8 - ROR) 15,14,14
   15 PRINT 16
   16 FORMAT (1X, 27HREDUCED DENSITY IS EXCEEDED)
      STOP
   10 DIF= 14.0E-8*(EXP(0.535*ROR) - 1.)
      GO TO 17
   13 DIF= 13.1E-8*(EXP(0.67*ROR) - 1.069)
      GO TO 17
   14 DIF= 2.976E-8*(EXP(1.155*ROR) + 2.016)
   17 CON= DIF/F + CONO
      CONL= CON
      RETURN
      END


      SUBROUTINE ENTH
      COMMON TL,P,XL,CONL,ZL,HAL
      PARTIAL MOLAL ENTHALPY OF CO2 IN CO2-N2 MIXTURE
      T= TL
      XA= XL
      PURE COMPONENT DATA
      TCA= 304.2
```

```
      TCB= 126.2
      PCA= 72.9
      PCB= 33.5
      R= 1.98588
      ENTHALPY OF CO2 AT LOW PRESSURE
      HAO= 5.10709*T + 7.71097E-3*T**2 - 3.30875E-6*T**3
     1+0.60068E-9*T**4
      GENERAL EXPRESSIONS
      TRA= T/TCA
      TRB= T/TCB
      ASA= SQRT(0.4278/(TRA**(5./2.)*PCA))
      ASB= SQRT(0.4278/(TRB**(5./2.)*PCB))
      BSA= 0.0867/(TRA*PCA)
      BSB= 0.0867/(TRB*PCB)
      ASM= XA*ASA + (1. - XA)*ASB
      BSM= XA*BSA + (1. - XA)*BSB
      ASMS= ASM**2
      CALL PVTX
      Z= ZL
      COMPRESSIBILITY FACTOR VIA R-K EQN. OF STATE
      ZM= Z
      F1= BSA/BSM
      F2= 1./(ZM - BSM*P)
      F3= ASMS/BSM
      F4= 2.*ASA/ASM
      F5= 1./(ZM + BSM*P)
      F6= BSM*P/ZM
      F7= - 3.5*P**2*ASMS*BSM/T
      F8= (P*ZM/T)*(2.5*ASMS - BSM - 2.*P*BSM**2)
      F9= 3.*ZM**2 - 2.*ZM + P*(ASMS - BSM - P*BSM**2)
      DZMT= (F7 + F8)/F9
      HA= HAO - ((F1 - F2 + F3*(F4 - F1)*P*BSM*F5/ZM)*DZMT
     1+ (BSM/T)*(F3*(F4-F1)*P*F5 - P*F2) + (1.5/T)*
     2(LOG(1.+F6)*F3*(F4-F1)))*R*T**2
      HAL= HA
      RETURN
      END
```

```
B. UNSTEADY VAPORIZATION AT HIGH PRESSURES

THIS PROGRAM COMPUTES THE VAPORIZATION HISTORY
OF A CO2 DROPLET VAPORIZING IN N2

INPUT DATA
TAMB IS THE AMBIENT TEMPERATURE
P IS THE TOTAL PRESSURE
R IS THE INITIAL DROPLET RADIUS
T(1,1) IS THE INITIAL DROPLET TEMPERATURE
T(I,1) IS THE INITIAL TEMPERATURE PROFILE
X(I,1) IS THE INITIAL COMPOSITION PROFILE
H IS THE SPACE INCREMENT SIZE, CM
ML-1 IS THE NUMBER OF SPACE INCREMENTS IN THE FILM
ISOBARIC FUNCTIONS DEFINED BELOW

OUTPUT DATA
DROPLET RADIUS, LIQUID TEMPERATURE, PERCENT-MASS-
VAPORIZED, AND VAPORIZATION RATE AS FUNCTIONS OF TIME.

 DIMENSION T(60,2), X(60,2), CT(60,2), CX(60,2)
 COMMON TL,P,XL,CONL,ZL,HAL,HBL
 DEFINE XVAPF(T)= 9.32293-24.97980*(T/TCA)+11.16181*
1(T/TCA)**2+15.94869*(T/TCA)**3-10.53194*(T/TCA)**4
 DEFINE DELTAF(T)= -11.03026+12.59688E3*(0.95-T/TCA)
1-7.89935E4*(0.95-T/TCA)**2+7.36357E5*(0.95-T/TCA)**3
2-4.03143E6*(0.95-T/TCA)**4+8.75409E6*(0.95-T/TCA)**5
 DEFINE CALF(T)= (81.75810-3.39598E2*(T/TCA)+4.45397E2*
1(T/TCA)**2+46.67570*(T/TCA)**3-6.05500E2*(T/TCA)**4+
25.12341E2*(T/TCA)**5-1.39428E2*(T/TCA)**6)*CCA
 DEFINE DCALTF(T)= (-3.39598E2/TCA+8.90794E2*T/(TCA**2)+
114.00271E1*T**2/(TCA**3)-24.22000E2*T**3/(TCA**4)+
225.61705E2*T**4/(TCA**5)-8.36568E2*T**5/(TCA**6))*CCA
 DEFINE CPAIF(T)= 5.10709+15.42195E-3*T-9.92626E-6*T**2+
12.40272E-9*T**3
 DEFINE DHALF(T)= CPAIF(T)-TCA*(1.01778E3/TCA-2.49614E3*T/
1(TCA**2)+11.41152E2*T**2/(TCA**3)+5.14988E1*T**3/(TCA**4)+
215.39960E2*T**4/(TCA**5)-12.82104E2*T**5/(TCA**6))
 DEFINE CDABF(T)= 1.14*CDABC*(T/TC)**(9./10.)
 DEFINE DCDABF(T)= (1.026/((T/TC)**(0.1)*TC))*CDABC
 THE ABOVE FCNS. DEFINE MOLE FRACTION AT THE INTERFACE,
 HEAT OF VAPORIZATION, LIQUID DENSITY, ITS DERIVATIVE,
 IDEAL SPECIFIC HEAT, LIQUID SPECIFIC HEAT, CDAB, AND
 ITS DERIVATIVE
 TOTAL PRESSURE EQUAL TO 112 ATM.
 DROP TEMP. RANGE 243-305 K.
 TEMPERATURE RANGE 240-1500 K.
 VAPORIZATION CONDITIONS
```

```
      TAMB= 1184.
      P= 112.
      R= 0.1
      T(1,1)= 273.78
      PRINT 1
    1 FORMAT (5X,4HTEMP,17X,8HPRESSURE)
      PRINT 2, TAMB,P
    2 FORMAT (2E20.6)
      PRINT 5
    5 FORMAT (6X,4HTIME,9X,6HRADIUS,8X,4HTEMP,8X,4HPERC,9X,
     14HFLOW,9X,7HERROR)
      H= 0.04
      DT= 0.001
      DX= 0.001
      ML= 26
      STAB= 0.5
      RMIN= 0.01
      LINES ARE PRINTED EVERY INDEX NUMBER OF TIME INCREMENTS
      INDEX= 1
      KL= ML-1
      JL= ML-2
      ITN= 1
      RG= 82.0567
      TCA= 304.2
      TCB= 126.2
      WA= 44.01
      WB= 28.016
      PCA= 72.9
      PCB= 33.5
      VCA= 94.0
      PI= 3.1415926
      CCA= 1./VCA
      CDABC= 3.05E-6*(1./WA+1./WB)**(1./2.)*(PCA*PCB)**(1./3.)/
     1((TCA*TCB)**(1./12.))
      TC= SQRT(TCA*TCB)
      DRIN= (4./3.)*PI*CALF(T(1,1))*R**3
      X(1,1)= XVAPF(T(1,1))
      INITIAL CONDITIONS ARE READ
      DO 3 IN= 2,ML
    3 READ 4, T(IN,1),X(IN,1)
    4 FORMAT (F10.0, F15.0)
      TINF= TAMB
      XINF= 0.
      TINF1= TINF+DT
      TL= TINF
      XL= XINF
      CALL PVTX
      ZINF= ZL
      CALL COND
      CALL ENTB
      CONINF= CONL
      HBINF= HBL
```

```
      TL= TINF1
      CALL PVTX
      CALL ENTB
      HBINF1= HBL
      CINF= P/(ZINF*RG*TINF)
      CPBINF= (HBINF1-HBINF)/DT
      ALFA= CONINF/(CINF*CPBINF)
      DIFF= CDABF(TINF)/CINF
      TIME INCREMENT IS DETERMINED
      IF (ALFA-DIFF) 22,21,21
   22 HK= STAB*H**2/DIFF
      GO TO 23
   21 HK= STAB*H**2/ALFA
   23 CONTINUE
      J= 1
      M= J+1
   18 AIK= ITN
      TIME= (AIK-1.)*HK
      TLO= T(1,J)
      ITE= 1
   29 CONTINUE
      XAO= X(1,J)
      XAO1= XAO+DX
      TO1= TLO+DT
      TL= TO1
      XL= XAO
      CALL PVTX
      ZOT1= ZL
      TL= TLO
      CALL PVTX
      ZO= ZL
      CALL COND
      CONO= CONL
      XL= XAO1
      CALL PVTX
      ZOX1= ZL
      COT1= P/(ZOT1*RG*TO1)
      CO= P/(ZO*RG*TLO)
      CT(1,J)= (COT1-CO)/DT
      COX1= P/(ZOX1*RG*TLO)
      CX(1,J)= (COX1-CO)/DX
      XH1= (-274.*X(1,J)+600.*X(2,J)-600.*X(3,J)+400.*X(4,J)-
     1150.*X(5,J)+24.*X(6,J))/(120.*H)
      TH1= (-274.*T(1,J)+600.*T(2,J)-600.*T(3,J)+400.*T(4,J)-
     1150.*T(5,J)+24.*T(6,J))/(120.*H)
      V= -CDABF(T(1,J))*XH1/(CO*(1.-X(1,J)))
      WY= 4.*PI*R**2*CO*V
      QCON= 4.*PI*R**2*CONO*TH1
      HEAT= DELTAF(T(1,J))
      CRITICAL MIXING LINE IS TESTED
      IF (HEAT-0.) 10,10,9
    9 CONTINUE
```

```
      FAC1= CO*X(1,J)/(CO*X(1,J)+CALF(T(1,J)))
      FAC2= (4./3.)*PI*R**3*(CALF(T(1,J))*DHALF(T(1,J))-
     1FAC1*DELTAF(T(1,J))*DCALTF(T(1,J)))
      TLT= (QCON-WY*DELTAF(T(1,J))*(1.-FAC1))/FAC2
      DR= (CDABF(T(1,J))*XH1-(R/3.)*(1.-X(1,J))*DCALTF(T(1,J))
     1*TLT)/((CO*X(1,J)+CALF(T(1,J)))*(1.-X(1,J)))
      W= WY+4.*PI*R**2*CO*X(1,J)*DR
      TNSC= TLT*HK+T(1,J)
      T(1,M)= TNSC
      X(1,M)= XVAPF(T(1,M))
      GO TO 11
   10 TLT= QCON/((4./3.)*PI*R**3*CALF(T(1,J))*DHALF(T(1,J)))
      TNEW= TLT*HK+T(1,J)
      DRC= (CDABF(T(1,J))*XH1-(R/3.)*(1.-X(1,J))*DCALTF(T(1,J))
     1*TLT)/((CO*X(1,J)+CALF(T(1,J)))*(1.-X(1,J)))
      DR= DRC
      RNEW= DR*HK+R
      WC= WY+4.*PI*R**2*CO*X(1,J)*DR
      W= WC
      IF (ITE-1) 32,31,32
   31 COP= CO
      CTP= CT(1,J)
      CXP= CX(1,J)
      VP= V
      WP= W
      QCP= QCON
      DRP= DR
      TLTP= TLT
      XH1P= XH1
      TH1P= TH1
      XP= X(1,J)
   32 CONTINUE
      DRON= (4./3.)*PI*CALF(TNEW)*RNEW**3
      DROC= (4./3.)*PI*CALF(T(1,J))*R**3
      DISC= DROC-DRON
      DELX= 0.005
      IF (2-ITE) 15,15,14
   14 X(1,J)= X(1,J)+DELX
      ITE= ITE+1
      DISCP= DISC
      GO TO 29
   15 SLOPE= (DISC-DISCP)/DELX
      BCONS= DISCP-SLOPE*XP
      X(1,M)= (WP*HK-BCONS)/SLOPE
      T(1,M)= TLTP*HK+T(1,J)
      CO= COP
      CT(1,J)= CTP
      CX(1,J)= CXP
      V= VP
      W= WP
      QCON= QCP
      DR= DRP
```

```
      TLT= TLTP
      XH1= XH1P
      TH1= TH1P
      X(1,J)= XP
   11 CONTINUE
      IF(ITN-1) 25,25,26
   25 WINIT= W
      VAPOR= 0.
      SUMV= 0.
      GO TO 27
   26 VAPOR= (HK/2.)*(WINIT+W+2.*SUMV)
      SUMV= SUMV+W
   27 CONTINUE
      DROP= (4./3.)*PI*CALF(T(1,J))*R**3
      PERC= (1.-DROP/DRIN)*100.
      ER= (PERC-(VAPOR/DRIN)*100.)*100./PERC
      OVERALL CONTINUITY IS CHECKED
      ERROR= ABS(ER)
      WGM= W*WA
      IF (1-INDEX) 8,7,8
    7 CONTINUE
      PRINT 6, TIME,R,T(1,J),PERC,WGM,ERROR
    6 FORMAT (1H0,6E13.6)
      INDEX= 0
    8 INDEX= INDEX+1
      SUM= 0.
      SUME= 0.
      INTEGRATION THROUGH THE BOUNDARY LAYER IS INITIATED
      DO 16 I= 2,KL
      K= I+1
      L= I-1
      AI= I
      Y= (AI-1.)*H
      T1= T(I,J)+DT
      X1= X(I,J)+DX
      TL= T(I,J)
      IF (304.2-T(1,J)) 34,33,33
   34 STOP
   33 CONTINUE
      IF (X(I,J)-0.) 500,501,501
  500 PRINT 502
  502 FORMAT (1X, 25HMOLE FRACTION IS NEGATIVE)
      STOP
  501 CONTINUE
      XA= X(I,J)
      XL= XA
      CALL PVTX
      Z= ZL
      CALL COND
      CALL ENTA
      CALL ENTB
      CON= CONL
```

```
      HAL1= HAL
      HBL1= HBL
      XL= X1
      CALL PVTX
      ZX1= ZL
      CALL COND
      CALL ENTA
      CALL ENTB
      CX1= CONL
      HAX1= HAL
      HBX1= HBL
      TL= T1
      XL= XA
      CALL PVTX
      ZT1= ZL
      CALL COND
      CALL ENTA
      CALL ENTB
      CT1= CONL
      HAT1= HAL
      HBT1= HBL
      CONX= (CX1-CON)/DX
      CONT= (CT1-CON)/DT
      HAX= (HAX1-HAL1)/DX
      HBX= (HBX1-HBL1)/DX
      CPA= (HAT1-HAL1)/DT
      CPB= (HBT1-HBL1)/DT
      C= P/(Z*RG*T(I,J))
      DCX1= P/(ZX1*RG*T(I,J))
      DCT1= P/(ZT1*RG*T1)
      CX(I,J)= (DCX1-C)/DX
      CT(I,J)= (DCT1-C)/DT
      TL= T(I,J)
      CPM= XA*CPA+(1.-XA)*CPB
      F1= CDABF(TL)/C
      F2= DCDABF(TL)/C
      H1= (1./CPM)*(XA*HAX+(1.-XA)*HBX)
      H2= CON/(C*CPM)
      H3= (1./(C*CPM))*(CONX+CDABF(TL)*(CPA-CPB))
      H4= (1./(C*CPM))*CONT
      H5= CDABF(TL)*(HAX-HBX)/(C*CPM)
      XH= (X(K,J)-X(L,J))/(2.*H)
      TH= (T(K,J)-T(L,J))/(2.*H)
      XHH= (X(K,J)-2.*X(I,J)+X(L,J))/(H**2)
      THH= (T(K,J)-2.*T(I,J)+T(L,J))/(H**2)
      EPS= (R**2/((Y+R)**2*C))*(H/2.)*(CX(1,J)*XH1+CT(1,J)*TH1)+
     1(1./C)*(H/2.)*(CX(I,J)*XH+CT(I,J)*TH)+H*SUME/((Y+R)**2*C)
      A= R**2*CO*(V+DR)/((Y+R)**2*C)
      B= DR*(1.-EPS)
      D= (R**2/((Y+R)**2*C))*(H/2.)*(CX(1,J)*(X(1,M)-
     1X(1,J))/HK+CT(1,J)*(T(1,M)-T(1,J))/HK)
      E= H*SUM/((Y+R)**2*C)
```

```
      FIX= F1*XHH+(F2*TH+2.*F1/(Y+R)-A+B+D+E)*XH
      THETA= H2*THH+(H3*XH+H4*TH+2.*H2/(Y+R)-A+B+D+E)*TH-H1*F1
     1*XHH+(H5*XH-F2*H1*TH-2.*F1*H1/(Y+R))*XH
      G1= CX(I,J)*XH*H/(2.*C)
      TT= (THETA*(1.-G1)+FIX*TH*CX(I,J)*H/(2.*C))/(1.-G1-CT(I,J)
     1*TH*H/(2.*C))
      XT= (FIX+CT(I,J)*XH*H*TT/(2.*C))/(1.-G1)
      T(I,M)= HK*TT+T(I,J)
      X(I,M)= HK*XT+X(I,J)
      SUM= SUM+(Y+R)**2*(CX(I,J)*(X(I,M)-X(I,J))/HK+CT(I,J)*
     1(T(I,M)-T(I,J))/HK)
   16 SUME= SUME+(Y+R)**2*(CX(I,J)*XH+CT(I,J)*TH)
      R= R+DR*HK
      DIS= KL
      DSW= DIS*H
      T(ML,M)= (TAMB-(T(JL,M)-4.*T(KL,M))*(DSW+R)/(2.*H))/
     1(1.+3.*(DSW+R)/(2.*H))
      X(ML,M)= -((X(JL,M)-4.*X(KL,M))*(DSW+R)/(2.*H))/
     1(1.+3.*(DSW+R)/(2.*H))
      INTEGRATION THROUGH THE BOUNDARY LAYER IS TERMINATED
      IF DROPLET RADIUS IS LESS THAN RMIN THE PROCESS STOPS
      IF(R-RMIN) 19,19,17
   17 ITN= ITN+1
      DO 24 IND= 1,ML
      TEMP= T(IND,M)
      T(IND,J)= TEMP
      FRAC= X(IND,M)
      X(IND,J)= FRAC
   24 CONTINUE
      GO TO 18
   19 STOP
      END


      SUBROUTINE PVTX
      COMMON TL,P,XL,CONL,ZL,HAL,HBL
      REDLICH-KWONG EQUATION OF STATE
      T= TL
      XA= XL
      TCA= 304.2
      TCB= 126.2
      PCA= 72.9
      PCB= 33.5
      TRA= T/TCA
      TRB= T/TCB
      ASA= SQRT(0.4278/(TRA**(5./2.)*PCA))
      ASB= SQRT(0.4278/(TRB**(5./2.)*PCB))
      BSA= 0.0867/(TRA*PCA)
      BSB= 0.0867/(TRB*PCB)
      ASM= XA*ASA + (1. - XA)*ASB
      BSM= XA*BSA + (1. - XA)*BSB
      ASMS= ASM**2
```

```
      NEWTON RAPHSON METHOD
      C3= 1.0
      C2= -1.0
      C1= P*(ASMS - BSM - P*BSM**2)
      C0= - ASMS*BSM*P**2
      Z0= 1.0
      ZM= Z0
      ITN= 0
   42 B= C3
      C= B
      B= C2 + ZM*B
      C= B + ZM*C
      B= C1 + ZM*B
      C= B + ZM*C
      B= C0 + ZM*B
      ZNEW= ZM - B/C
      IF (ABS((ZM - ZNEW)/ZNEW) - 0.01) 43,44,44
   44 ITN= ITN + 1
      IF (ITN - 20) 45,46,46
   45 ZM= ZNEW
      GO TO 42
   46 PRINT 3
    3 FORMAT (1X, 34HFAILS TO CONVERGE IN 20 ITERATIONS)
      PRINT 64, ZM
   64 FORMAT (E10.3)
      STOP
   43 ZM= ZNEW
      Z= ZM
      ZL= Z
      RETURN
      END


      SUBROUTINE COND
      COMMON TL,P,XL,CONL,ZL,HAL,HBL
      THERMAL CONDUCTIVITY OF THE MIXTURE
      T= TL
      XA= XL
      TCA= 304.2
      TCB= 126.2
      WA= 44.01
      WB= 28.016
      SIGA= 3.941
      SIGB= 3.798
      TBA= 195.2
      TBB= 71.4
      R= 1.98588
      ZCA= 0.274
      ZCB= 0.291
      VCA= 94.0
      VCB= 90.1
      TRA= T/TCA
```

```
      TRB= T/TCB
      VISCOSITIES AT LOW PRESSURE, POISES
      TSA= T/TBA
      TSB= T/TBB
      OMAR= 0.697*(1. + 0.323*LOG(TSA))
      OMBR= 0.697*(1. + 0.323*LOG(TSB))
      VISA= 2.669E-5*OMAR*SQRT(WA*T)/(SIGA**2)
      VISB= 2.669E-5*OMBR*SQRT(WB*T)/(SIGB**2)
      SPECIFIC HEATS AT LOW PRESSURE, CAL/GMOLE K
      IF (T - 240.) 20,21,21
   20 PRINT 22
   22 FORMAT (1X, 25HHEAT CAPACITY IS EXCEEDED)
      STOP
   21 CONTINUE
      IF (1500. - T) 20,23,23
   23 CONTINUE
      CVA= 5.10709+15.42195E-3*T-9.92626E-6*T**2+
     12.40272E-9*T**3-R
      CVB= 7.08396-1.28565E-3*T+3.21241E-6*T**2-
     11.20800E-9*T**3-R
      THERMAL CONDUCTIVITY AT LOW PRESSURE
      CONA= (VISA/WA)*(1.30*CVA + 3.40 - 0.70/TRA)
      CONB= (VISB/WB)*(1.30*CVB + 3.40 - 0.70/TRB)
      BROKAW METHOD
      Q= 0.31713 + 0.28784*(1. - XA) - 0.23806*(1. - XA)**2 +
     10.42739*(1. - XA)**3
      CML= XA*CONA + (1. - XA)*CONB
      CMRR= XA/CONA + (1. - XA)/CONB
      CMR= 1./CMRR
      CONO= Q*CML + (1. - Q)*CMR
      THERMAL CONDUCTIVITY AT HIGH PRESSURE
      TCM= XA*TCA + (1. - XA)*TCB
      ZCM= XA*ZCA + (1. - XA)*ZCB
      W= XA*WA + (1. - XA)*WB
      VCM= XA*VCA + (1. - XA)*VCB
      PCM= 82.0544*ZCM*TCM/VCM
      Z= ZL
      V= 82.0544*Z*T/P
      ROR= VCM/V
      GAM= TCM**(1./6.)*SQRT(W)/(PCM**(2./3.))
      F= GAM*ZCM**5
      IF (0.5 - ROR) 11,10,10
   11 IF (2.0 - ROR) 12,13,13
   12 IF (2.8 - ROR) 15,14,14
   15 PRINT 16
   16 FORMAT (1X, 27HREDUCED DENSITY IS EXCEEDED)
      STOP
   10 DIF= 14.0E-8*(EXP(0.535*ROR) - 1.)
      GO TO 17
   13 DIF= 13.1E-8*(EXP(0.67*ROR) - 1.069)
      GO TO 17
   14 DIF= 2.976E-8*(EXP(1.155*ROR) + 2.016)
```

```
   17 CON= DIF/F + CONO
      CONL= CON
      RETURN
      END

      SUBROUTINE ENTA
      COMMON TL,P,XL,CONL,ZL,HAL,HBL
      PARTIAL MOLAL ENTHALPY OF CO2 IN CO2-N2 MIXTURE
      T= TL
      XA= XL
      PURE COMPONENT DATA
      TCA= 304.2
      TCB= 126.2
      PCA= 72.9
      PCB= 33.5
      R= 1.98588
      ENTHALPY OF CO2 AT LOW PRESSURE
      HAO= 5.10709*T + 7.71097E-3*T**2 - 3.30875E-6*T**3
     1+0.60068E-9*T**4
      GENERAL EXPRESSIONS
      TRA= T/TCA
      TRB= T/TCB
      ASA= SQRT(0.4278/(TRA**(5./2.)*PCA))
      ASB= SQRT(0.4278/(TRB**(5./2.)*PCB))
      BSA= 0.0867/(TRA*PCA)
      BSB= 0.0867/(TRB*PCB)
      ASM= XA*ASA + (1. - XA)*ASB
      BSM= XA*BSA + (1. - XA)*BSB
      ASMS= ASM**2
      Z= ZL
      COMPRESSIBILITY FACTOR VIA R-K EQN. OF STATE
      ZM= Z
      F1= BSA/BSM
      F2= 1./(ZM - BSM*P)
      F3= ASMS/BSM
      F4= 2.*ASA/ASM
      F5= 1./(ZM + BSM*P)
      F6= BSM*P/ZM
      F7= - 3.5*P**2*ASMS*BSM/T
      F8= (P*ZM/T)*(2.5*ASMS - BSM - 2.*P*BSM**2)
      F9= 3.*ZM**2 - 2.*ZM + P*(ASMS - BSM - P*BSM**2)
      DZMT= (F7 + F8)/F9
      HA= HAO - ((F1 - F2 + F3*(F4 - F1)*P*BSM*F5/ZM)*DZMT
     1+ (BSM/T)*(F3*(F4 - F1)*P*F5 - P*F2) + (1.5/T)*(LOG(1.
     2+ F6)*F3*(F4 - F1)))*R*T**2
      HAL= HA
      RETURN
      END
```

```
      SUBROUTINE ENTB
      COMMON TL,P,XL,CONL,ZL,HAL,HBL
      PARTIAL MOLAL ENTHALPY OF N2 IN CO2-N2 MIXTURE
      T= TL
      XA= XL
      PURE COMPONENT DATA
      TCA= 304.2
      TCB= 126.2
      PCA= 72.9
      PCB= 33.5
      R= 1.98588
      ENTHALPY OF N2 AT LOW PRESSURE
      HBO= 7.08396*T-0.64282E-3*T**2+1.0708E-6*T**3-
     10.3020E-9*T**4
      GENERAL EXPRESSIONS
      TRA= T/TCA
      TRB= T/TCB
      ASA= SQRT(0.4278/(TRA**(5./2.)*PCA))
      ASB= SQRT(0.4278/(TRB**(5./2.)*PCB))
      BSA= 0.0867/(TRA*PCA)
      BSB= 0.0867/(TRB*PCB)
      ASM= XA*ASA + (1. - XA)*ASB
      BSM= XA*BSA + (1. - XA)*BSB
      ASMS= ASM**2
      Z= ZL
      COMPRESSIBILITY FACTOR VIA R-K EQN. OF STATE
      ZM= Z
      F1= BSB/BSM
      F2= 1./(ZM - BSM*P)
      F3= ASMS/BSM
      F4= 2.*ASB/ASM
      F5= 1./(ZM + BSM*P)
      F6= BSM*P/ZM
      F7= - 3.5*P**2*ASMS*BSM/T
      F8= (P*ZM/T)*(2.5*ASMS - BSM - 2.*P*BSM**2)
      F9= 3.*ZM**2 - 2.*ZM + P*(ASMS - BSM - P*BSM**2)
      DZMT= (F7 + F8)/F9
      HB= HBO - ((F1 - F2 + F3*(F4 - F1)*P*BSM*F5/ZM)*DZMT
     1+ (BSM/T)*(F3*(F4 - F1)*P*F5 - P*F2) + (1.5/T)*(LOG(1.
     2+ F6)*F3*(F4 - F1)))*R*T**2
      HBL= HB
      RETURN
      END
```

TYPICAL INITIAL PROFILES DATA

```
421.385    0.223212
```

514.089	0.166914
570.815	0.133860
...	...

C. SEMI-EMPIRICAL VAPORIZATION MODEL (REF. 10)

```
      THIS PROGRAM COMPUTES THE VAPORIZATION HISTORY
      OF A CO2 DROPLET VAPORIZING IN N2

      INPUT DATA
      R IS THE INITIAL DROPLET RADIUS
      T IS THE INITIAL DROPLET TEMPERATURE
      TAMB IS THE AMBIENT TEMPERATURE
      P IS THE TOTAL PRESSURE
      DELTA IS THE TIME INCREMENT IN NUMERICAL TECHNIQUE

      OUTPUT DATA
      DROPLET TEMPERATURE, RADIUS, VAPORIZATION RATE,
      AND PERCENT-MASS-VAPORIZED AS FUNCTIONS OF TIME

      COMMON TL,P,PVL,CONL
      DEFINE CPAF(TD)= 5.10709+15.42195E-3*TD-9.92626E-6*
     1TD**2+2.40272E-9*TD**3
      DEFINE VAPF(TD)= 8.2208*(TD/100.-1.281)**(3.852)
      DEFINE CALF(TD)= (0.468+123.265E-3*(TCA-TD)**(0.391377)
     1-616.157E-6*(TCA-TD)+7.030546E-6*(TCA-TD)**2)/WA
      DEFINE DCALF(TD)= (-0.391377*123.265E-3/((TCA-TD)
     1**0.608623)+616.157E-6-14.061092E-6*(TCA-TD))/WA
      DEFINE DELF(TD)= TD*(7.90*TD/TCA-7.82-7.11*LOG(VAPF(TD)
     1/PCA)/2.30259)/(1.07-TD/TCA)
      DEFINE CPLF(TD)= (2.35579-2.56148E-2*(TD-273.15)+
     112.28015E-5*(TD-273.15)**2+17.35195E-5*(TD-273.15)
     2**3+37.68386E-7*(TD-273.15)**4)*WA/FAC
      DEFINE DABF(TD)= 2.745E-4*(TD/TC)**(1.823)*CT/P
      THE ABOVE FCNS. DEFINE IDEAL SPECIFIC HEAT, VAPOR
      PRESSURE, LIQUID DENSITY, ITS DERIVATIVE, LATENT
      HEAT, LIQUID SPECIFIC HEAT, AND DIFFUSIVITY
      LOW PRESSURE PROPERTIES
      PRINT 3
    3 FORMAT (1H1,8X,24HQUASI STEADY STATE MODEL)
      PRINT 4
    4 FORMAT (8X,4HTIME,11X,4HTEMP,12X,6HRADIUS,9X,4HFLOW,
     111X,4HPERC)
      FAC= 4.18605
      CCA= 1./94.
      TCA= 304.2
      TCB= 126.2
      PCA= 72.9
      PCB= 33.5
```

```
      WA= 44.01
      WB= 28.016
      TC= SQRT(TCA*TCB)
      CT= (PCA*PCB)**(1./3.)*(TCA*TCB)**(5./12.)*(1./WA+1./WB)
     1**(1./2.)
      DELTA= 26.7459E-2
      VAPORIZATION CONDITIONS
      T= 243.36
      R= 0.1
      TAMB= 373.769
      P= 112.0
      TIME= 0.
      PI= 3.1416
      WGTIN= 4.188*CALF(T)*R**3
      WGT= WGTIN
      RG= 82.0567
    8 PV= VAPF(T)
      HEAT= DELF(T)
      IF (HEAT-0.) 11,11,12
   11 STOP
   12 CONTINUE
      DEN= CALF(T)
      DENT= DCALF(T)
      SPH= CPLF(T)
      TAV= (T+TAMB)/2.
      DAB= DABF(TAV)
      CPA= CPAF(TAV)
      TL= TAV
      PVL= PV
      CALL COND
      CON= CONL
      W= 4.*PI*R*DAB*P*LOG(P/(P-PV))/(RG*TAV)
      WM= W*WA
      PERC= (1.-WGT/WGTIN)*100.
      PRINT 5, TIME,T,R,WM,PERC
    5 FORMAT (1HO, 5E15.6)
      Z= W*CPA/(4.*PI*R*CON)
      TLT= 4.*PI*R*CON*(TAMB-T)*Z/(WGT*SPH*(EXP(Z)-1.))-
     1W*HEAT/(WGT*SPH)
      DR= (-4.188*DENT*R**3*TLT-W)/(4.*PI*R**2*DEN)
      HEUN METHOD
      R1= R+(1./3.)*DELTA*DR
      T1= T+(1./3.)*DELTA*TLT
      WGT1= WGT-(1./3.)*DELTA*W
      PV1= VAPF(T1)
      HEAT1= DELF(T1)
      DEN1= CALF(T1)
      DENT1= DCALF(T1)
      SPH1= CPLF(T1)
      TAV1= (TAMB+T1)/2.
      DAB1= DABF(TAV1)
      CPA1= CPAF(TAV1)
```

```
      TL= TAV1
      PVL= PV1
      CALL COND
      CON1= CONL
      W1= 4.*PI*R1*DAB1*P*LOG(P/(P-PV1))/(RG*TAV1)
      Z1= W1*CPA1/(4.*PI*R1*CON1)
      TLT1= 4.*PI*R1*CON1*(TAMB-T1)*Z1/(WGT1*SPH1*(EXP(Z1)-1.))-
     1W1*HEAT1/(WGT1*SPH1)
      DR1= (-4.188*DENT1*R1**3*TLT1-W1)/(4.*PI*R1**2*DEN1)
      R2= R+(2./3.)*DELTA*DR1
      T2= T+(2./3.)*DELTA*TLT1
      WGT2= WGT-(2./3.)*DELTA*W1
      PV2= VAPF(T2)
      HEAT2= DELF(T2)
      DEN2= CALF(T2)
      DENT2= DCALF(T2)
      SPH2= CPLF(T2)
      TAV2= (TAMB+T2)/2.
      DAB2= DABF(TAV2)
      CPA2= CPAF(TAV2)
      TL= TAV2
      PVL= PV2
      CALL COND
      CON2= CONL
      W2= 4.*PI*R2*DAB2*P*LOG(P/(P-PV2))/(RG*TAV2)
      Z2= W2*CPA2/(4.*PI*R2*CON2)
      TLT2= 4.*PI*R2*CON2*(TAMB-T2)*Z2/(WGT2*SPH2*(EXP(Z2)-1.))-
     1W2*HEAT2/(WGT2*SPH2)
      DR2= (-4.188*DENT2*R2**3*TLT2-W2)/(4.*PI*R2**2*DEN2)
      TIME= TIME+DELTA
      R= R+DELTA*((1./4.)*DR+(3./4.)*DR2)
      T= T+DELTA*((1./4.)*TLT+(3./4.)*TLT2)
      WGT= WGT-DELTA*((1./4.)*W+(3./4.)*W2)
      IF (TCA-T) 9,9,10
    9 GO TO 7
   10 CONTINUE
      IF THE RADIUS IS LESS THAN 100 MICRONS THE PROCESS STOPS
      IF (R-0.01) 7,7,6
    6 GO TO 8
    7 STOP
      END


      SUBROUTINE COND
      COMMON TL,P,PVL,CONL
      AVERAGE THERMAL CONDUCTIVITY
      TCA= 304.2
      TCB= 126.2
      WA= 44.01
      WB= 28.016
      SIGA= 3.941
      SIGB= 3.798
```

```
      TBA= 195.2
      TBB= 71.4
      A= PVL/(2.*P)
      TRA= TL/TCA
      TRB= TL/TCB
      TSA= TL/TBA
      TSB= TL/TBB
      OMAR= 0.697*(1.+0.323*LOG(TSA))
      OMBR= 0.697*(1.+0.323*LOG(TSB))
      VISA= 2.669E-5*OMAR*SQRT(WA*TL)/(SIGA**2)
      VISB= 2.669E-5*OMBR*SQRT(WB*TL)/(SIGB**2)
      CVA= 5.10709+15.42195E-3*TL-9.9 626E-6*TL**2+2.40272E-9
     1*TL**3-1.98588
      CVB= 7.08396-1.28565E-3*TL+3.21241E-6*TL**2-1.20800E-9
     1*TL**3-1.98588
      CONA= (VISA/WA)*(1.30*CVA+3.40-0.70/TRA)
      CONB= (VISB/WB)*(1.30*CVB+3.40-0.70/TRB)
      CONL= A*CONA+(1.-A)*CONB
      RETURN
      END
```

REFERENCES

1. Arpaci, V. S., Conduction Heat Transfer, Addison-Wesley, 1966, p. 505.

2. Bird, R. B., Stewart, W. E. and Lightfoot, E. N., Transport Phenomena, Wiley, 1960, chap. XVI.

3. Borman, G. L., and Johnson, J. H., "Burning a Wide Range of Fuels in Diesel Engines," SAE Progress in Technology Series, vol. 11, 1967, pp. 13-29.

4. Brokaw, R. S., "Estimating Thermal Conductivities of Nonpolar Gas Mixtures," Ind. Eng. Chem., vol. 47, no. 11, Nov., 1955, pp. 2398-2400.

5. Chueh, P. L., and Prausnitz, J. M., "Vapor-Liquid Equilibria at High Pressures. Vapor-Phase Fugacity Coefficientes in Nonpolar and Quantum-Gas Mixtures," Ind. Eng. Chem. Fundamentals, vol. 6, no. 4, Nov., 1967, pp. 492-498.

6. Chueh, P. L., and Prausnitz, J. M., "Vapor-Liquid Equilibria at High Pressures: Calculation of Critical Temperatures, Volumes, and Pressures of Nonpolar Mixtures," A.I.Ch.E. Journal, vol. 13, no. 6, Nov., 1967, pp. 1107-1113.

7. Chueh, P. L., and Prausnitz, J. M., "Calculation of High Pressure Vapor-Liquid Equilibria," Ind. Eng. Chem., vol. 60, no. 3, March, 1968, pp. 34-52.

8. Crandall, S. H., Engineering Analysis, McGraw-Hill, 1966, chap. III, p. 177.

9. Dominicis, D. P., "An Experimental Investigation of Near Critical and Supercritical Burning of Bipropellant Droplets," NASA CR-72399, April, 1968.

10. El Wakil, M. M., Uyehara, O. A., and Myers, P. S., "A Theoretical Investigation of the Heating-up Period of Injected Fuel Droplets Vaporizing in Air," NACA TN 3179, 1954.

11. Faeth, G. M., "Investigation of Near Critical and Supercritical Burning of Fuel Droplets," Quarterly Progress Report No. 7, NASA Grant NGR 39-009-077, 1968.

12. Heidmann, M. F., and Wieber, P. R., "Analysis of n-Heptane Vaporization in Unstable Combustor with Traveling Transverse Oscillations," NASA TN D-3424, 1966.

13. Heidmann, M. F., and Wieber, P. R., "Analysis of Frequency Response Characteristics of Propellant Vaporization," NASA TN D-3749, 1966.

14. Hougen, O. A., Watson, K. M., and Ragatz, R. A., Chemical Process Principles Charts, 3rd ed., Wiley, 1964.

15. Keyes, F. G., "Measurements of Heat Conductivity in Nitrogen-Carbon Dioxide Mixtures," Trans. ASME, vol. 73, July, 1951, pp. 597-603.

16. Lightfood, E. N., and Cussler, E. L., "Diffusion in Liquids," Selected Topics in Transport Phenomena, Chem. Eng. Progr. Symp. Series, vol. 61, no. 58, 1965, pp. 66-85.

17. MacKay, D. M. and Fisher, E. F., Analogue Computing at Ultra-High Speed, Chapman & Hall Ltd., 1962, chap. XVII.

18. Muirbrook, N. K., and Prausnitz, J. M., "Multicomponent Vapor-Liquid Equilibria at High Pressures: Part I. Experimental Study of the Nitrogen-Oxygen-Carbon Dioxide System at 0°C.," A.I.Ch.E. Journal, vol. 11, no. 6, Nov., 1965, pp. 1092-1096.

19. National Bureau of Standards, "Selected Values of Properties of Hydrocarbons," C461, No., 1947, p. 281.

20. Obert, E. F., Concepts of Thermodynamics, McGraw-Hill, 1960, p. 494.

21. Priem, R. J., "Vaporization of Fuel Droplets Including the Heating-up Period," Ph.D. Thesis, University of Wisconsin, 1955.

22. Redlich, O., and Kwong, J.N.S., "On the Thermodynamics of Solutions," Chem. Rev., vol. 44, 1949, pp. 233-244.

23. Reid, R. C., and Sherwood, T. K., The Properties of Gases and Liquids, 2nd ed., McGraw-Hill, 1966, pp. 316, 398, 400, 463, Appendices A and G.

24. Rosner, D. E., "On Liquid Droplet Combustion at High Pressures," AIAA Journal, vol. 5, no. 1, Jan., 1967, pp. 163-166.

25. Sengers, J. V., "Behavior of Viscosity and Thermal Conductivity of Fluids Near the Critical Point," Critical Phenomena, National Bureau of Standards, Misc. Publ. 273, 1966, pp. 165-178.

26. Sotter, J. G., "Nonsteady Evaporation of Liquid Propellant Drops: The Grossman Model," JPL Technical Report 32-1061, Jan., 1968.

27. Spalding, D. B., "Theory of Particle Combustion at High Pressures," ARS Journal, vol. 29, no. 11, Nov., 1959, pp. 828-835.

28. Stewart, W. E., Personal Communication, University of Wisconsin, April, 1967.

29. Stiel, L. I., and Thodos, G., "The Thermal Conductivity of Nonpolar Substances in the Dense Gaseous and Liquid Regions," A.I.Ch.E. Journal, vol. 10, no. 1, Jan., 1964, pp. 26-30.

30. Tee, L. S., Kuether, G. F., Robinson, R. C., and Stewart, W. E., "Diffusion and Principles of Corresponding States," American Petroleum Institute, Division of Refining, vol. 46, 1966, pp. 235-243.

31. Vukalovich, M. P., and Altunin, V. V., Thermophysical Properties of Carbon Dioxide, translated into English under the direction of the United Kingdom Atomic Energy Authority, Collet's Ltd., 1968, pp. 30, 94, 243, and 244.

32. Wieber, P. R., "Calculated Temperature Histories of Vaporizing Droplets to the Critical Point," AIAA Journal, vol. 1, no. 12, Dec., 1963, pp. 2764-2770.

33. Wilson, G. M., "Vapor-Liquid Equilibria, Correlation by Means of a Modified Redlich-Kwong Equation of State," Advances in Cryogenic Engineering, vol. 9, 1964, pp. 168-176.

34. Zenner, G. H., and Dana, L. E., "Liquid-Vapor Equilibrium of Carbon Dioxide-Oxygen-Nitrogen Mixtures," Thermodyanmics, Chem. Eng. Progr. Symp. Series, vol. 59, no. 44, 1963, pp. 36-41.

35. Ziebland, H., "Heat Conduction in Near-Critical Fluids: A Survey," Explosives Research and Development Establishment, Waltham Abbey, Essex.

DISTRIBUTION LIST

NASA Lewis Research Center
21000 Brookpark Road
Cleveland, Ohio 44135
Attn: Dr. R.J. Priem (2)

NASA Lewis Research Center
21000 Brookpark Road
Cleveland, Ohio 44135
Attn: Norman T. Musial

NASA Lewis Research Center
21000 Brookpark Road
Cleveland, Ohio 44135
Attn: Library (2)

NASA Lewis Research Center
21000 Brookpark Road
Cleveland, Ohio 44135
Attn: Repart Control Office

NASA Scientific and Technical
Information Facility
P.O. Box 33
College Park, Maryland 20740
Attn: NASA Representative (6)

NASA Lewis Research Center
21000 Brookpark Road
Cleveland, Ohio 44135
Attn: E.W. Conrad

NASA Headquarters
6th and Independence Ave, S.W.
Washington, D.C. 20546
Attn: R.W. Levine, Code RPL

NASA
George C. Marshall Space
Flight Center
R-P and VE-PA
Huntsville, Alabama 35812
Attn: R.J. Richmond

NASA
Manned Spacecraft Center
Houston, Texas 77058
Attn: J.G. Thibadaux

AFRPL(RPRRC)
Edwards, California 93523
Attn: B.R. Bornhorst

AFRPL(RPPZ)
Edwards, California 93523
Attn: Capt. C.J. Abbe

Air Force Office of Scientific
Research
1400 Wilson Blvd.
Arlington, Virginia 22209
Attn: B.T. Wolfson

Chemical Propulsion Information
Agency
8621 Georgia Avenue
Silver Spring, Maryland 20910
Attn: T.W. Christian

U.S. Naval Weapons Center
China Lake, California 93555
Attn: D. Couch

Office of Naval Research
Navy Department
Washington, D.C. 20360
Attn: R.D. Jackel, 429

U.S. Naval Weapons Center
China Lake, California 93555
Attn: E.W. Price, Code 508

U.S. Army Missile Command
AMSMI-RKL, Attn: W.W. Wharton
Redstone Arsenal, Alabama 35808

ARL(ARC)
Attn: K. Scheller
Wright-Patterson AFB
Dayton, Ohio 45433

University of California
Department of Aeronautical Sciences
Attn: A.K. Oppenhiem
6161 Etcheverry Hall
Berkeley, California 94720

University of California
Mechanical Engineering,
Thermal System
Attn: Dr. R.F. Sawyer
Berkeley, California 94720

University of California
Aerospace Engineering Department
Attn: F.A. Williams
P.O. Box 109
LaJolla, California 92038

Jet Propulsion Laboratory
California Institute of Technology
Attn: R.M. Clayton
4800 Oak Grove Drive
Pasadena, California 91103

Jet Propulsion Laboratory
California Institute of Technology
Attn: J.H. Rupe
4800 Oak Grove Drive
Pasadena, California 91103

Colorado State University
Attn: C.E. Mitchell
Fort Collins, Colorado 80521

Dartmouth University
Attn: P.D. McCormack
Hanover, New Hampshire 03755

Georgia Institute of Technology
Aerospace School
Attn: B.T. Zinn
Atlanta, Georgia 30332

Illinois Institute of Technology
Rm 200 M.H.
Attn: T.P. Torda
3300 S. Federal Street
Chicago, Illinois 60616

Massachusetts Institute of
Technology
Department of Mechanical Engr.
Attn: T.Y. Toong
Cambridge, Massachusetts 02139

The Pennsylvania State University
Mechanical Engineering Department
Attn: G.M. Faeth
207 Mechanical Engineering Blvd.
University Park, Pa. 16802

Princeton University
James Forrestal Campus Library
Attn: I. Glassman
P.O. Box 710
Princeton, New Jersey 08540

Princeton University
James Forrestal Campus Library
Attn: D. Harrje
P.O. Box 710
Princeton, New Jersey 08540

Purdue University
School of Mechanical Engineering
Attn: J.R. Osborn
Lafayette, Indiana 47907

Sacramento State College
School of Engineering
Attn: F.H. Reardon
6000 J. Street
Sacramento, California 95819

Purdue University
Jet Propulsion Center
Attn: R. Weiss
W. Lafayette, Indiana 47907

University of Southern California
Attn: M. Gerstein, Dept. Mech. Engr.
University Park
Los Angeles, California 90007

University of Michigan
Aerospace Engineering
Attn: J.A. Nicholls
Ann Arbor, Michigan 48104

Ohio State University
Dept. of Aeronautical and
Astronautical Engineering
Attn: R. Edse
Columbus, Ohio 43210

Bell Aerosystems Company
Attn: L.M. Wood
P.O. Box 1
Mail Aone J-81
Buffalo, New York 14205

Multi-Tech., Inc.
Attn: F.B. Cramer
601 Glenoaks Blvd.
San Fernando, California 91340

Rocketdyne
A Division of
North American Aviation
Attn: E.C. Clinger
6633 Canoga Avenue
Canoga Park, California 91304

Rocketdyne
A Division of
North American Aviation
Attn: R.B. Lawhead
6633 Canoga Avenue
Canoga Park, California 91304

Purdue University
School of Aeronautics, Astronautics,
and Engineering Sciences
Attn: Dr. A.A. Ranger
Lafayette, Indiana

Aerojet-General Corporation
Attn: R. McBride
P.O. Box 296
Dept. 4921 Bldg. 160
Azusa, California 91703

Aerospace Corporation
Attn: O.W. Dykema
P.O. Box 95085
Los Angeles, California 90045

Dynamic Science, a Division
of Marshall Industries
Attn: B.P. Breen
1900 Walker Avenue
Monrovia, California 91016

Pratt and Whitney Aircraft
Florida Research and Development
Center
Attn: G.D. Garrison
P.O. Box 2691
West Palm Beach, Florida 33402

TRW Systems
Attn: G.W. Elverum
1 Space Park
Redondo Beach, California 90278

University of Connecticut
Aerospace Department
Attn: Dr. E.K. Dabora
Storrs, Connecticut 06268